COOPERATIVE INSTITUTE FOR RESEARCH
IN ENVIRONMENTAL SCIENCES (CIRES)
UNIVERSITY OF COLORADO AT BOULDER
BOULDER, COLORADO 80309

Report Documentation Page

ORIGINATING ACTIVITY

Institute for Telecommunication Sciences
NTIA/U.S. Dept. of Commerce
Boulder, Colo. 80303

REPORT SECURITY CLASSIFICATION

Unclassified

REPORT TITLE

ELECTROMAGNETIC THEORY OF TECHNIQUES FOR THE NON-DESTRUCTIVE TESTING OF WIRE ROPES

DESCRIPTIVE NOTE

Summary Report for Period 1 March 1978 to 28 February 1979

AUTHOR(S)(Last name, first name, initial)

WAIT, JAMES R. Principal Investigator
HILL, DAVID A.

REPORT DATE

28 February 1979

TOTAL NO. OF PAGES

177

CONTRACT NO.

H0155008

CONTRACT TITLE

Analytical Investigations of Electromagnetic Fields in Mine Environments

AVAILABILITY/LIMITATION NOTICE

SUPPLEMENTARY NOTE

The views and conclusions contained in this document are those of the authors and should not be interpreted as necessarily representing the official policies or recommendations of the Departments of Interior and Commerce.

SPONSORING ACTIVITY

U.S. Bureau of Mines,
Pittsburgh Mining and Safety Research Center
U.S. BOM Technical Project Officer,
Dr. H.K. Sacks

ABSTRACT

This report contains a summary of analytical research on electromagnetic methods of nondestructive testing of cylindrical conductors. The principal objective is to provide theoretical insight to the operation of electromagnetic sensing of the internal properties of wire ropes that are used extensively in mine hoists. An overall review of past work is also included.

KEY WORDS

Nondestructive testing, nondestructive evaluation, electromagnetic probing, mine safety, cable testing, electromagnetic induction.

Table of Contents

Section 1

EXECUTIVE SUMMARY

Here we present an overall summary of the principal achievements during the course of the investigations carried out under this phase of the research contract.

In Section 2 we give an overall summary of the Non-Destructive Methods that utilize the interaction of electromagnetic fields with the sample. Some specific topics are: Some Early NDT Work in England, The Important Efforts by Semmelink in South Africa, More Recent Applications and Practices, Early Theoretical Investigations, Related Investigations in Geophysical Prospecting, More Recent Analytical Studies, An Alternative Formulation for Solenoid Excitation, The Dual Problem, and finally we introduce The Prolate Spheroidal Void Model of Hill and Wait that is covered in more detail in later sections.

In Section 3 we deal with the electromagnetic theory of an infinitely long cylinder for the case when the electrical conductivity and the magnetic permeability are uni-axial tensors. This is an idealized yet relevant model for a stranded wire rope or cable that is to be excited by an external alternating-current source. The general and special forms of the solution are discussed in the context of non-destructive testing (NDT) of the rope. The method of deducing the electromagnetic response for a finite source is described in the special case where azimuthal symmetry prevails.

In Section 4 a remarkably simple and novel solution is obtained for the fields induced in an anisotropic cylindrical shell that is located coaxially within a long solenoid. This could be the basis of a non-destructive measuring scheme for stranded wire rope when we have actually accounted for the winding geometry in a relatively crude fashion.

In Section 5 we extend a previous analysis for the series impedance of a long solenoid to allow for the cylindrical layering of the encircled conductor. The results are discussed in the context of non-destructive testing of steel ropes that may have external or internal corrosion. It is shown that even an internal layer of reduced conductivity and permeability will be detectable if the frequency is sufficiently low to permit penetration of the primary field.

In Section 6 we present a self-contained analysis for the impedance of a solenoid that encircles a conducting cylinder that has an internal flaw or anomaly that is also cylindrical in form. A perturbation method is used to obtain an expression for the fractional change of the impedance as a function of the size and location of the anomaly.

In Section 7 we consider the effect of a thin prolate spheroidal void in an infinite conducting circular cylinder. This is used as model for a broken strand in a wire rope. The rope is excited by an azimuthal magnetic line current which is a model for a thin toroidal coil. The anomalous

external fields are computed from the induced electric and magnetic dipole moments of the void.

In Section 8 we consider again the thin prolate spheroidal void in an infinite conducting circular cylinder. But now the rope is excited by an electric ring current which is a model for a thin solenoid or multi-turn wire loop. The anomalous external fields are computed from the induced electric and magnetic dipole moments of the void. For this type of excitation, the induced axial magnetic dipole moment is the dominant contributor to the scattered field.

In Section 9 a stranded wire rope is again idealized as a homogeneous conducting and permeable cylinder of circular cross section and of infinite length. The rope is excited by a coaxial solenoid or finite length multi-turn coil that carries an azimuthally directed alternating current. The novel feature here is that the rope and the enclosing solenoid may have a uniform velocity relative to each other. Using a non-relativistic analysis, the nature of this dynamic interaction is examined and numerical results are presented for parameter values that are relevant to both static and dynamic conditions in non-destructive testing of such cylindrical conductors. It is shown that the dynamic interaction with the rope specimen is not appreciably modified from that for the static condition unless the motional velocity is somewhat greater than about 10 m/s.

Section 2

SURVEY OF ELECTROMAGNETIC METHODS OF NON-DESTRUCTIVE TESTING

INTRODUCTION

Wire ropes are used extensively in many life sustaining situations. Elevator and mine hoist cables are two notable examples but we might also mention the support cable for aerial tramways, ski chairlifts and gondolas, helicopter and suspension cables. In this review, we will restrict attention to wire ropes used in mine hoists. There is an obvious need to perform tests of the integrity of such ropes without in any way impairing their function. Apart from careful visual examination and measurements of the external diameter, the non-destructive test methods available utilize electromagnetic fields, x-rays or mechanical waves. Here we will review progress in the electromagnetic methods.

The early history of the subject will be described briefly since this provides a remarkably good introduction to the working principles. We will then progress rather quickly in time up to the currently used techniques and operating procedures. Next we drop back in time to summarize some of the basic papers that deal with the basic concepts and the techniques for dealing with the testing of cylindrical conductors by both electric and magnetic methods. At this juncture, we call attention to the extensive related work on electromagnetic probing of geophysical targets such as ore bodies and other sub-surface conductors. Finally, we turn to the various investigations, primarily of a theoretical nature, that have been carried out; we include here the most recent work. In the later sections of this interim summary report we deal with specific aspects in more detail.

SOME EARLY NDT WORK IN ENGLAND

Wall [1] gives an early account of the design and operation of electromagnetic rope testers. The test results were given for specially constructed ropes. Using basically an A.C. technique, his method makes it possible to detect broken wires within a rope that represent less than 5% reduction in the total cross-sectional area. As the author indicates, the investigation was motivated by testing of wire ropes used in collieries in England. But the author also indicates that other important applications are to tram cables, airship mooring ropes, and to suspension bridge ropes.

Wall is an early proponent of the A.C. method as opposed to D.C. magnetic testing favored in more recent times. He lists some of the advantages as follows: a) the rope need not continuously move through the magnetic system, b) the A.C. signal is easy to detect and c) any remnant magnetism due, say, to a previous test is wiped out.

He is interested in testing colliery ropes of the locked coil type up to 2¼ inch diameter. In such locked ropes, the outer and one or more of the inner layers are locked together to form flexible sheaths. This constrains the rope to maintain its circular form as it passes over the winding drum. He then quotes a classical skin depth formula that gives a guide to the penetration of the A.C. currents into the core of the rope. He points out cogently that, once the A.C. energy penetrates through the outer locked coil sheaths, it will be "practically" uniformly distributed through the remainder of the cross-section since the wires are so effectively stranded.

The tests were made by means of a laminated iron yoke that has projecting limbs with machined tunnelled holes as indicated in Fig. 1a. The sample length of the rope was fixed concentrically in the holes. A search

coil of 20 turns was wound around the center portion of the rope that is midway between the projecting limbs. The relationship between the flux density in the rope and the peak value of the magnetizing excitation at 20 and 50 Hz was measured. Wall was able to ascertain that the flux penetration was almost complete at 20 Hz but only partially so at 50 Hz.

In the same pioneering paper, Wall studies the effect of mechanical strain on the magnetic permeability with special reference to A.C. excitation. He also examines the change in the reluctance of the air space due to the eccentricity of the rope in the magnet system.

He concludes that "whilst a flaw of about 3% of the total cross section is detectable, a flaw of about 5% produces a pronounced effect, whilst a flaw of about 18% gives a very striking disturbance of the record". Some of Wall's results are summarized in Fig. 1b.

In a follow-up study, Wall and Hainsworth [2] investigate the way in which the flux is distributed within the rope. As they point out, this information is relevant to the estimation of the depth of a flaw in a locked coil or similar rope as used in collieries. They feel a mathematical approach to the problem is intractable. Instead, they build up a special sample or physical model with embedded search coils.

The experimental configuration was chosen to be a replica of a locked coil rope except that the layers of wires were not so close as in actual ropes. Straight mild steel wire rods of 1/8" diameter were employed; each rod was coated with insulating enamel before assembly. A first layer or central group of 7 wires was formed and a search coil (A) of 200 turns was arranged to embrace this group. A second layer of 20 wires was then added and the search coil (B) embraced this layer. Next came the third layer with a further embracing search coil (C). Finally, a fourth layer of 44

wires was formed and the search coil (D) embraced it. Each of the four search coils had 200 turns. Then, by connecting pairs of consecutive search coils in opposition, it was possible to measure the flux magnitude associated with each layer.

The differences between the waveform of the induced EMF's in the various layers are very striking as indicated in Fig. 2. Also, as indicated in Fig. 3, the B-H response curves are shown for central group and the surface layer. Here the screening effect for the central group is very apparent. For the surface layer, the situation is somewhat different since apparently the A.C. excitation has the effect of increasing the apparent permeability. To some extent this tends to counteract the eddy current screening.

THE IMPORTANT EFFORTS BY SEMMELINK IN SOUTH AFRICA

Semmelink [3] gives an extremely interesting account of the early history of electromagnetic testing of wire ropes in South Africa. He indicated that in a paper read to the Transvaal Institute of Mechanical Engineering in 1906, Mr. C. McCann proposed an "electrical apparatus" for ascertaining the cross sectional area of wire ropes. In this scheme, a detachable coil around the rope was supplied through a stepdown transformer from the mains supply. A laminated yoke completed the magnetic circuit and an ammeter was connected in series with the coil. It was claimed that "the current falls exactly in proportion to the size of the rope". Semmelink was also well aware of T.F. Wall's [1] work in England that we described above. He points out that the disadvantage of Wall's method is that the rope speed must be very slow due to the very low frequencies being adopted. Furthermore, the locked type ropes and the use of high

A.C. flux densities causes severe heating of the rope.

The first experiments described by Semmelink were conducted in 1946. A magnetizing coil of twenty turns of welding cable was used carrying a current of 100 amps at 50 Hz together with a co-axial search coil of several thousand turns. The rope was passed through the centers of both coils. It was found that all visible corrosion and broken wires caused voltage variations in the search coil that were measured by a peak reading voltmeter and an oscilloscope. Semmelink [3] then tested about fifty main winding (hoist) ropes. The tensile strength of the wire was either 123/134 tons (2000 lb.) per square inch or 128/140 tons per square inch. The ropes have six strands of approximately thirty wires laid on a sisal core which is impregnated with lubricant. The diameter of the ropes varied from 1¼ inches to 2 inches. The ropes were similar to the type shown in Fig. 4. The steel was ascertained to have the following magnetic properties: relative permeability = 44 for a magnetizing force less than 1 oersted, maximum permeability = 320 for a magnetizing force of 25 oersteds, maximum flux density = 14000 gauss for a magnetizing force of 200 oersteds, retentivity = 9500 gauss, coercive force = 20 oersted, hysteresis loss = 0.35 watts per c.c. at 50 Hz. He found, what is now generally known, that an increase of tensile stress in the wire causes an increase of permeability. For example, a stress of 65 tons per square inch causes an associated increase of permeability of 14% even for a magnetizing force of less than 1 oersted. He also noted that twisting of the wire caused a decrease of 8% of permeability for 180° of twist per foot of wire. Semmelink [3] also measured the change of D.C. resistance of the wire rope for stresses varying from zero to 70 tons/square inch. Only 1.1% increase was noted over this range that was in accord with the percentage increase of length due to elasticity.

In deciding on an A.C. method, Semmelink chose to employ a low magnetizing current. This has two advantages: 1) internal heating is minimized and b) better penetration of the rope due to the relatively small initial permeability (i.e. he is working on the virgin part of the B-H curve). A schematic of his measuring scheme is indicated in Fig. 5.

In a later paper, Semmelink [4] describes a more sophisticated approach to the eddy current testing of wire ropes. The schematic diagram of his measurement set up is illustrated in Fig. 6. As indicated, the rope is excited by spaced coaxial coils and the pick up coil is located centrally. The output of the pick up coil is amplified and detected by a phase sensitive detector.

In the absence of eddy currents, the pick up or search coil voltage leads the magnetizing current by 90 degrees. However, because of the eddy current losses, the phase shift is modified as indicated in Fig. 6. Both the reactive component E_x and the resistive component E_R can be balanced out in an appropriate adjustment of the potentiometers. Thus, the "output" for a given rope can be indicated on a double pen recorder.

The rope speed during a test depends on the response of the recorder and of the detector circuit. Furthermore, due to the choice of a low operating frequency (e.g. 80 Hz), the response of the detectors can not be fast and Semmelink chooses a time constant of 0.1 second. Thus, if the shortest variation to be detected along the rope is 10 cm, the rope speed should not exceed 10 cm in 0.1 second (i.e. the rope speed should be less that 200 feet per minute).

The coils, wound on a bakelite former, are 6 inches long, 5 inches outer diameter and 3 inches inner diameter. The two magnetizing coils have 10 turns each. For a magnetizing current of 1 amps, this gives an exciting

field at the center of 0.43 oersted. The pick up or search coil also has ten turns. The whole assembly is hinged with spring loaded contacts to maintain the electrical integrity needed when the two halves are clamped around the rope.

A number of interesting results have been obtained by Semmelink [4]. For example, a decrease of eddy currents causes an increase of flux with a resulting increase on the E_x trace and a corresponding decrease on the E_R trace. This often is associated with decreased contact between the strands. The reverse situation has also been found when there is increased contact between the strands. Such stressful situations occur at the cross-over points where ropes pass from one layer to another on winding drums.

Slight corrosion in the rope leads to a deposit of non-conducting material between the wires and to a reduction of eddy currents. This usually means a decrease of both E_x and E_R traces. Semmelink also indicates that internal corrosion appears to occur usually over relatively short lengths often at intervals corresponding to the circumference of the drum.

External corrosion manifests itself in a large reduction of the E_x trace but only a small reduction in the E_R trace. Such corrosion can occur over long lengths of the rope (e.g. 1000 feet).

Semmelink [4] found that inadvertent D.C. magnetization of the rope (e.g. from the earth's magnetic field) could lead to violent transients in the E_x trace when the rope moves at high speed through the coil assembly. In one case, the rope had remained at rest for long periods with one section of the rope extending from the drum to the headgear sheave in a northerly direction.

MORE RECENT APPLICATIONS AND PRACTICES

Hiltbrunner [5] gives a good description of what is known now as the D.C. magnetic testing method. This approach has been highly developed in Switzerland for the non-destructive testing of tram-way wire ropes. Essentially the method is based on imposing a strong axial magnetic field to the sample by either a solenoid coil and/or or permanent magnet. The search coil is oriented in the radial direction and produces a voltage response only when there is some type of lateral non-uniformity.

Lang [6] gives an extensive description of an A.C. testing device for wire ropes. Although he does not acknowledge the fact, the concept, method, and operational procedure seem to be based on the earlier work of Semmelink [3,4]. However, Lang uses only one single-turn transmitting coil with a coaxial search coil. Most of his data are shown for a frequency of 30 Hz. Lang found that in all cases of broken wires detected, the "X" trace shows a sharp reduction presumably due to a decrease in the axial magnetic flux. In a number of cases, sections of rope with apparent missing wires were found. This was believed to indicate a wire separation at a faulty spot weld. It is unfortunate that the numerous test results published by Lang are not accompanied by "ground truth" information on the actual state of the rope. He does show a few interesting comparisions between the measured breaking tensile strength and the "R" and "X" readings at 10 Hz for locked coil ropes. Such data, however, were not provided for the 30 and 80 Hz tests on the stranded ropes.

Larsen et al [7] describes various devices for both D.C. and A.C. rope testing that are currently available. They mention that the Rotesco device as described by Lang [6] has been successful in 1970 in predicting tensile

reductions of about 5%, although the extensive comparisons were not "quantitative".

Morgan [8] presents a general review of electromagnetic non-destructive test methods applied to wire ropes. The discussion is entirely qualitative. He makes a number of recommendations for further development in Australia. Morgan and Symes [9] then describe the activities that led to the creation of a government sponsored project at the University of New South Wales. They give a largely qualitative description of their current research on both methods of testing wire ropes. They also describe some tentative ideas about an A.C. device that is to operate at a frequency of 1 kHz. Surprisingly, they make no mention of many A.C. devices that hitherto have been used elsewhere. It is possible they will find that 1 kHz is rather too high a frequency for effective penetration to the core of most mine hoist ropes.

Stachurski [10] gives a very useful summary of the physical concepts employed in D.C. magnetic testing for flaws in wire ropes. A number of interpretative schemes are outlined in a qualitative manner. Also, he uses prescribed forms of flaws, breaks, and cracks to calibrate the device. Much useful data on the design and implementation of the defectograph device are also given. It is evident that this Polish group have highly developed the D.C. magnetic technique.

Egen and Benson [11] describe some interesting tests on a special prepared rope with prescribed types of imperfections. There were seven types of faults: 1) splice, 2) 2 to 3 wires filed half-way through, over a length of about ½ inch, 3) an added No. 18 AWG wire laid into groove of core, 4) spike inserted into core and wires were spread apart, 5) 3 wires of 2 inch

length were removed from the core, 6) one wire in core was cut and 7) a two inch length of core was removed. Using three D.C. devices (the Polish MD-8 Defectoscope, the Swiss PMK-75 Kundig device and the Canadian Rotesco device). None of these devices detected fault No. 6 and the Kundig device did not detect fault No. 2. Otherwise, all other faults were detected by all three instruments. The results indicated that, for the rope tested (i.e. 7/8 inch diameter, 6 × 25, FW, RLL, FC, XIPS), each instrument observed about the same magnetic field variations. The very similar performance of these three instruments is probably a consequence of the basic similarity of the operating principle of each of these D.C. devices. It is a pity that the A.C. Rotesco device was not tested on the same rope.

Bergander [12] International, Inc. describes the Polish D.C. magnetic device for NDT of wire ropes known as the Defectograph MD-8 that he developed with Dr. J. Stachurski. The rope being tested moves through the permanent magnet which is magnetized to its saturation point. He claims that a 0.2% change of the rope cross-section can be detected via a measurement of the external magnetic leakage field. The e.m.f. induced in the search coil can also be compensated for changes in the rope speed. Using an empirical approach the probe coil response is related to such parameters as the loss of cross section of the rope, the length over which the loss occurs and the radial location of the internal flaw.

EARLY THEORETICAL INVESTIGATIONS

Hochschild [13] gives a review of papers by Förster [14-18] and presents some useful plots of the current density in conducting cylinders for A.C. excitation by a solenoidal coil. He points out that no matter how carefully the test coil system is designed, small defects will go undetected

unless the response time of the instrument is less than the time taken from the defect to pass through the effective region of the coils. For example, a localized defect passing through at 0.03 inch wide differential test coil at 100 feet per minute will not be detected unless the response extends upwards to at least 200 Hz. A common limitation on bandwidth is the ink-pen recording devices, whose frequency response seldom exceeds 200 Hz.

McClurg [19] also exhibits some of the results of Förster and colleagues in graphical form. In particular, he shows that the impedance variations of solenoids (i.e. feed through coils) encircling cylindrical conductors that have surface and sub-surface cracks. The empirical data used are from Förster's papers. McClurg discusses the application of these eddy current techniques to metal cutting operations where such things as uniformness of the hardness is desirable.

Graneau [20] introduces the interesting concept that induced currents in a conductor, flowing along closed curves, can be represented by a number of filamentary circuits. These currents and the energizing current can then be deduced in principle from a system of circuit equations with self and mutual inductances that are postulated from the physics of the problem. Using somewhat heuristic reasoning, Graneau obtains an expression for the current anywhere in the metallic object by infinite series of increasing powers of the energizing frequency. The coefficients are undetermined functions of the filament circuit resistance, and mutual inductances between the filaments. He concludes that there is a clear division between quantities depending on geometry and properties. As a consequence, the induced currents can be expressed as an explicit function of frequency. This is really quite strange since exact solutions of idealized forms such as layered cylinders with external dipole excitation do not exhibit this behavior [21-25].

RELATED INVESTIGATIONS IN GEOPHYSICAL PROSPECTING

Electromagnetic methods of non-destructive testing of solid conductors are closely akin to techniques that are now used in geophysical prospecting for metallic ore bodies [21-34]. It is unfortunate that these two groups have had little interaction. This writer was involved in the theoretical developments in multi-frequency and transient electromagnetic methods in geophysical exploration. In fact, as long ago as 1950 it was proposed that conductivity and permeability of a spherical ore body could be ascertained from its electromagnetic response in either the frequency or its time domain. A similar analysis was carried out for a cylindrical ore body with a specified conductivity and permeability. The basic concept was that geometrical configuration of the source and receiver coils with respect to the target could be arranged to have a negligible effect of the determination of ore body size, conductivity and permeability. The subject has advanced considerably since those "early days" and modern accounts are published regularly in Geophysics, the journal of the (U.S.) Society of Exploration Geophysicists and Geophysical Prospecting, the journal of the European Society of Geophysical Exploration.

The work that is relevant to the electromagnetic probing of wire ropes is the analysis of a homogeneous conductive and permeable cylinder of infinite length. In an "early" paper [22], a general solution was given for the total fields produced when a line source or current-carrying cable was located parallel to the cylinder. An exact two-dimensional solution was obtained using a wave impedance approach. The low frequency version of the general solution was expressed in a quasi-static form and numerical results for the induced dipole term were given. Some examples are shown in Figs. 7 and 8

for the induced magnetic dipole responses of spheres and cylinders. In each case the ordinates are proportional to the induced dipole moment. Strictly speaking, the monopole term should also be considered when dealing with cylinders that are effectively infinite in length. This type of analysis was later extended to dipolar excitation of the infinite cylinder when again the monopole or azimuthally independent induced current was not considered in the numerical examples [22].

Further work on this subject was carried out by David A. Hill and the writer [30] where more realistic situations were treated such as the excitation of a conductive cylinder of finite length by an external magnetic dipole where all significant induced monopole, dipole, and multipole contributions were retained in the calculations. The analytical and numerical techniques used in these papers would seem to be applicable in a quantitative analyses of electromagnetic non-destructive testing of solid conductors.

MORE RECENT ANALYTICAL STUDIES

Vein [35] points out, what is usually accepted, that the mutual impedance between two closed circuits is dependent on conducting solids in the immediate environments. He promotes the concept of transfer impedance but feels ill at ease in relating this to the reciprocity theorem for generally continuous media. With this motivation, he works through the analytical details of a number of classical problems such as the mutual impedance between coaxial circular loops in the presence of planar, cylindrical, and spherical conductors. He assumes, without really providing a justification, that azimuthal symmetry prevails in each case. No real harm is done, however, since no numerical results of any kind are provided. The derivations seem to be unnecessarily complicated and, even then, reliance is made on formulas

quoted from exercises in W.R. Smythe's [36] classic text.

Burrows [37], in a significant thesis, exploits the reciprocity theorem in eddy-current testing and the subsequent development of a flaw-detection theory. He is very quick to recognize the limitations of quasi-static theory such as assumed by Vein [35]. But it should be stressed immediately that Burrows actually assumes azimuthal symmetry of his detection coils even though the "flaws" may be asymmetrical. This is a valid procedure but it appears that some fundamental information is lost when both the source and the probe coil fully encircle the cylindrical sample. Burrows represents internal flaws in terms of induced electric and magnetic dipoles that, in turn, produces the secondary influence. He also provides some very useful tabulations of the infinite integrals that describe the internal fields within both solid cylindrical and tubular samples of circular cross sections for azimuthally symmetric excitation. These same integrals can be used to predict the response in a corresponding azimuthally symmetric detector coil due to an internal (small) flaw. Actually, this same approach has been followed up very recently by Hill and Wait [38] who did not restrict the results to azimuthal symmetry of the probe coil.

Dodd, Deeds and Luquire [39] have obtained integral solutions for the vector potential produced by a circular coil for a number of different geometrical configurations. The solutions are limited to axial symmetry. In calculating the exciting fields of a rectangular cross-section circular coil, they assume that a straight-forward superposition of current over the cross-section is valid. This is a quasi-static assumption that probably needs to be investigated, particularly when the coil of finite width and length encircles a highly conducting cylinder.

Dodds et al quote Burrows' [37] formulation for deducing the secondary induced voltages due to a defect or flaw in an adjacent conductor. Here they write down a formula for the defect-produced voltage, induced in coil 2, by a current in coil 1 in terms of the electric and magnetic scattering matrices for an electrically small defect.

In the same paper, Dodds et al give explicit solutions in integral form for the rectangular cross-section coil located over a two-layer planar conductor. Actually, the form of these solutions are very similar to earlier investigations of electromagnetic induction in layered models of the earth's crust. The NDT community is apparently not aware of this extensive literature. An example is the book by Keller and Frischknecht [40] that reviews the current status of such problems at least up to 1965. Of course, Dodds et al give the explicit form of the fields of a circular coil with rectangular cross-section, while the geophysicists restrict their attention to small loops. Dodds et al also gives solutions for various combinations of pick-up coils and the corresponding secondary effects due to embedded defects that can be characterized by the polarizability matrices mentioned above.

Cheng, Dodds and Deeds [41] have presented a general formulation for the time-harmonic eddy currents, produced by a circular coil of rectangular cross-section, for a underlying planar conductor of any number of layers. The integral solutions obtained in a straight-forward fashion yield algebraically complicated results. A number of these results could have been obtained by using impedance methods based on analogies with transmission line theory (see for example [42] and [43]).

Dodd, Cheng and Deeds [44] give a formal vector potential solution to a coil coaxial with any number of cylindrical conductors. While they state the derivation is quite general, the solution is only carried through for complete symmetry about the common axis.

Dodd and Deeds [45] give the same solutions for a uniform coil with uniform A.C. current excitation over a two layer planar conductor. They then repeat the solution for the coil encircling a two-layer cylindrical conductor of infinite length. A single numerical example is given for the normalized impedance of the coil as over the two-layer planar structure that exhibits the effect of the thickness of the upper layer.

Kahn et al [46] present an interesting analysis of how eddy currents in a solid conductor are diverted around a surface crack. One of the basic assumptions is that the magnetic field tangent to the surface is a constant even in the presence of the crack. They also present solutions for diffraction by a semi-infinite crack (i.e. a half-plane) in an otherwise infinite medium. Neither of these solutions are "rigorous" as claimed by the authors but the results do provide considerable insight into how defects, of other than infinitesimal size, will modify to external fields. Kahn and Spal [47] have also presented some results for the calculations of eddy currents in a long cylinder with a radial crack at the surface. Details of the analytical method are not yet available but presumably the approach is similar to that used in treating the surface crack in the planar conductor. It is appropriate to call attention to the close similarity of such problems to earlier theoretical studies in geophysics where one is interested in the perturbation of time-varying geomagnetic fields near coastlines [48] and other laterally varying features in the earth's crust [49].

AN ALTERNATIVE FORMULATION FOR SOLENOID EXCITATION

As we have indicated, a commmon method of non-destructive testing (NDT) of metal rods and tubes is to induce eddy currents by means of an encircling solenoid carrying an alternating current. The impedance of the solenoid is related to the cross-sectional area and the electrical properties of the sample. A formula for this impedance was obtained by Förster and Stambke [16] on the assumption that end effects could be ignored. Also, they assumed that the cylindrical sample was centrally located within the solenoid. The same derivation was essentially repeated by Hochschild [13] and Libby [51].

A feature of the Förster-Stambke derivation is that the effect of the air gap is introduced in a somewhat heuristic fashion wherein the field in this concentric region is assumed to be the same as the one for the empty solenoid. We feel it is worthwhile to provide a more general derivation of the impedance formula. We also show it applies to the case of a non-concentric air gap. Finally, we mention the relevance of the current analysis to the dual problem where the cylindrical sample is excited by a toroidal coil.

To simplify the discussion, we consider first the concentric air gap model with a homogeneous cylindrical sample of radius a with conductivity σ and magnetic permeability μ. The situation is indicated in Fig. 9 where the solenoid of radius b encloses the sample, both of which are assumed to be infinite in length. Our objective is to find an expression for the impedance of the solenoid per unit length since this is the basis of the NDT eddy current methods that are commonly used.

In terms of cylindrical coordinates (ρ,ϕ,z), the only component of the magnetic field is H_z since the exciting current in the solenoid is uniform in both the axial and in the azimuthal direction. Within the sample, H_z satisfies the Helmholtz equation

$$(\nabla^2 - \gamma^2)H_z = 0 \tag{1}$$

where $\gamma^2 = i\sigma\mu\omega$ and where we have adopted a time factor $\exp(i\omega t)$. Here ω is the angular frequency that is sufficiently low that displacement currents in the sample can be neglected. If not, we merely replace σ by $\sigma + i\varepsilon\omega$ where ε is the permittivity. Also, it goes without saying that the field amplitude is sufficiently small that non-linear effects can be ignored.

For the highly idealized situation described, we can immediately write [52]

$$H_z = AI_o(\gamma\rho) \tag{2}$$

for $\rho < a$ where I_o is a modified Bessel function of argument $\gamma\rho$ and where A is a constant. From Maxwell's equations the azimuthal component of the electric field is

$$E_\phi = -(1/\sigma)\partial H_z/\partial\rho = -A(\gamma/\sigma)I_1(\gamma\rho) \tag{3}$$

also for $\rho < a$. Now we can immediately form an expression for the "impedance" Z_c of the cylinder:

$$Z_c = \left[-E_\phi/H_z\right]_{\rho=a} = \eta I_1(\gamma a)/I_o(\gamma a) \tag{4}$$

where $\eta = \gamma/\sigma = (i\mu\omega/\sigma)^{\frac{1}{2}}$ is the intrinsic or wave impedance of the sample material.

Now, for the air gap region $a < \rho < b$, we write corresponding field expressions

$$H_{oz} = BI_o(\gamma_o\rho) + CK_o(\gamma_o\rho) \tag{5}$$

and

$$E_{o\phi} = -B\eta_o I_1(\gamma_o\rho) + C\eta_o K_1(\gamma_o\rho) \tag{6}$$

where B and C are constants and where $\eta_o = \gamma_o/(i\varepsilon_o\omega) = (\mu_o/\varepsilon_o)^{\frac{1}{2}} \cong 120\pi$ in terms of the permittivity ε_o and permeability μ_o of the air region. Here and in the above, the Bessel function identities $\partial I_o(x)/\partial x = I_1(x)$ and $\partial K_o(x)/\partial x = -K_1(x)$ have been employed.

Compatible with the requirement that tangential fields must be continuous at $\rho = a$ we can write

$$\left[E_{o\phi} + Z_c H_{oz}\right]_{\rho=a} = 0 \tag{7}$$

This immediately tells us that

$$\frac{C}{B} = \frac{\eta_o I_1(\gamma_o a) - Z_c I_o(\gamma_o a)}{\eta_o K_1(\gamma_o a) + Z_c K_o(\gamma_o a)} \tag{8}$$

In the external region $\rho > b$, the field expressions must clearly have the form:

$$H_{oz} = DK_o(\gamma_o\rho) \tag{9}$$

$$E_{o\phi} = D\eta_o K_1(\gamma_o\rho) \tag{10}$$

where D is another constant.

Now the solenoid current is idealized as a continuous current distribution j_o amps/m in the azimuthal direction defined such that

$$\lim_{\Delta \to 0} \begin{cases} H_{oz}(\rho=b+\Delta) - H_{oz}(\rho=b-\Delta) = -j_o & (11) \\ E_{o\phi}(\rho=b+\Delta) - E_{o\phi}(\rho=b-\Delta) = 0 & (12) \end{cases}$$

Application of these conditions immediately leads to

$$D = C - I_1(\gamma_o b)B/K_1(\gamma_o b) \tag{13}$$

and

$$B = j_o\gamma_o bK_1(\gamma_o b) \tag{14}$$

Among other things, this tells us that the magnetic field external to the solenoid (i.e. $\rho > b$) has the form

$$H_{oz} = \{-B[I_1(\gamma_o b)/K_1(\gamma_o b)] + C\}K_o(\gamma_o \rho) \tag{15}$$

The quantity of immediate interest is the impedance Z of the solenoid itself. Clearly, within the limits of our basic assumptions,

$$Z = \text{const.} \times E_{o\phi}(\rho=b)/j_o \tag{16}$$

The corresponding impedance of the empty solenoid is denoted Z_o. Thus, it follows that

$$\frac{Z}{Z_o} = 1 - \frac{C}{B}\,\frac{K_1(\gamma_o b)}{I_1(\gamma_o b)} \tag{17}$$

which is explicit since C/B is given by (8).

We now can simplify the impedance ratio formula if we invoke the small argument approximations for Bessel functions of order $\gamma_o a$ and $\gamma_o b$. That is, we use $I_o(x) \simeq 1$, $I_1(x) \simeq x/2$, $K_o(x) \simeq -\log x$ and $K_1(x) \simeq 1/x$. This exercise leads to

$$\frac{Z}{Z_o} \simeq \left[1 - \frac{a^2}{b^2} + \frac{\mu}{\mu_o}\,\frac{a^2}{b^2}\,\frac{2}{\gamma a}\,\frac{I_1(\gamma a)}{I_o(\gamma a)}\right] = \frac{R + iX}{Z_o} \tag{18}$$

where no restriction has been placed on the magnitude of γa. Here R and X denote the resistance and reactance, respectively.

The formula for Z/Z_o given by (18) is in agreement with Förster and Stambke [16] (if one remembers they used the old German designations J_o and J_1 for modified Bessel functions). Förster and Stambke [16], Hochschild [13] and Libby [51] present extensive numerical data for this quasi-static approximation to Z/Z_o in Argand diagrams in the complex plane for various values of $|\gamma a|$ and μ/μ_o. Two examples, using dimensionless parameters,

are shown in Figs. 10 and 11 when the ordinates and abscissae are normalized by X_o which is the reactance of the empty solenoid. That is, we assume $Z_o \simeq iX_o$ corresponding to negligible ohmic losses in the solenoid itself. The real parameter α is defined by $\alpha = \gamma a \exp(-i\pi/4) = (\sigma\mu\omega)^{\frac{1}{2}}a$. In Fig. 10 the sample radius b is assumed to be the same as the sample radius a (i.e. no air gap). Different values of the magnetic permeability are shown. Not surprisingly, when α is small, R vanishes and X/X_o tends to μ/μ_o. However, in general, the eddy-currents have the effect of reducing X/X_o, which is the effective flux, and to introduce a resistive portion R/X_o. In Fig. 11, the relative permeability of the sample $\mu/\mu_o = 1$ but the filling factor a^2/b^2 assumes different values. The results indicate that the presence of the air gap reduces the sensitivity of the device for probing the conductivity but the effect is predictable.

Actually, if α is sufficiently small (i.e. $|\gamma a| << 1$), (18) reduces to

$$Z/Z_o \simeq X/X_o \simeq 1 + (a^2/b^2)[\mu/\mu_o - 1] \tag{19}$$

which is consistent with the curves in Figs. 10 and 11. In this D.C. limit the results only depend on the magnetic permeability of the sample.

The formal extension of the theory to the case where the exciting solenoid is no longer concentric with the cylindrical sample can also be dealt with. The situation is indicated in Fig. 12. As before, cylindrical coordinates (ρ,ϕ,z) are chosen co-axial with the sample. But now, the shifted coordinates (ρ',ϕ',z) are chosen to be coaxial with the exciting solenoid. The shift is ρ_o as indicated in Fig. 12 where we do impose the rather obvious physical restriction that $b > \rho_o + a$. We may show that the field in the non-concentric air gap has the form [50]

$$H_{oz} = BI_o(\gamma_o\rho') + \sum_{m=-\infty}^{+\infty} C_m \sum_{n=-\infty}^{+\infty} K_{m+n}(\gamma_o\rho')I_n(\gamma_o\rho_o)(-1)^n e^{-i(n+m)\phi'} \tag{20}$$

This is valid in the non-concentric air gap region (i.e. $\rho > a$ and $\rho' < b$). The needed azimuthal component is obtained from

$$E_{o\phi'} = -\eta_o \partial H_{oz}/\partial(\gamma_o\rho') \tag{21}$$

The relevant quantity for the impedance calculation is the "average" field $\bar{E}_{o\phi'}$ at the solenoid. Then it follows that the impedance Z per unit length of the solenoid with the sample divided by the impedance Z_o of the empty solenoid is given by

$$\frac{Z}{Z_o} = 1 - \frac{K_1(\gamma_o b)}{I_1(\gamma_o b)} \sum_{m=0}^{\infty} \varepsilon_m \frac{C_m}{B} (-1)^m I_m(\gamma_o\rho_o) \tag{22}$$

where $\varepsilon_o = 1$ and $\varepsilon_m = 2$ for $m \neq 0$ and where C_m/B is known [50]. Not surprisingly, (22) reduces to (17) for the centrally located sample, i.e. $I_m(\gamma_o\rho_o) = 0$ for $\rho_o \to 0$ when $m \neq 0$.

We again may invoke the small argument approximations for Bessel functions of order $\gamma_o a$, $\gamma_o b$, and $\gamma_o\rho_o$. Lo and behold, these show that Z/Z_o reduces again to the formula given by (18). This confirms the conjecture of Förster and Stambke [16] who seemed to be gifted with keen physical insight into such problems. Of course, we do not expect the result to hold in any sense when the dimensions of the solenoid become comparable with the free-space wavelength. In that case, many other complications arise such as the assumed uniformity of the solenoid current.

THE DUAL PROBLEM

There is an extremely interesting dual to the problem we have discussed. That is, rather than exciting the cylindrical sample with an *azimuthal electric current*, we employ an *azimuthal magnetic current*. This

is an idealized representation for a thin toroidal coil but, again, it effectively is of infinite length in the z or axial direction. The assumed source discontinuity is now in the electric field at $\rho = b$ which has only a z component. The much more complicated case of the toroidal coil of finite axial extent was analyzed recently [53].

Under the present assumption of axial uniformity, the admittance Y per unit length of the toroid is the dual of the impedance Z of the solenoid discussed above. Thus, all the earlier equations apply if we make the following transformations: $i\mu\omega \to \sigma$, $\mu_o \to \varepsilon_o$, $\eta \to \eta^{-1}$, $\eta_o \to \eta_o^{-1}$, $H_z \to E_z$, $E_\phi \to -H_\phi$, $H_{oz} \to E_{oz}$, and $E_{o\phi} \to -H_{o\phi}$. Then the dual of (18) is the ratio of the admittance Y of the toroidal coil with the sample to the admittance Y_o without the sample. It is written explicitly

$$\frac{Y}{Y_o} = \left[1 - \frac{a^2}{b^2} + \frac{\sigma}{i\varepsilon_o\omega}\frac{a^2}{b^2}\frac{2}{\gamma a}\frac{I_1(\gamma a)}{I_o(\gamma a)}\right] \tag{23}$$

for the case where $|\gamma_o b| \ll 1$. That is, the radius of the toroidal coil should be much smaller than the free-space wavelength. Also, in full analogy to the earlier discussion, the quasi-static result holds for any location of the cylindrical sample within the toroid. Furthermore, in the low frequency limit where $|\gamma a| = \alpha \ll 1$, we see that

$$Y \simeq Y_o[1 + (a^2/b^2)[(\sigma/i\varepsilon_o\omega) - 1]] \tag{24}$$

which depends only on the conductivity of the sample. Thus this type of excitation should be preferred with probing the effective conductivity in the axial direction in the sample.

THE PROLATE SPHEROIDAL VOID MODEL OF HILL AND WAIT

As we have indicated, an appropriate source for excitation of axial electric currents is a toroidal coil which encircles the rope, and a magnetic current model for the toroidal source coil has been analyzed [53]. Expressions for both the interior and exterior fields were derived for a homogeneous wire rope. As we shall outline here, the presence of a small slender void within the rope can be treated. Such a void can be considered a model for a broken strand. The void is also allowed to be oriented at any arbitrary angle to the rope axis to account for the winding geometry of the wire rope. The induced electric and magnetic dipole moments are computed from the primary fields and the electric and magnetic polarizabilities of the void. We then obtain expresssions for the external fields of electric and magnetic dipoles of arbitrary orientation. Of course, it is these external fields which are the observable quantities in any EM nondestructive testing method. The particular expressions, derived for the external fields of internal electric and magnetic dipoles, should be useful in future analyses of other types of small imperfections in wire ropes. Of course, in such cases, the electric and magnetic polarizabilities would be different.

In a previous analysis [53], we analyzed an azimuthal current sheet source which encircled the rope. The current sheet was allowed to have arbitrary width in the z or axial direction and arbitrary azimuthal extent. This source results in fairly complicated expressions for the electric and magnetic fields. Since, in this paper, we are primarily concerned with the fields scattered by the void, we take the simpler special case for the source shown in Fig. 13. Specifically, a magnetic current ring of strength K is

located at a radius b in the plane $z = 0$. This is a model for a thin toroidal coil which completely encircles the rope. The rope is assumed to be infinitely long and has radius a. It has conductivity σ_w, permittivity ε_w, and permeability μ_w. The surrounding free space has permittivity ε_o and permeability μ_o. For now, we defer discussion of the void properties and consider only the homogeneous rope.

Because of the symmetry of the source and the rope, the fields are TM (Transverse Magnetic) and independent of ϕ. The magnetic field has only a nonzero azimuthal component H_ϕ^{pr}, and the electric field has only nonzero axial and radial components E_z^{pr} and E_ρ^{pr}. The superscript pr denotes the fields in the absence of the void. These primary fields are derived elsewhere [53], and the explicit forms both inside and outside the rope are given in Appendix A of a recent report [38]. We note that E_ρ^{pr} and H_ϕ^{pr} are zero for $\rho = 0$. On the other hand, E_z^{pr} is nearly independent of ρ inside the rope for sufficiently low frequencies.

We now select a thin prolate spheroid of conductivity σ_v, permittivity ε_v, and permeability μ_v in order to model a broken strand. The prolate spheroidal shape is a convenient one because its electric and magnetic polarizabilities are known. However, we would not expect a significant difference for a thin circular cylinder of the same length and volume. To account for the winding geometry of the rope, we allow a rotation of the major axis of the spheroid about the ρ' axis by an angle α. Thus, the major axis is oriented at an angle α to the unit vector $\hat{z}'$ and an angle $\pi/2 + \alpha$ to the unit vector $\hat{\phi}'$ as indicated in Fig. 1c.

Since the void has a contrast in both the electric and magnetic properties, both electric and magnetic dipole moments will be induced [36]. The electric polarizabilities for the incident electric field applied along the

major axis, α^e_{maj}, or along the minor axis, α^e_{min}, are given by

$$\alpha^e_{maj} = -V(\sigma_w - \sigma_v) \tag{25}$$

and

$$\alpha^e_{min} = \frac{-2V(\sigma_w - \sigma_v)}{1 + \sigma_v/\sigma_w} \quad , \tag{26}$$

where V is the volume of the thin prolate spheroid. Since we anticipate the use of very low frequencies, we have neglected displacement currents. To include them, σ_w would be replaced by $\sigma_w + i\omega\varepsilon_w$ and σ_v would be replaced by $\sigma_v + i\omega\varepsilon_v$ in (25) and (26). The magnetic polarizabilities for the incident magnetic field applied along the major axis, α^m_{maj}, or along the minor axis, α^m_{min}, are similarly given by

$$\alpha^m_{maj} = -Vi\omega(\mu_w - \mu_v) \tag{27}$$

and

$$\alpha^m_{min} = \frac{-2Vi\omega(\mu_w - \mu_v)}{1 + \mu_v/\mu_w} \tag{28}$$

In order to compute the induced dipole moments, it is first necessary to resolve the incident electric and magnetic fields into components along the major and minor axes. The resultant induced dipole moments can then be resolved into the more convenient ρ, ϕ, and z components. When this is done, the induced electric dipole moments are found to be

$$(Ids)_z = E^{pr}_z(\alpha^e_{maj}\cos^2\alpha + \alpha^e_{min}\sin^2\alpha) \ , \tag{29}$$

$$(Ids)_\phi = E^{pr}_z(\alpha^e_{min} - \alpha^e_{maj})\sin\alpha\cos\alpha \ , \tag{30}$$

$$(Ids)_\rho = E^{pr}_\rho \alpha^e_{min} \tag{31}$$

In (29)-(31), the primary electric field components E^{pr}_z and E^{pr}_ρ are evaluated at ρ', ϕ', z'. Similarly, the induced magnetic dipole moments are found to be

$$(Kd\ell)_z = H_\phi^{pr}(\alpha_{min}^m - \alpha_{maj}^m)\sin\alpha\cos\alpha \ , \tag{32}$$

$$(Kd\ell)_\phi = H_\phi^{pr}(\alpha_{min}^m \cos^2\alpha + \alpha_{maj}^m \sin^2\alpha) \ , \tag{33}$$

$$(Kd\ell)_\rho = 0 \ . \tag{34}$$

Note that the units of the induced electric dipole moments in (29)-(31) are ampere meters, and the units of the induced magnetic dipole moments in (32) through (34) are volt-meters. These induced dipole moments are the sources of the scattered field.

The scattered field external to the rope is the observable quantity in any NDT system. Since we anticipate the use of coils for sensors, we have considered the scattered magnetic field components $H_\rho^{sc}(\rho,\phi,z)$, $H_\phi^{sc}(\rho,\phi,z)$, and $H_z^{sc}(\rho,\phi,z)$ [38]. Each of these components can be written as a superposition of the contributions from each of the six induced dipole sources. (Actually, there are only five nonzero sources since $(Kd\ell)_\rho$ is zero for the specific configuration considered here). Explicit expressions for the three scattered field components are given elsewhere [38].

The quantities of most interest in NDT are the external ($\rho>a$) magnetic field components which are observed with the sensing coils. The primary magnetic field has only a ϕ component H_ϕ^{pr} but the scattered magnetic field has all three components. For the numerical results, the following parametric values remain fixed: $a = 1$ cm, $\sigma_w = 1.1 \times 10^6$mho/m, $\mu_w = 200\ \mu_o$, $b = 2$ cm, frequency = 10 Hz, $\rho = 2$ cm, $\sigma_v = 0$, and $\mu_v = \mu_o$. For this low frequency, the conduction currents dominate, and the permittivities ε_w and ε_v are unimportant. The above values of σ_w and μ_w

are roughly representative of stainless steel, but the permeability of steel is quite variable [54]. For the above parameters, the radius a is approximately one skin depth. For convenience here, we also choose $z = z' = 0$ and $\phi' = 0$.

In Figs. 14, 15, and 16, we show the magnitude of the scattered magnetic field components normalized by VH_{ϕ}^{pr} as a function of ϕ. The reason for showing the ϕ dependence is that, although the primary field is independent of ϕ, the scattered field varies considerably in ϕ. This variation might dictate the use of multiple sensing coils spaced in azimuth around the rope. The curves are normalized by the primary field because the anomalous scattered field is measured in the presence of the primary field and their ratio is thus of interest. We also normalize the results to the volume V of the void in order to make the curves more general. However, a typical value for V might be on the order of $10^{-8}m^3$ (=1 cm × 1 mm × 1 mm). As indicated in Figs. 14 and 15, H_{ρ}^{sc} and H_{ϕ}^{sc} are of approximately the same level, but H_{ρ}^{sc} is odd in ϕ while H_{ϕ}^{sc} is even. We also may note the decrease in scattered field as the void is moved from the outer region ($\rho'/a = 0.9$) toward the center ($\rho'/a = 0.1$) of the rope. Because $\alpha = 0°$ in Figs. 14 and 15, only the axial and radial electric dipole moments and the azimuthal magnetic dipole are excited. Also, the radial electric dipole is very small because its exciting field E_{ρ}^{pr} is small. The calculations reveal that $(Ids)_z$ and $(Kd\ell)_{\phi}$ contribute approximately equally to the scattered field. In Fig. 16, we have $z = z' = 0$ and $\rho'/a = 0.5$, but we allow α to vary from 0° to 30°. Nonzero values of α allow two additional dipole moments (the azimuthal electric and the axial magnetic dipoles) to be induced. The result is a decrease in the level of H_{ϕ}^{sc} and H_{ρ}^{sc}

and an increase in the level of H_z^{sc}. These new results are described elsewhere [38].

The phase of the scattered field was also computed, but was found to be of less interest. Also, the individual dipole contributions were computed, and they are of individual interest since they will be excited differently for other sources or other void configurations.

Although we have generated numerical results for the specific case of a thin prolate spheroidal void, the formulation given here actually yields the external fields for arbitrary induced electric and magnetic dipole moments. Thus the formulation is useful for any type of rope imperfection that can be characterized by induced electric and magnetic dipole moments. This requires only that the rope imperfection be small in terms of the rope radius and the rope skin depth. Larger imperfections should have a similar qualitative behavior, but could probably be rigorously analyzed only by solving an integral equation for the fields in the imperfection. Also, it would be a simple matter to perform similar calculations for a solenoidal coil of the type used in present NDT systems. The scattered field calculation remains unchanged, but the primary field would be $TE(E_z^{pr} = 0)$ rather than $TM(H_z^{pr} = 0)$. Some calculations for this case have been carried out by Burrows [37] for the special case where both exciting and sensing coils are coaxial with the tubular specimen.

CONCLUDING REMARKS

We have attempted to give an overall view of NDT electromagnetic methods. As indicated, the investigations have proceeded along different lines. The very practical and perhaps most useful work to date has been empirical in nature. There has been no attempt made to deduce the magni-

tude of the secondary fields due to the internal flaw; instead a large number of actual ropes are tested and the results presented. On the other hand, the analytical approaches have considered only highly idealized situations. Nevertheless, some important principles are disclosed that may have an important bearing on operating procedures. For example, the toroidal coil exciter could be utilized in practical schemes in conjunction with localized sensor coils that can characterize the three-dimensional field configuration in an adequate fashion.

A basic theoretical aspect of the NDT problem that we have not really addressed is to account for the anisotropic nature of the effective conductivity and the permeability of the wire rope. The spiral construction of stranded wire ropes sometimes described as a "twisted bunch of spaghetti" defies any simple microscopic description. However, from a macroscopic point, we might describe the effective anisotropy by conductivity and permeability tensors. Some preliminary efforts in this direction have begun [55]. It is obvious that much remains to be done and we have addressed some of these topics in the subsequent sections.

REFERENCES

[1] T.F. Wall, "Electromagnetic testing for mechanical flans in steel wire ropes", *J. Inst. Elect. Engrs.*, vol. 67, pp. 899-911, 1929.

[2] T.F. Wall and C.H. Hainsworth, "The penetration of alternating magnetic flux in wire ropes", *J. Inst. Elect. Engrs.*, vol. 71, pp. 374-379, 1932.

[3] A. Semmelink, "Electro-magnetic testing of winding ropes", *Trans. of the South African Institute of Electrical Engrs.*, vol. 43, no. 5, pp. 113-129, May 1953.

[4] A. Semmelink, "Electromagnetic testing of winding ropes", *Trans. of the South African Institute of Electrical Engrs.*, vol. 47, No. 8, pp. 206-244, Aug. 1956.

[5] R.H. Hiltbrunner, "Le Controle Magnétique des câbles avec le défectoscope integra", *Économie et Technique des Transports*, no. 119, June 1957.

[6] J.G. Lang, "The principle and practice of electromagnetic wire rope testing", *Canadian Mining and Metallurgical Bulletin*, pp. 415-424, April 1969.

[7] C.H. Larsen, P.A. Egen, R.D. Jones, and H.A. Cross, "Wire rope applications and practices associated with underground coal mining in the U.S.", *Final Report (from Battelle Laboratories) on U.S. Bureau of Mines Contract No. HO101741*, 22 June 1971.

[8] J.P. Morgan, "Investigations on wire ropes in mine hoisting system", *Proc. Australian Inst. of Min. and Metal*, no. 215, pp. 59-85, 1965.

[9] J.P. Morgan and H.E.J. Symes, "Non-destructive testing of wire ropes", Bulletin No. 6, *Australian Mineral Industries Research Assoc. Ltd.* (National Library of Australia Card No. ISSN 0313-6973), 1976.

[10] J. Stachurski, "Magnetic testing of steel wire ropes", *Report from Laboratory for Testing Wire Ropes, University of Mining and Metallurgy*, Cracow, Poland, 1976.

[11] R.A. Egen and D.K. Benson, "Wire rope retirement criteria and procedures", Progress Report No. 16 (from *Midwest Research Inst., 425 Volker Blvd., Kansas City, MO 64110) on U.S. Bureau of Mines Contract No. J0155187,* 10 Nov. 1976.

[12] M.J. Bergander, "Principles of magnetic defectoscopy of steel ropes", Paper presented at *47 Annual Convention of the Wire Association, Boston,* November 1977.

[13] H. Hochschild, "Electromagnetic methods of testing metals", *Progress in Non-Destructive Testing,* vol. 1, pp. 59-109, The Macmillan Co., New York, 1959.

[14] F. Förster, "Theoretical and experimental foundation of non-destructive testing using eddy currents I. Test coil Methods", *Zeitschrift Metallkunde,* vol. 43, no. 5, pp. 163-171, 1952 (in German).

[15] F. Förster and H. Breitfeld, "Non-destructive testing using eddy current methods II. Practical results and industrial applications of methods using test coils", *Zeitschrift Metallkunde,* vol. 43, no. 5, pp. 172-180, 1952 (in German).

[16] F. Förster and K. Stambke, "Theoretical and experimental foundation of non-destructive testing using eddy currents III. Quantitative methods of non-destructive testing using test object encircling coils", *Zeitschrift Metallkunde,* vol. 45, no. 4, pp. 166-179, 1954 (in German).

[17] F. Förster, "Theoretical and experimental foundation of non-destructive testing using eddy currents IV. Practical apparatus for non-destructive testing using encircling coils for eddy currents", *Zeitschrift Metallkunde,* vol. 45, no. 4, pp. 180-187, 1954 (in German).

[18] F. Förster and H. Breitfeld, "Theoretical and experimental foundation of non-destructive testing using eddy currencts V. Quantitative testing for cracks in metallic objects using test object encircling coils", *Zeitschrift Metallkunde*, vol. 45, no. 4, pp. 188-199, 1954 (in German).

[19] G.O. McClurg, "Non destructive eddy current testing", *IRE Trans.*, vol. IE-11, no. 1, pp. 20-26, 1959.

[20] P. Graneau, "Coupled circuit theory for electromagnetic testing", *Progress in Non-Destructive Testing* (ed. by E.G. Stanford and J.H. Fearson), vol. 2, pp. 163-188, 1961.

[21] J.R. Wait, "A conducting sphere in a time varying magnetic field", *Geophys.*, vol. XVI, pp. 666-672, Oct. 1951.

[22] J.R. Wait, "The cylindrical ore body in the presence of a cable carrying an oscillating current", *Geophys.*, vol. XVII, pp. 378-386, April 1952. [In eqn. (13), replace μ_2/μ_1 by $n\mu_2/\mu_1$ both in the numerator and denominator, similarly, in (14), replace $(k\pm n)$ by $n(k\pm 1)$. Also, the summations in (66), (67), etc. should include the $n = 0$ terms].

[23] J.R. Wait, "A conducting permeable sphere in the presence of a coil carrying an oscillating current", *Can. J. Phys.*, vol. 31, pp. 670-678, May 1953.

[24] J.R. Wait, "Some solutions for electromagnetic problems involving spheroidal, spherical and cylindrical bodies", *J. Res. NBS*, vol. 64B, pp. 15-32, Jan./Mar. 1960.

[25] S.H. Ward and D.C. Fraser, "A conducting permeable sphere and cylinder in an elliptically polarized alternating magnetic field", *J. Geomag. and Geoelectricity*, vol. 18, no. 1, pp. 23-41, 1966.

[26] S.H. Ward, "The electromagnetic method", *Mining Geophysics*, vol. II, pp. 224-372, Oct. 1967 [Ward's quasi-static solution, Sec. 7a, does not include the effect of the induced monopole or azimuthally invariant currents, i.e. the $n = 0$ terms are missed].

[27] S.K. Singh, "Transient electromagnetic response of a conducting infinite cylinder embedded in a conducting medium", *Geofisica Internacional (Mexico)*, vol. 12, no. 1, pp. 7-21, 1972.

[28] S.K. Singh, "Transient electromagnetic response of a conducting cylinder in a conducting medium: numerical resutls", *Geofisica Internacional (Mexico)*, vol. 12, no. 4, pp. 267-280, 1972.

[29] Von J. Meyer, "Über die Richtungsveränderlichkeit des geomagnetischen Induktionspfeiles bei endlicher Leitfähigkeit", *Zeits. für Geophysik*, vol. 38, pp. 195-221, 1968.

[30] D.A. Hill and J.R. Wait, "Electromagnetic response of a conducting cylinder of finite length", *Geofisica Internacional (Mexico)*, vol. 12, no. 4, pp. 245-266, 1972.

[31] J.R. Wait, "On the electromagnetic induction in elongated ore bodies", *Geophysics*, vol. 38, no. 5, pp. 984-985, 1973. Correction: vol. 39, no. 2, p. 235, 1974.

[32] W. Kertz, "Leitungsfähiger Zylinder im transversalen magnetishen Wechselfeld, *Gerl. Beitr. Geophys.*, vol. 69, pp. 4-28, 1960.

[33] S.H. Ward, "Unique determination of conductivity susceptibility, size and depth in multi-frequency electromagnetic exploration", *Geophysics*, vol. 24, no. 3, pp. 531-546, July 1959.

[34] J.R. Wait, "Electromagnetic coupling between a circular loop and a conducting sphere", *Geophysics*, vol. 18, pp. 970-971, Oct. 1953.

[35] P.R. Vein, "Inductance between two loops in the presence of solid conducting bodies", *J. Electronic Control*, vol. 13, no. 5, pp. 471-494, 1962.

[36] W.R. Smythe, *Static and Dynamic Electricity*. New York: McGraw-Hill Book Co., 1950, 2nd Ed. (Third revised edition now available).

[37] M.L. Burrows, "A theory of eddy-current flaw detection", *Ph.D Thesis, University of Michigan*, 1964 (available from Univeristy Microfilms, Ann Arbor, MI, Order No. 64-12,568).

[38] D.A. Hill and J.R. Wait, "Scattering by a slender void in a homogeneous conducting wire rope", *Applied Physics*, vol. 16, 391-398 (and, by same authors, "Electromagnetic field perturbation by an internal void in a conducting cylinder excited by a wire loop", *Applied Physics*, in press).

[39] C.V. Dodd, W.E. Deeds, and J.W. Luquire, "Integral solutions to some eddy current problems", *Int'l. J. of NDT*, vol. 1, pp. 29-90, 1969/1970.

[40] G.V. Keller and F.C. Frischknecht, *Electrical Methods in Geophysical Prospecting*. NewYork: Pergamon Press, 1966.

[41] C.C. Chang, C.V. Dodd, and W.E. Deeds, "General analysis of probe coils near stratified conductors", *Int'l. J. of NDT*, vol. 3, pp. 109-130, 1971/1972.

[42] J.R. Wait, *Electromagnetic Waves in Stratified Media*. Pergamon Press, Chap. 2, 1st Ed. 1962 and 2nd Ed. 1970.

[43] J.R. Wait, "Fields of a horizontal dipole over a stratified half-space", *IEEE Trans. Antennas Propagat.*, vol. AP-14, no. 6, pp. 790-792, Nov. 1966.

[44] C.V. Dodd, C.C. Cheng, and W.E. Deeds, "Induction coils coaxial with an arbitrary number of cylindrical conductors", *J. Appl. Phys.*, vol. 45, no. 2, pp. 638-647, Feb. 1974.

[45] C.V. Dodd and W.E. Deeds, "Analytical solution to eddy current probe coil problems", *J. Appl. Phys.*, vol. 39, no. 6, pp. 2829-2838, May 1968.

[46] A.H. Kahn, R. Spal, and A. Feldman, "Eddy current losses due to a surface crack in conducting material", *J. Appl. Phys.*, vol. 48, no. 11, pp. 4454-4459, Nov. 1977.

[47] A.H. Kahn and R.D. Spal, "Electromagnetic theory and its relationship to standards", *Proceedings of the Workshop on Eddy Current Non-Destructive Testing*, National Bureau of Standards, Gaithersburg, MD, Nov. 3-4, 1977 (to be issued as an NBS Special Publication).

[48] J.T. Weaver, "The electromagnetic field within a discontinuous conductor with reference to geomagnetic micropulsations near a coast-line", *Can. J. Phys.*, vol. 41, pp. 484-495, 1963.

[49] J.R. Wait and K.P. Spies, "Magneto-telluric fields for a segmented overburden", *J. Geomag. and Geoelectricity*, vol. 26, pp. 449-458, 1974.

[50] J.R. Wait, "The electromagnetic basis for non-destructive testing of cylindrical conductors", *IEEE Trans. Instrumentation & Measurement*, vol. IM-27, No. 3, 235-238, September 1978.

[51] H.L. Libby, *Introduction to Electromagnetic Nondestructive Test Methods*. New York: John Wiley & Sons, 1971, Sec. 5.2, pp. 135-150.

[52] J.R. Wait, *Electromagnetic Radiation from Cylindrical Structures*. Oxford and New York: Pergamon Press, 1959.

[53] D.A. Hill and J.R. Wait, "Analysis of alternating current excitation of a wire rope by a toroidal coil", *J. Appl. Phys.*, vol. 48, no. 12, pp. 4893-4897, 1977.

[54] A.G. Kandoian, *Reference Data for Radio Engineers*. New York: ITT Corp., 1968, pp. 4-32.

[55] J.R. Wait, "Electromagnetic response of an anisotropic conducting cylinder to an external source, *Radio Science*, Vol. 13, No. 5, 789-792, September/October 1978.

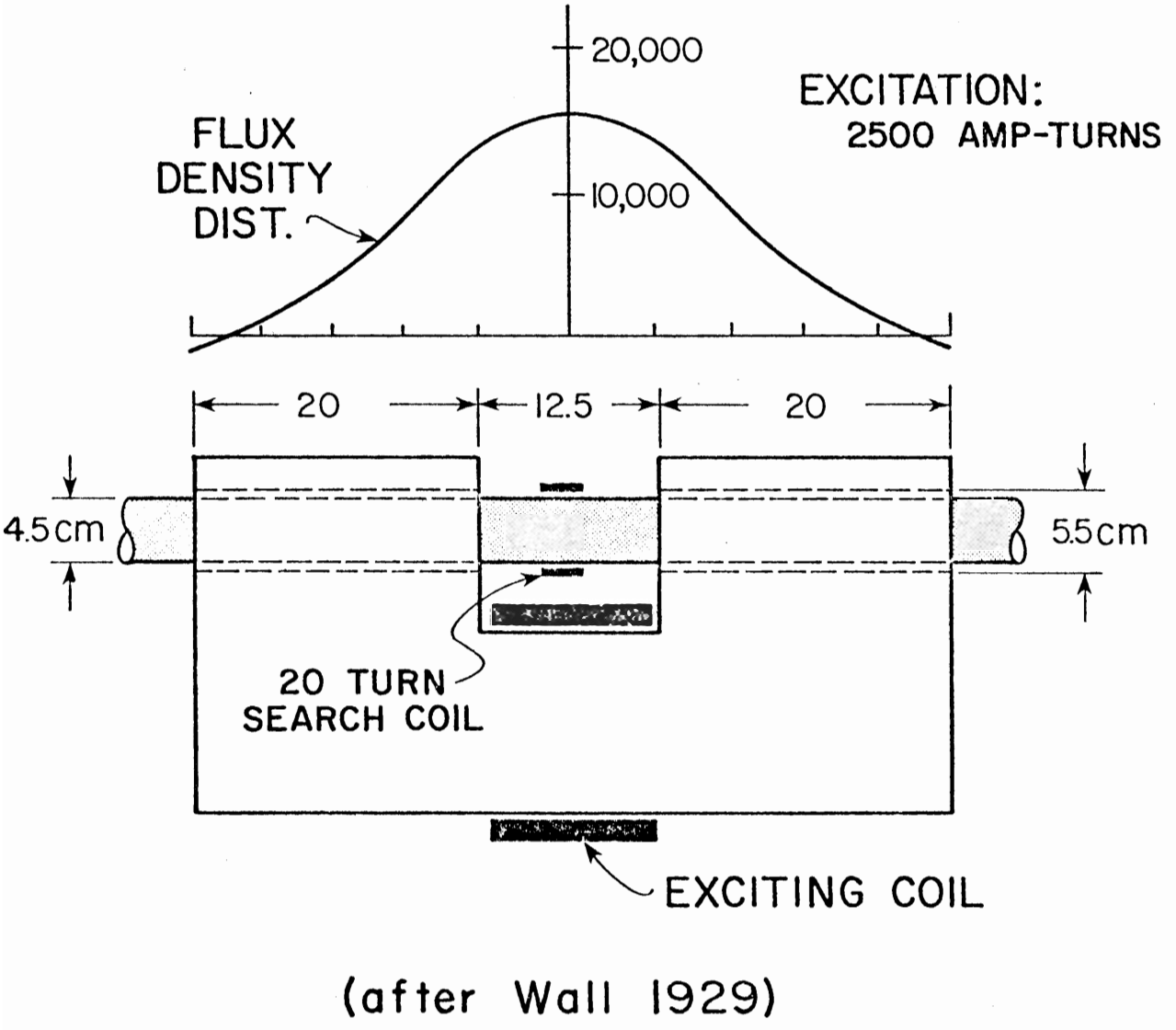

Fig. 1a. Sketch of Wall's device (1929), the B-H curve, and the resulting induced EMF in the search coil.

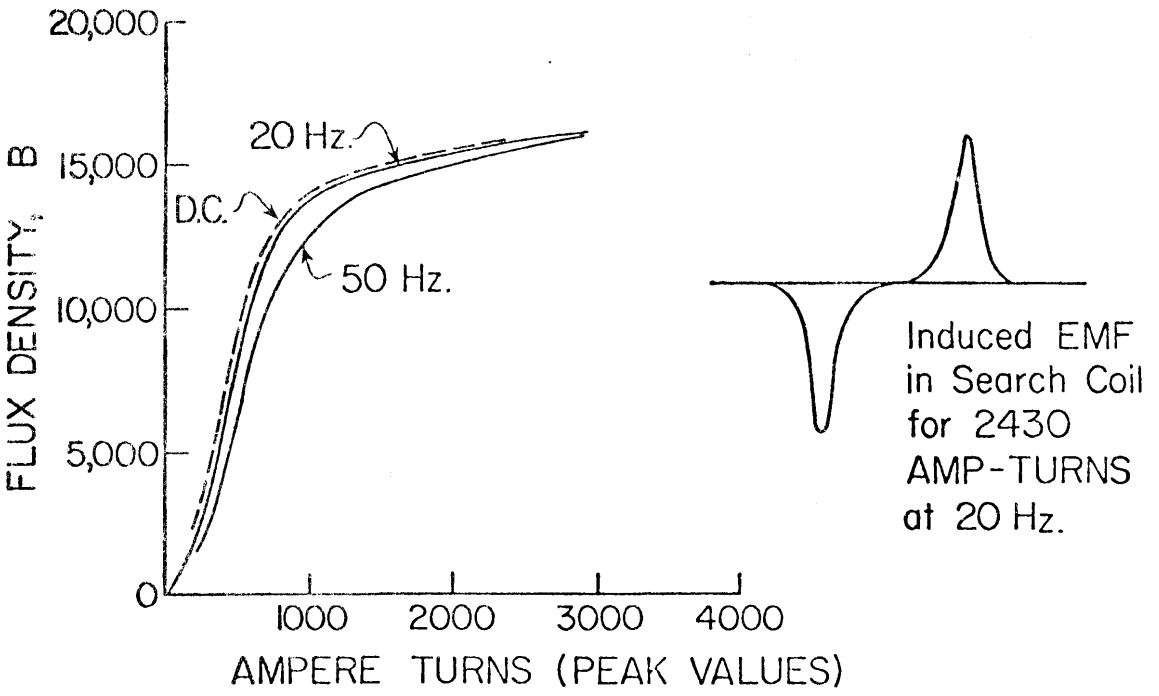

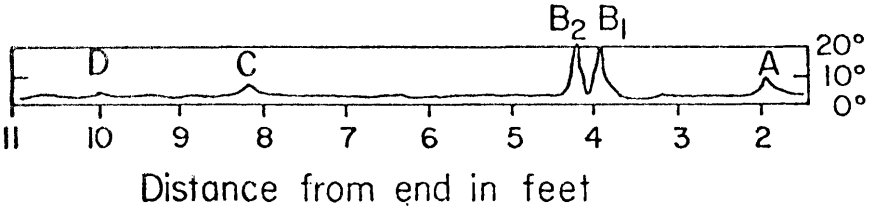

(After Wall 1929)

Fig. 1b. Some data from Wall's test of a locked coil rope. (EMF Waveform Amplitude not given).

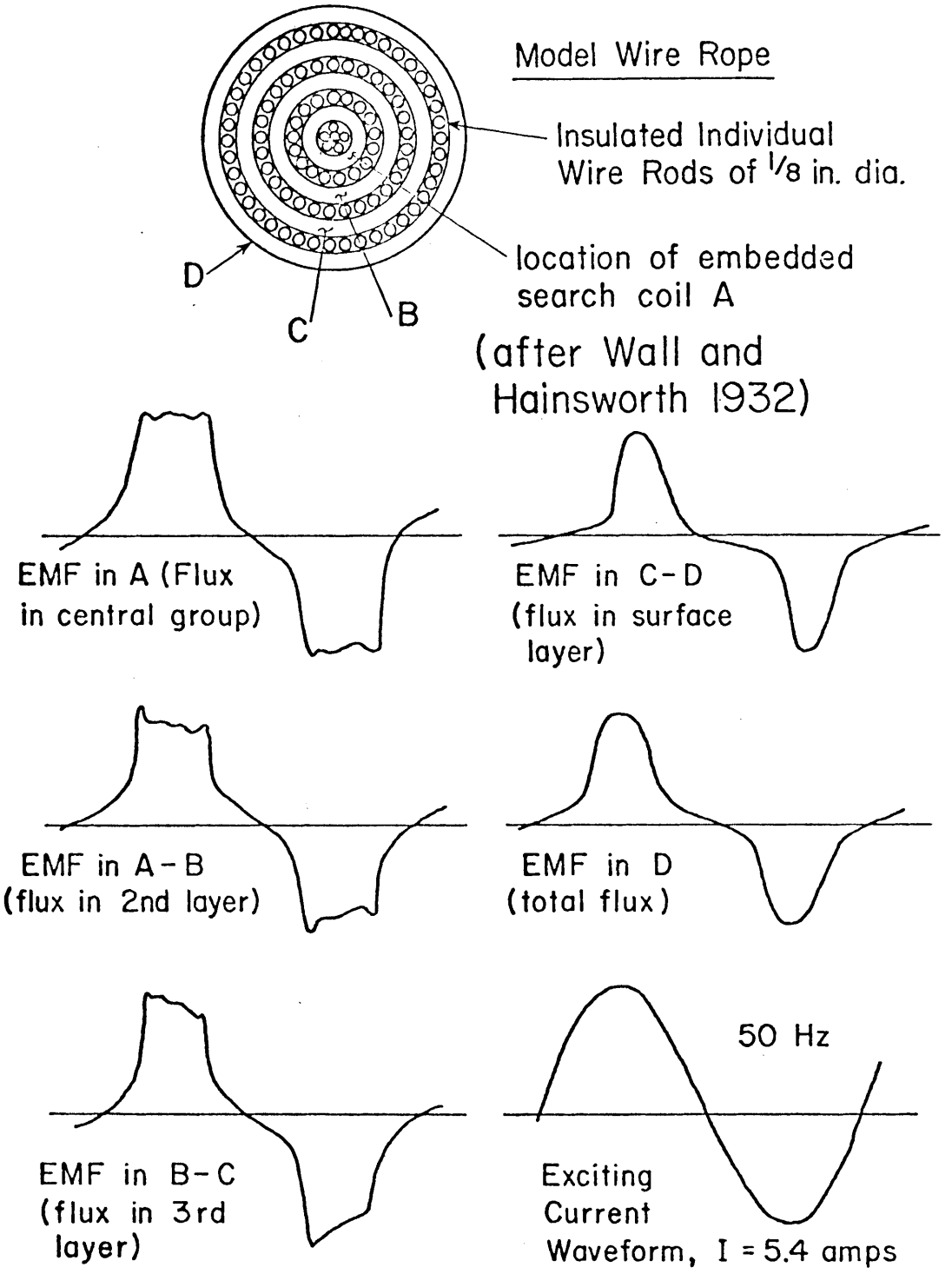

Fig. 2. Special model of a wire rope used by Wall and Hainsworth (1932) to study internal fields.

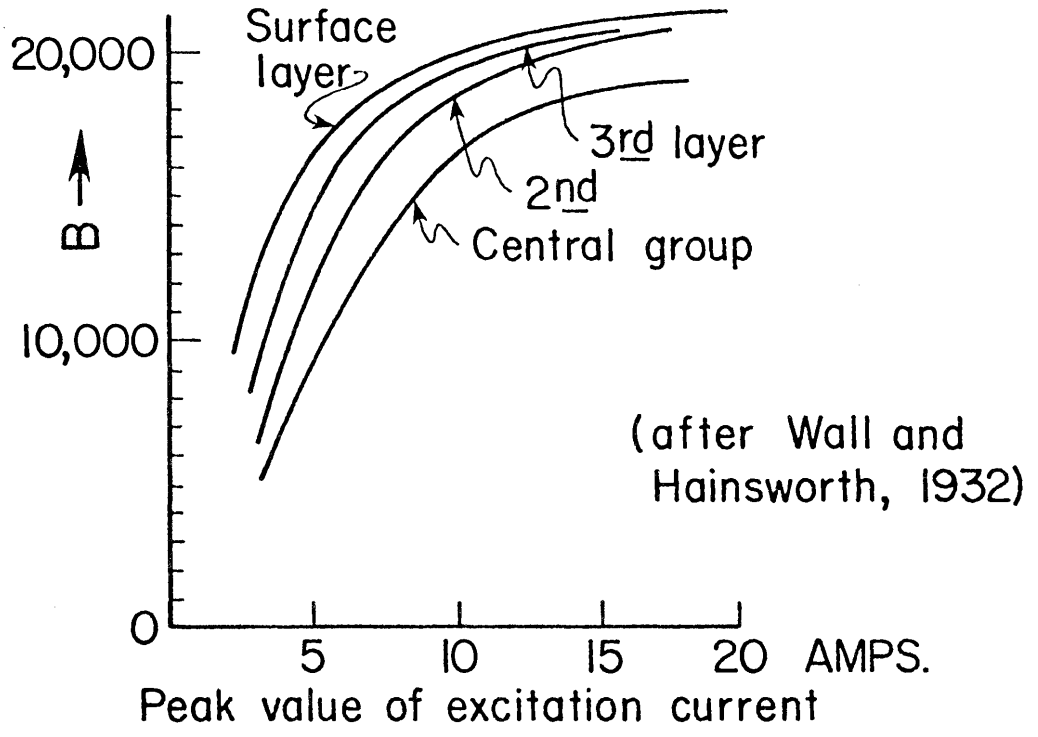

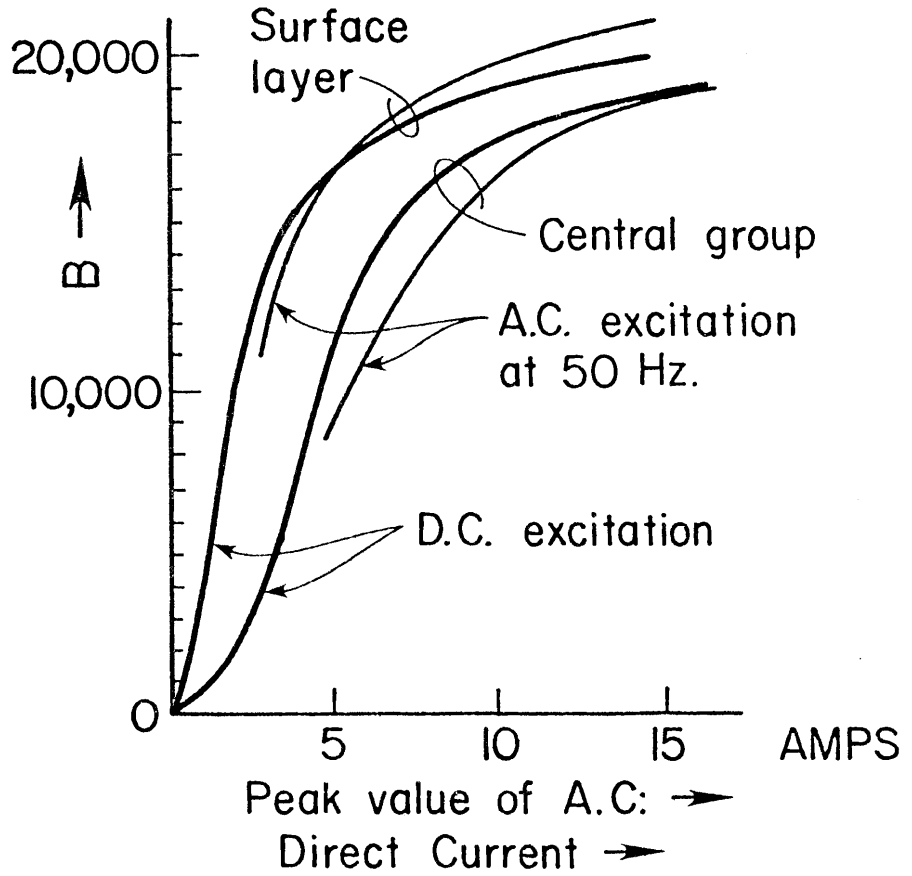

Fig. 3. Some measured data for the special wire rope model.

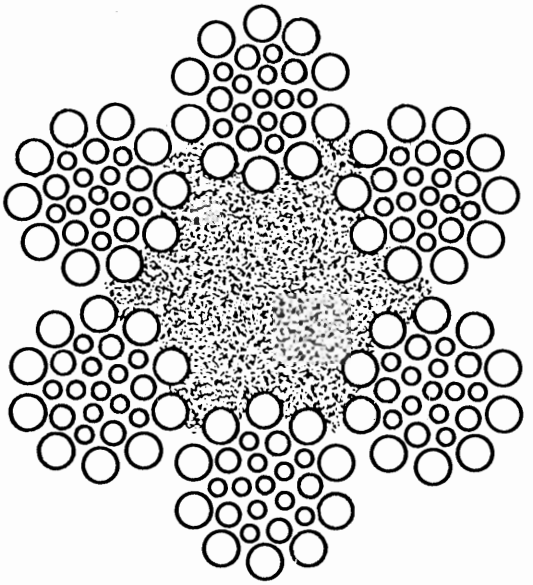

Fig. 4. Stranded wire rope.

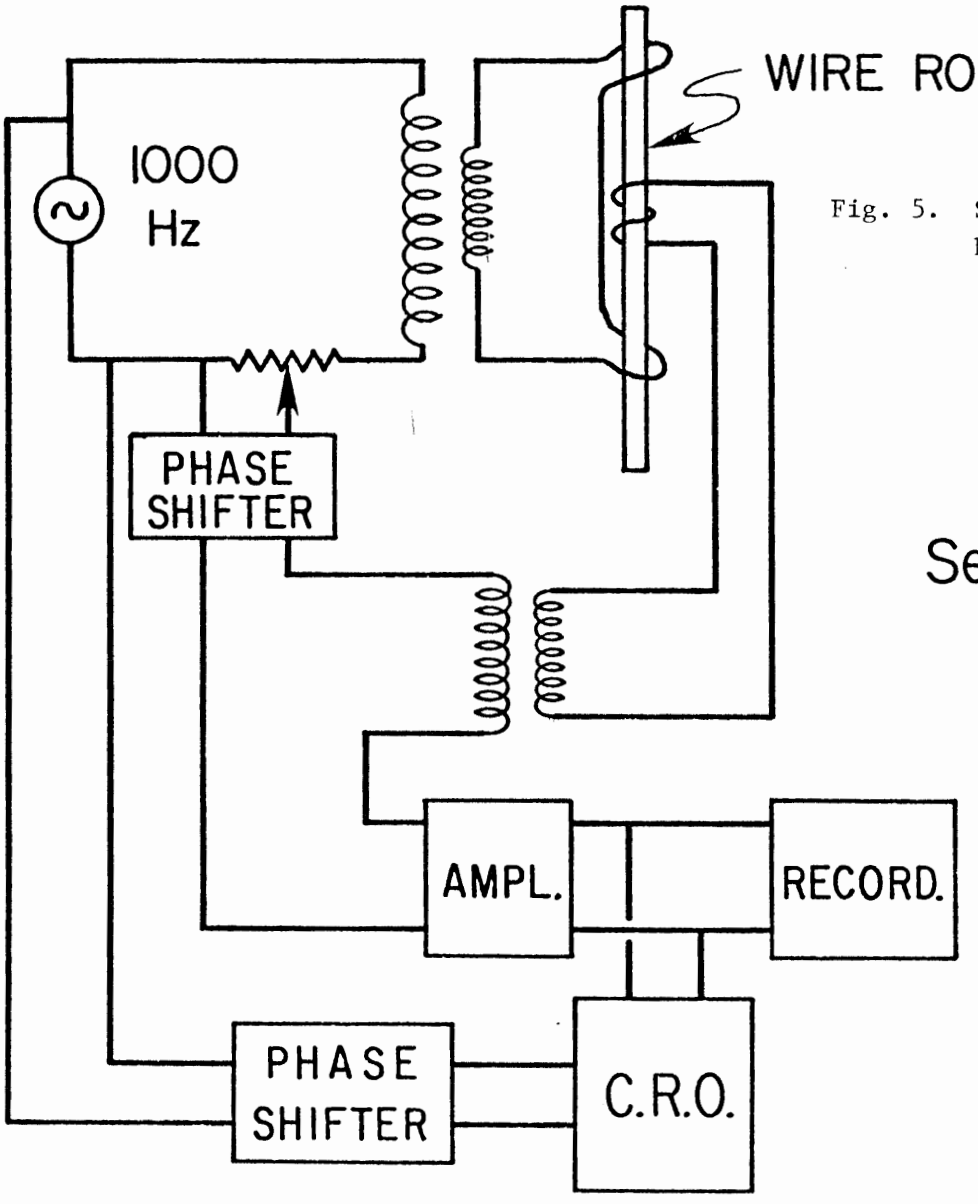

Fig. 5. Semmelink's (1953) prototype A.C. scheme.

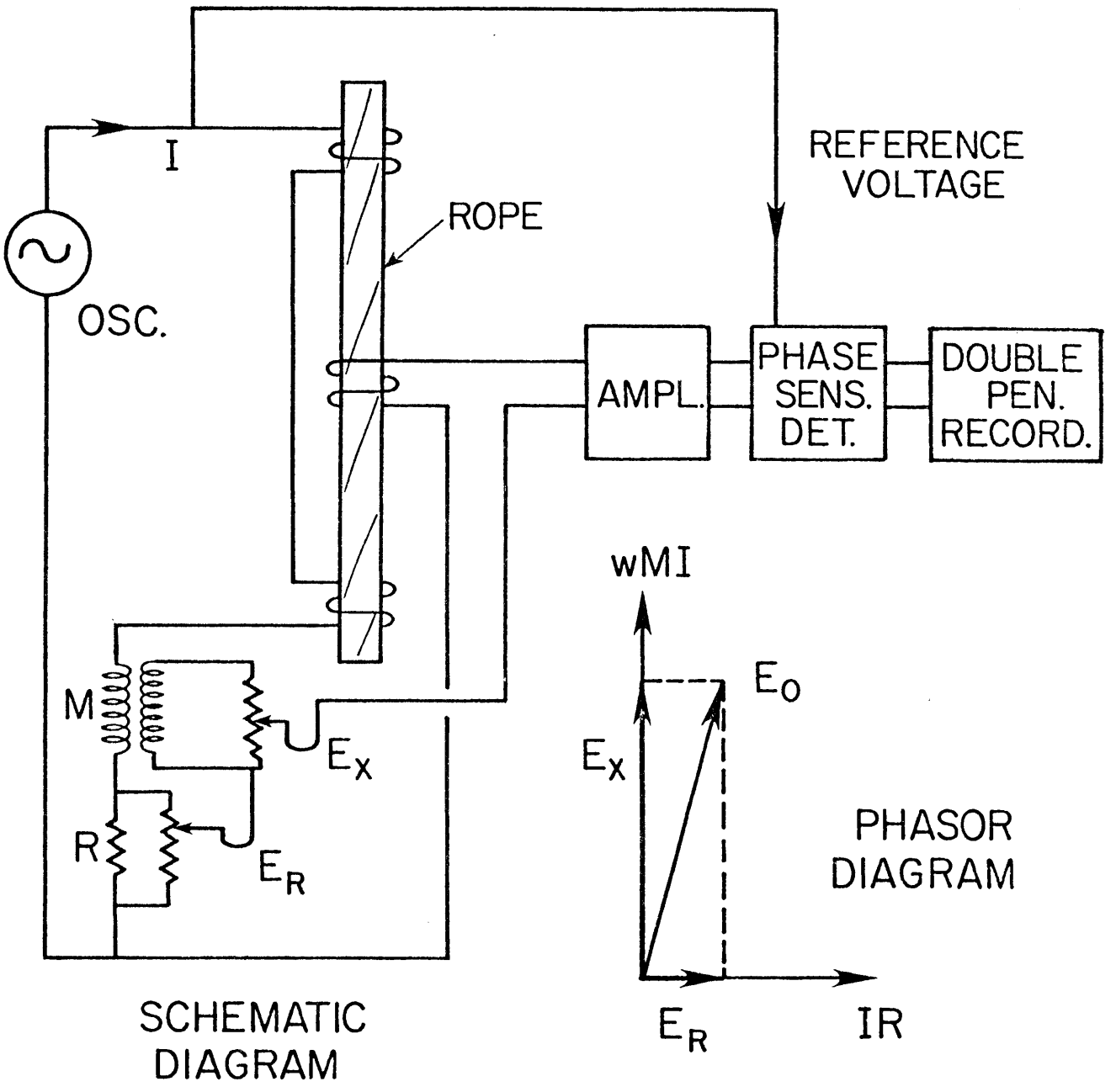

(after Semmelink, 1956)

Fig. 6. Improved model use by Semmelink (1956).

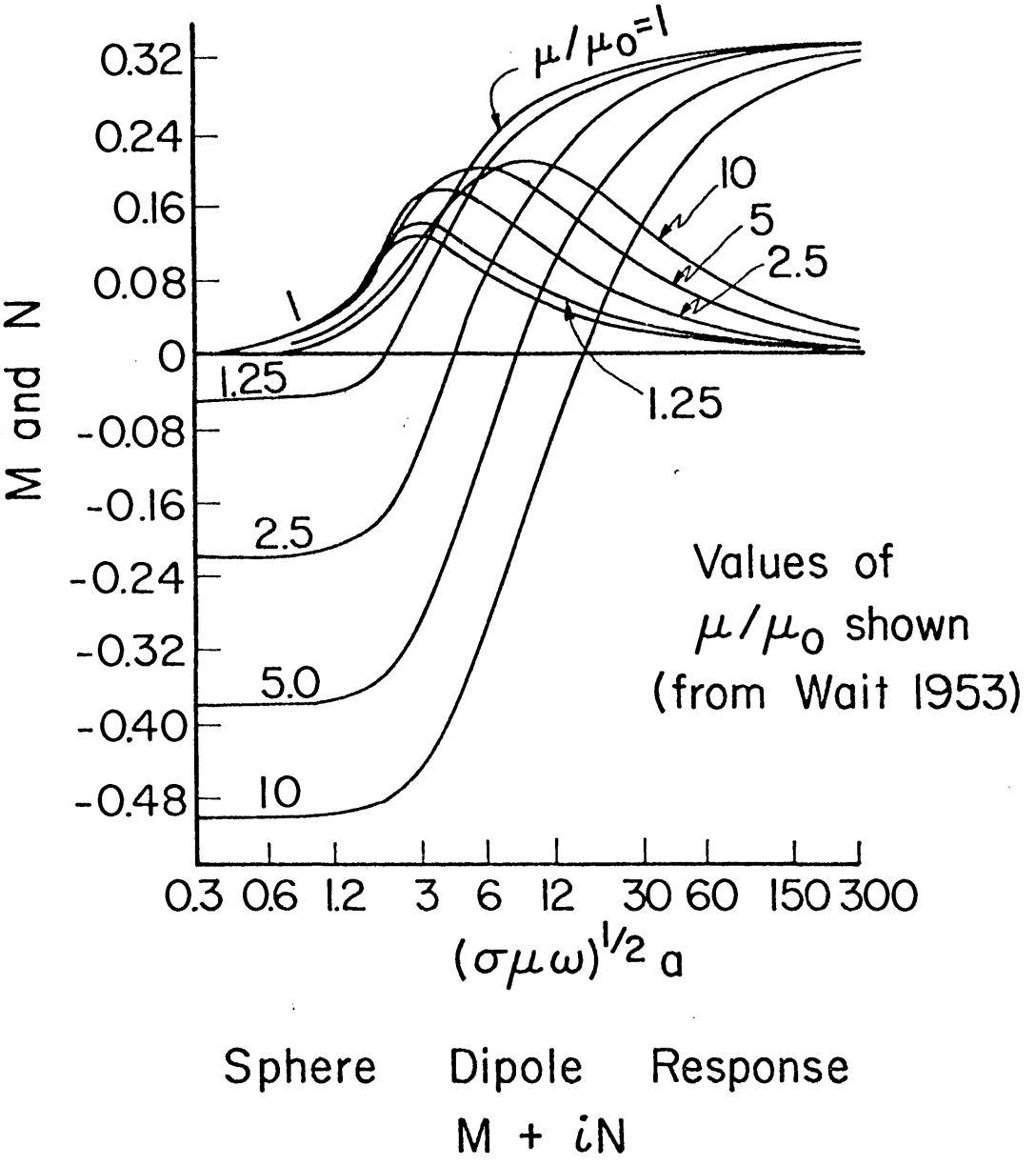

Fig. 7. Induced magnetic dipole for a conducting permeable sphere as a function of its conductivity σ, permeability μ, angular frequency ω, and radius a.

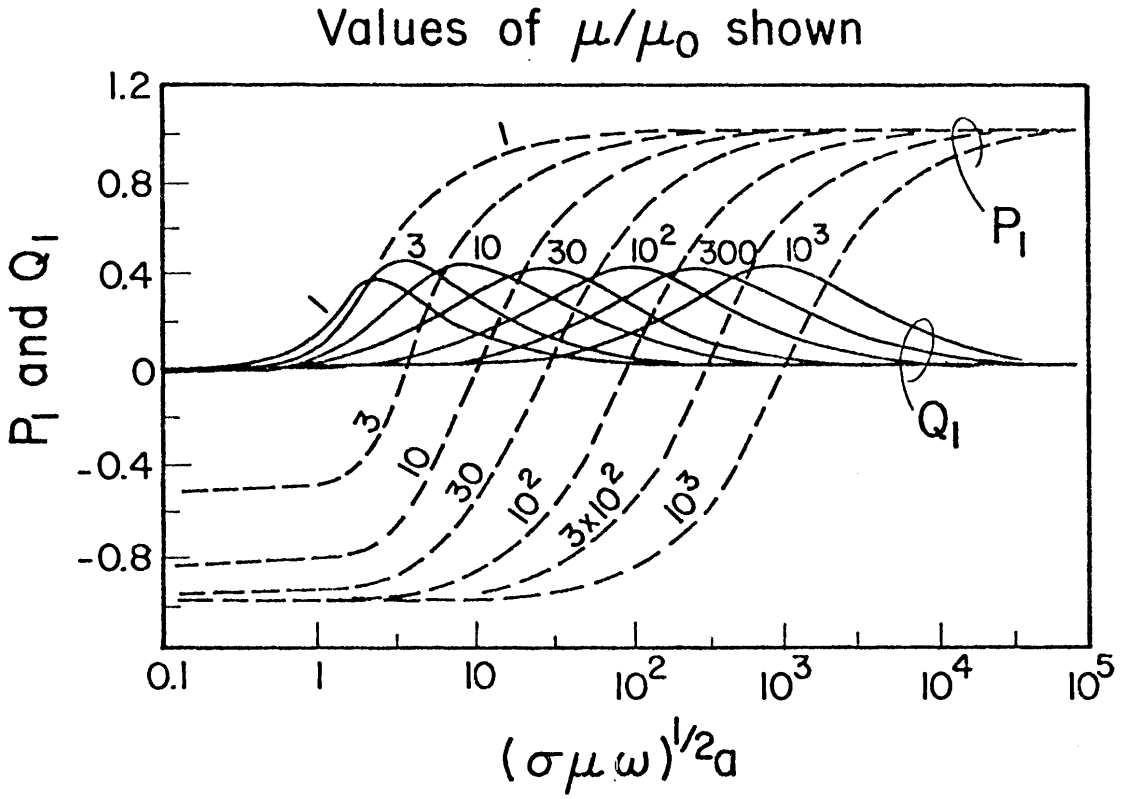

Cylinder Dipole Response

$R_1 = P_1 + \iota Q_1$

(from Wait 1952, 1960)

Fig. 8. Induced (line) magnetic dipole for a conducting permeable cylinder.

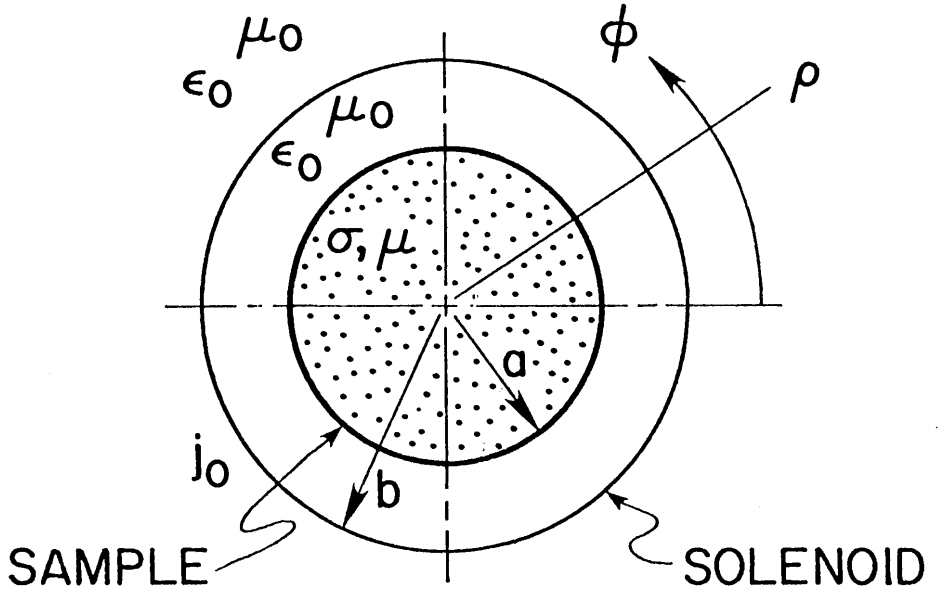

Fig. 9. Cross-sectional view of cylindrical sample located centrally.

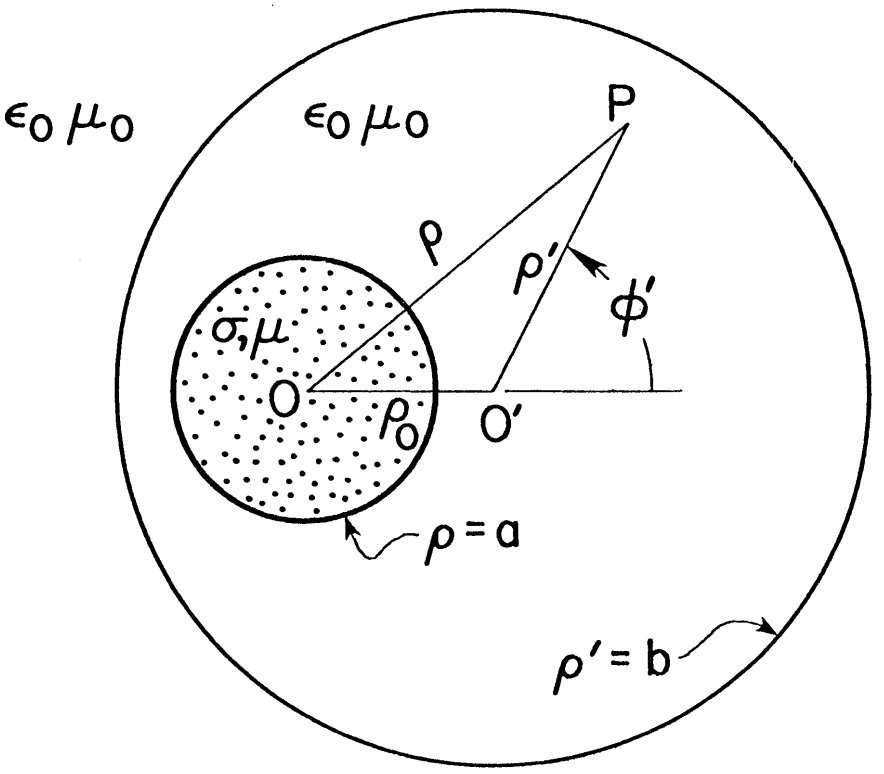

Fig. 12. Cross-section view of the non-concentrically located sample.

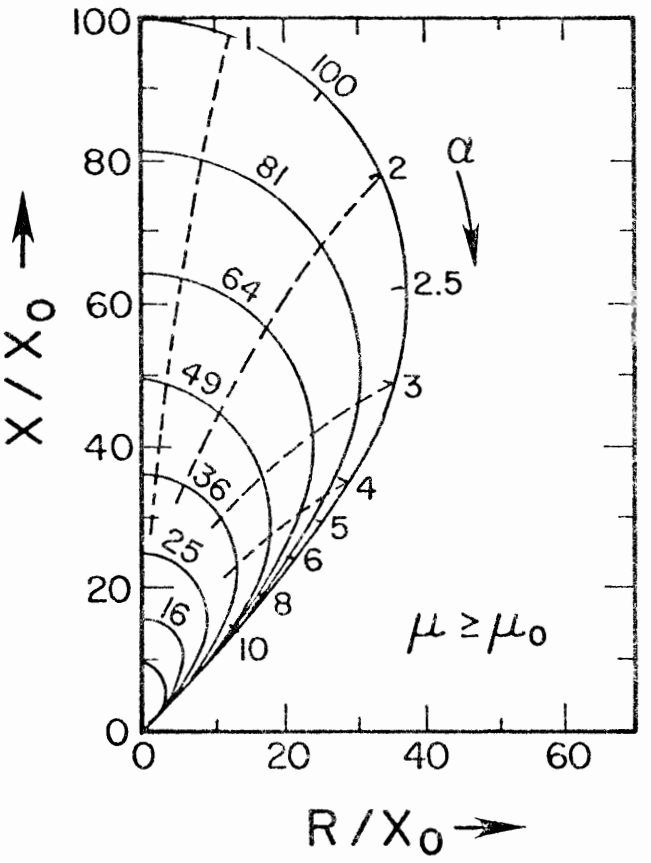

Values of Relative Permeability μ/μ_0 shown

Fig. 10. Argard plot of the impedance $Z = R + iX$ normalized to the reactance X_0 of the empty solenoid, for a = b.

$$\alpha = (\sigma\mu\omega)^{1/2}a$$

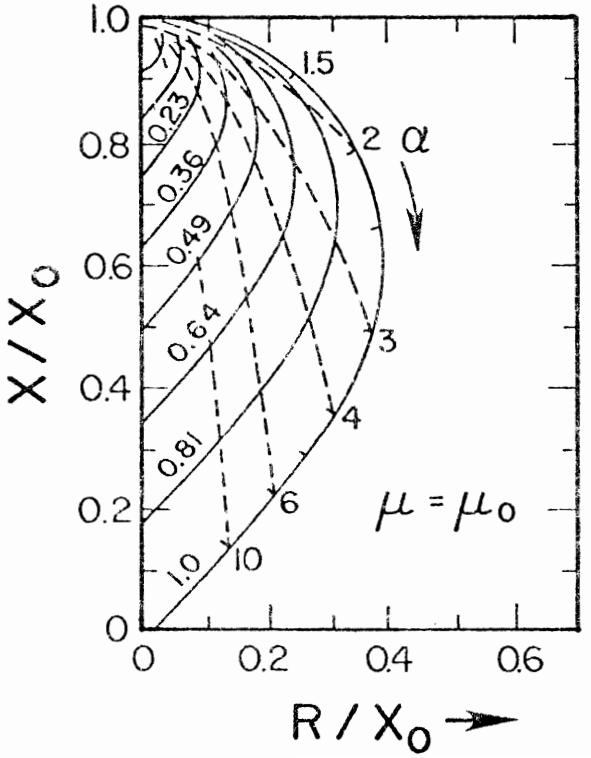

Values of filling factor a^2/b^2 shown

Fig. 11. Argand plot of the impedance $Z = R + iX$ normalized to the reactance X_0 of the empty solenoid, for $\mu = \mu_0$.

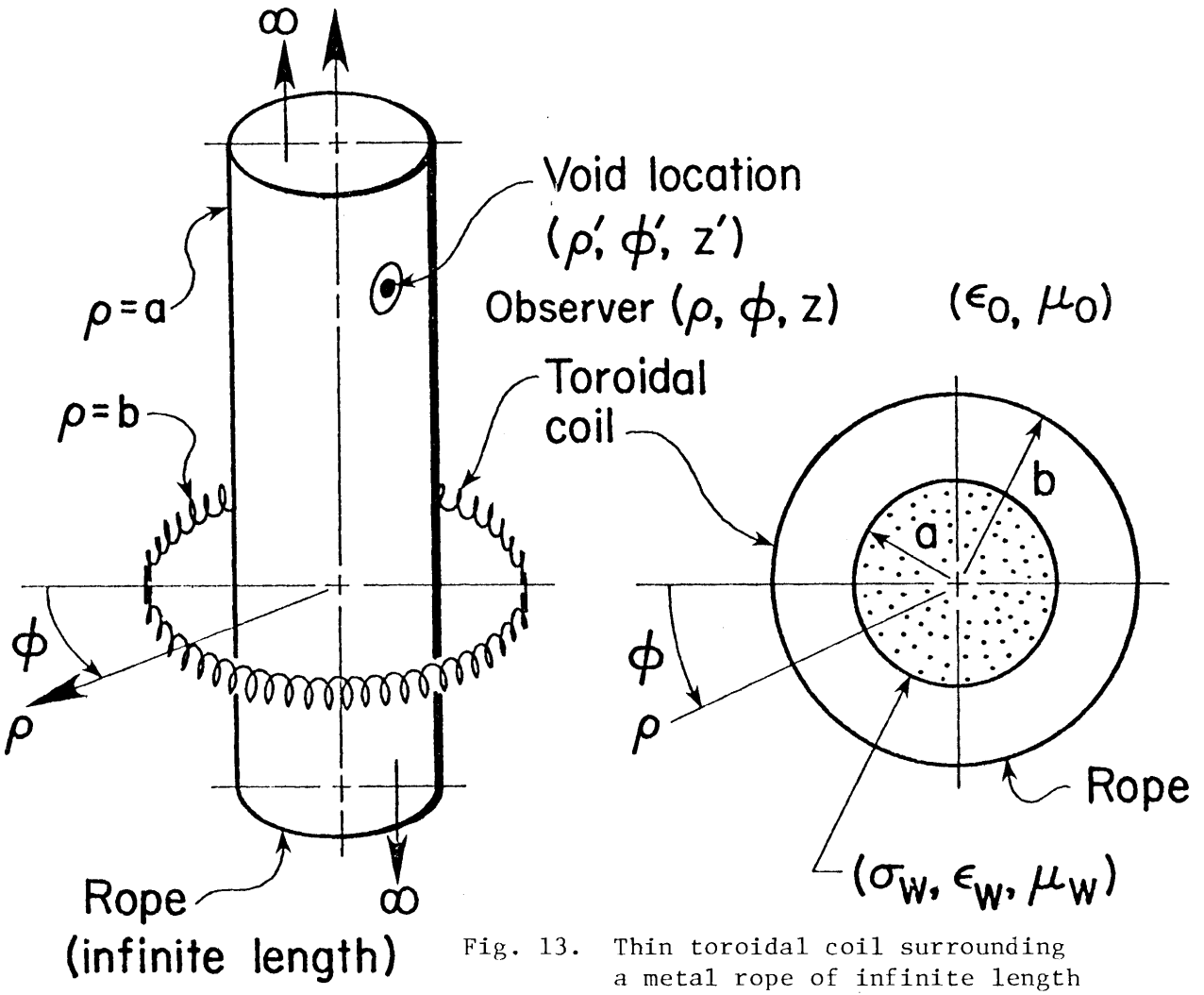

Fig. 13. Thin toroidal coil surrounding a metal rope of infinite length a) Perspective view, b) Top view, c) Prolate spheroidal void.

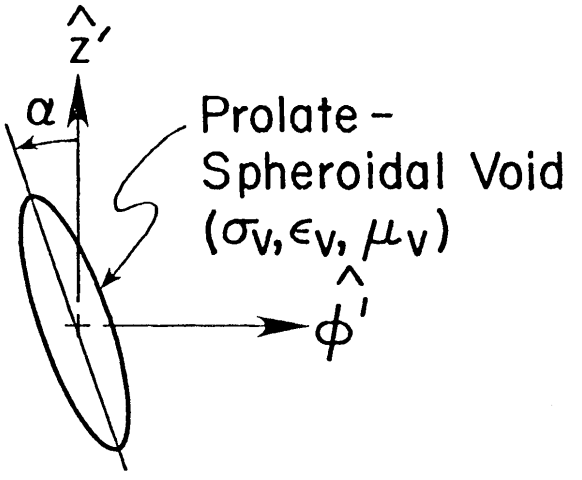

Fig. 14. The normalized magnitude of the scattered radial magnetic field for various void locations ρ'.

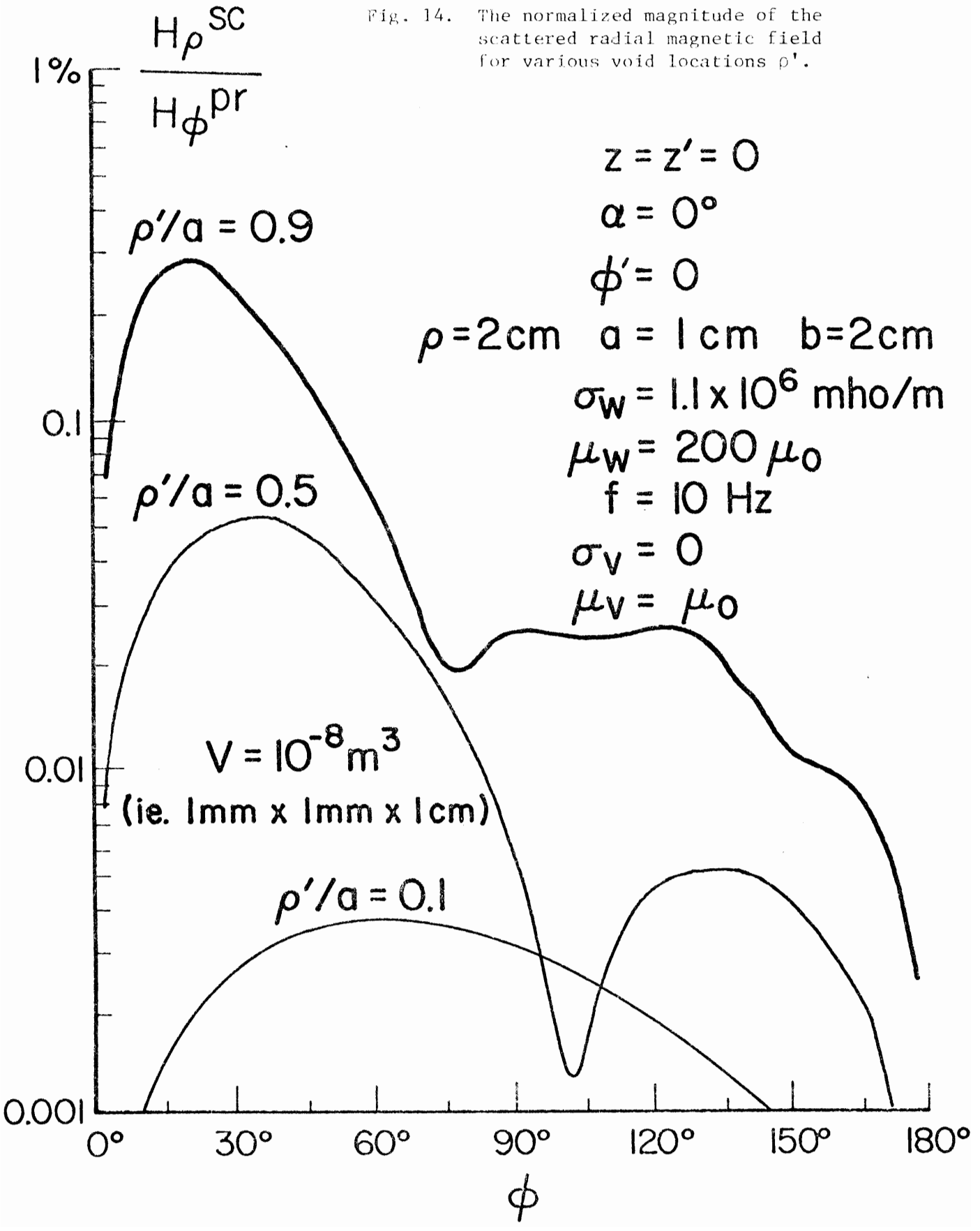

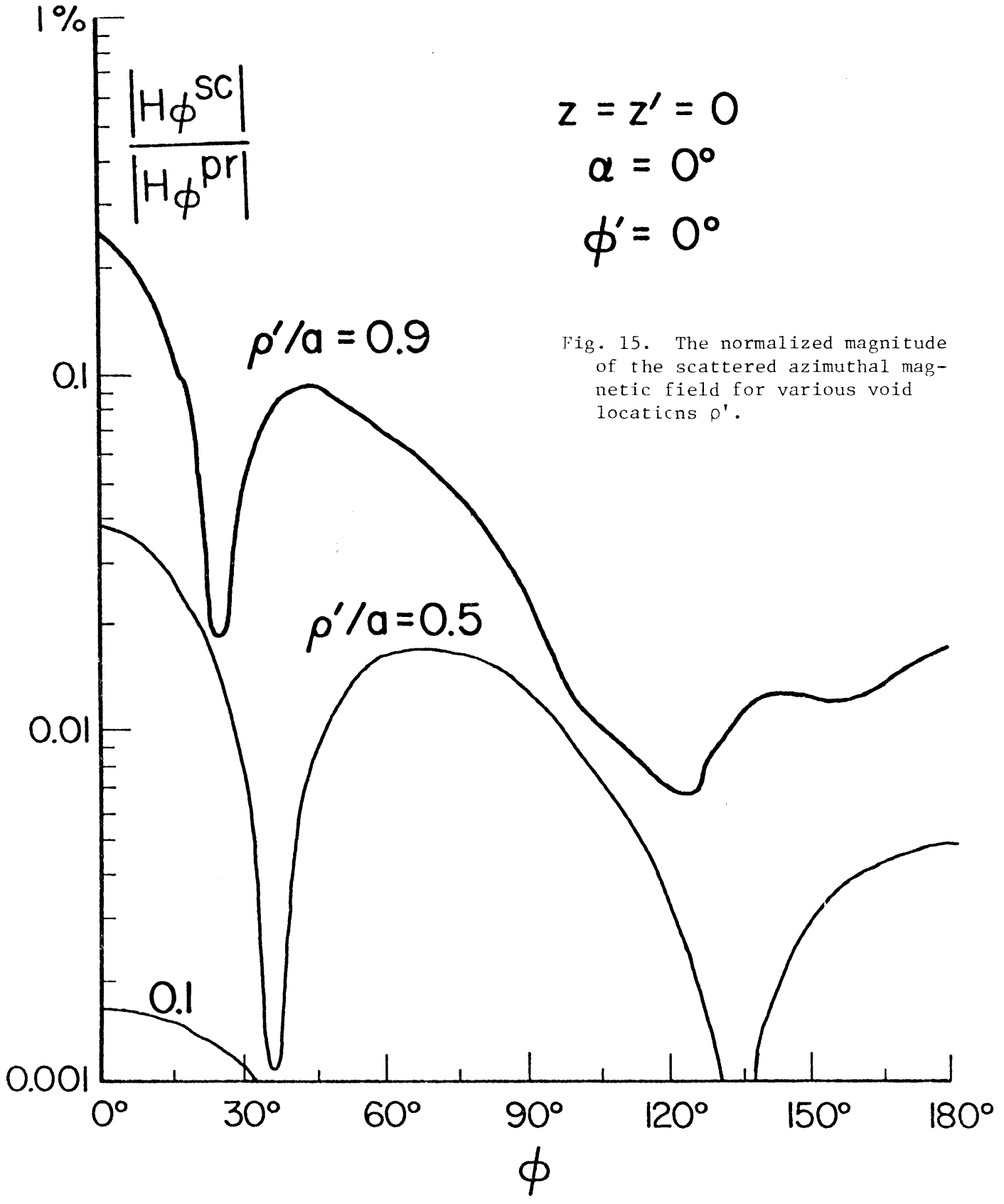

Fig. 15. The normalized magnitude of the scattered azimuthal magnetic field for various void locations ρ'.

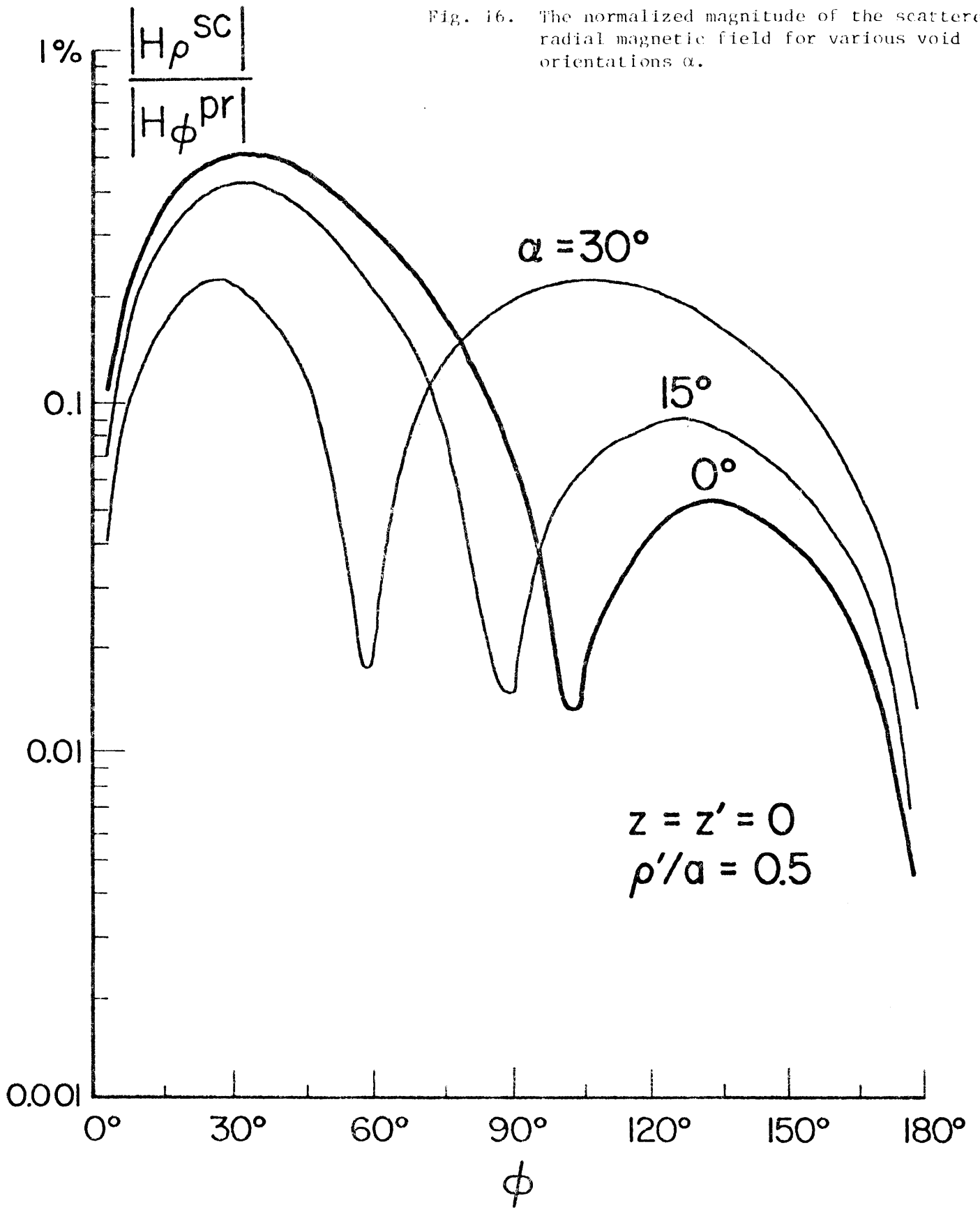

Fig. 16. The normalized magnitude of the scattered radial magnetic field for various void orientations α.

ADDITIONAL BIBLIOGRAPHY

FOR SECTION 2

Richard Hochschild, *Applications of Microwaves in Nondestructive Testing*, Non-Destructive Testing, Vol. 21, pp. 115-120, March/April, 1963.

C.T. Tai, *A Study of Electrodynamics of Moving Media*, Proceedings of the IEEE, Vol. 52, No. 6, pp. 685-691, June, 1964.

(This study contains a digest of Minkowski's theory of electrodynamics of moving media in the three-dimensional form and a critical review of some current writings on this subject from the point of view of Minkowski's theory. The invariant nature of the Maxwell-Minkowski equations is explained in terms of a conventional language. The important role played by the constitutive relations in formulating a complete theory of electrodynamics of moving media is pointed out.)

C.T. Tai, *Electrodynamics of Moving Anisotropic Media: The First-Order Theory*, Radio Science Journal of Research NBS/USNC-URSI, Vol. 69D, No.3, pp. 401-405, March 1965.

(Minkowski's theory of moving media is extended hereby to the anistropic case. The corresponding Maxwell-Minkowski equations have been derived under the condition that the velocity of the moving medium is small compared to the velocity of light. As an application of that theory, it is shown that the characteristics of a plane wave propagating in a drifting magneto-ionic plasma can conveniently be determined from the constitutive parameters of the plasma without drifting. The equivalence between the convection current model adopted by Bell and Helliwell and the polarization current model suggested by Unz and correctly interpreted by Epstein, Bell, Smith, and Brice is also pointed out.)

Theresa M. Lavelle, *Microwaves in Nondestructive Testing*, Materials Evaluation, Vol. 25, No. 11, pp. 254-258, Nov., 1967.

(The use of microwave radiation in nondestructive testing of nonmetals is investigated. Techniques involving reflection, transmission and scattering are discussed and applied to general nondestructive tests. The paper also discusses the results of a laboratory test program in which the following measurements are considered:

1. Dimensional Measurements - Determination of range and accuracy for thickness variations.
2. Flaw Detection - Determination of types of flaws and specimen configuration.
3. Material Property - Determination of types of physical and chemical properties that can be detected and possible degree of resolution.

The general test procedure is to irradiate the sample with microwave energy and to monitor the transmitted or reflected energy for phase or amplitude change. The tests are conducted at X-band

(9.6 gigahertz) or Ka band (35 gigahertz). Reflection tests can detect thickness of nonmetals to a resolution of 0.1 mm. Lack of bond can be detected using a "magic tee" reflection arrangement. Degree of cure can be monitored using a microwave transmission technique. Scattering is useful in detecting the presence of a flaw within epoxy samples.)

V.V. Klyuev, *A Problem in the Analysis of the Characteristics of Superposed Eddy-Current Displacement Converters*, Defektoskopiya, Vol. 4, pp. 42-49, January/February 1968.

(Expressions are derived for the components of the electromagnetic field of a turn during motion of a current conducting plate in the direction of the axis of the turn, and certain problems in the determination of the inertia of converters are analyzed.)

G.A. Barill and V.S. Sobolev, *Analysis of the Reaction of a Conducting Ferromagnetic Polarizing Sphere Placed in the Field of an Insertion-Type Induction Transducer*, Defektoskopiya, Vol. 5, pp. 417-422, July/August 1969.

(This article analyzes the solution of the problem of a sphere placed in a uniform magnetic field of an insertion-type induction transformer transducer, and it determines the value of the signal obtained as a function of the parameters of the sphere material, i.e., the dielectric constant, the permeability, the conductivity, and the loss angle. Special attention is devoted to an evaluation of the effect of the sphere's dielectric constant on signal magnitude.)

V.V. Klyuev, G.G. Kapelin, *Experimental and Theoretical Research in Feed-Through Transducers for Monitoring Moving Objects*, Defektoskopiya, Vol. 6, pp. 701-, 1969.

V.V. Klyuev, M.L. Faingolz, and G.G. Kapelin, *Movement of a Current-Conducting Plate Parallel to the Plane of a Striding-Type Transducer*, Defektoskopiya, Vol. 6, pp. 425-432, July/August 1970.

(The emf of a square striding-type transducer located over a parallel moving plate is determined. The voltage hodographs obtained analytically are confirmed experimentally. Recommendations are given for tuning out the effect of the travel speed of the object being inspected.)

Yu. K. Fedosenko, *Calculation of Insertion EMF During Testing of Bimetallic Cylinders with a Thin Surface Layer*, Defektoskopiya, Vol. 6, pp. 433-437, July/August 1970.

(A general expression is analyzed for the insertion emf of a penetrating pickup with a bimetallic ferromagnetic cylinder whose surface layer has a thickness equal to 0.01-0.06 of the outer radius. Simplified equations are found for designing pickups. Cases are considered in which there are various relations

V.V. Vlasov and V.A. Komarov, *Electromagnetic Phenomena Which Occur When a Transverse Uniform Alternating Magnetic Field Acts on a Conducting Cylinder*, Defektoskopiya, Vol. 7, No. 2, pp. 128-133, 1971.

(The results of analytical and experimental investigations of the electromagnetic phenomena which arise when an external transverse uniform alternating magnetic field acts on an electrically conducting (magnetic and nonmagnetic) cylinder are presented. The results of these investigations as they apply to the nondestructive monitoring of cylindrical steel articles using eddy currents are analyzed.)

Yu. N. Russkevich, *Establishment of the Electromagnetic Field of a Turn Over a Conducting Nonferromagnetic Layer*, Defektoskopiya, Vol. 7, No. 3, pp. 264-269, 1971.

(The solution to the problem of determining the vector potential of the nonstationary field of eddy currents induced in a conducting layer of arbitrary thickness by a jump in the external annular current is presented. The solution is obtained for the zone situated over the surface of separation of the media; it constitutes the basis of a model for the attenuation of a field of eddy currents, giving a clear representation of the character of this process.)

Yu. M. Shkarlet and N.N. Lokshina, *Eddy Current Density During Pulse Excitation of an Applied Transducer*, Defektoskopiya, Vol 7, No. 3, pp. 281-285, 1971.

(This article considers the problem of determining the nonstationary density of eddy currents in a conductive magnetic half-space exciting an applied transducer powered by current in the form of a single step. The resultant formula is used to compute the relative density of eddy currents during a continuous change of the time of the transient process for certain fixed distances from the surface into the depth of a metallic medium. The distribution of current density is computed with respect to the depth of a metallic half-space for various instants of time.)

M.M. Shel, *Harmonic Structure of the Secondary EMF of a Deposited Sensor*, Defektoskopiya, Vol. 7, No. 4, pp. 378-382, 1971.

(An approximate expression is obtained which can be used to calculate the higher harmonics of the secondary emf of a deposited sensor in checking ferromagnetic parts. The relationship between the harmonic structure and the shape of the hysteresis loop of the specimen being investigated is determined. Experimental results are cited which confirm the correctness of the basic theoretical premises.)

V.V. Vlasov and V.A. Komarov, *The Magnetic Field of Eddy Currents Above A Surface Crack in Metal With Excitation of Them by an Applied Inductor*, Defektoskopiya, Vol 7, No. 6, pp. 665-675, 1971.

(A method is proposed for a qualitative estimate of the magnetic field of eddy currents occurring along the walls of cracks spread on the surface in metal with a comparatively highly developed skin effect.)

A.L. Zelenkov and V.N. Rudakov, *Detection of Local Defects in Dielectrics With a Radiodefectoscope Working in the "Reflection" Mode*, Defektoskopiya, No. 5, pp. 5-10, September/October, 1971.

(A calculation of the diffraction fields formed in the scattering of electromagnetic waves by a local defect in a dielectric sheet when the radiodefectoscope with mechanical scanning employed for detecting the defect is operating in the "reflection" mode is presented. The calculation allows for the directional characteristics of the probes. The experimental data obtained agree closely with calculations.)

D.L. Waidelich, *Response of Pulsed Dipoles in Conductors*, International Symposium on Antennas & Propagation, pp. 5-6, Sept. 1971.

V.V. Klyuev and M.L. Faingoiz, *Nondestructive Testing of Moving Articles by Means of Superimposed and Superimposed Screen Converters Using the Constant Magnetic Field Method*, Defektoskopiya, Vol 8, No. 1, pp. 100-106, 1972.

(The distortion of the field H_z is determined for superimposed and superimposed screen converters of rectangular form and excited with a direct current during the motion of the test object. Analysis is carried out on the basis of accurate computations of imporper integrals defining the cases considered.)

V.A. Sandovskii, *Field of the Vector-Potential in a Conductive Semispace During Its Movement Relative to a Wall Having a Current*, Defektoskopiya, Vol. 8, No. 1, pp. 75-80, January/February 1972.

(The problem of the steady-state field of the vector-potential in a conductive semispace is solved for its movement relative to a wall having a current. The rigorous solution with generally accepted assumptions for problems of such a class is presented in quadratures. This solution is analyzed for the case of a moving semispace of magnetic and nonmagnetic materials and is extended to any source of a constant magnetic field.)

V.V. Vlasov and B.I. Volkov, *Applied Eddy-Current System Having a Hall Element as the Searcher and Reacting to the Tangential Component of the Defect Field*, Defektoskopiya, Vol. 8, No. 1, pp. 84-89, January/February, 1972.

V.V. Klyuev and M.L. Faingoiz, *Nondestructive Testing of Moving Current-Conducting Articles by Means of Pass-Through Converters Using the Constant-Field Method*, Defektoskopiya, Vol. 8, No. 2, pp. 27-31, March/April, 1972.

(A determination is made of the induced vector potential of outer and inner cylindrical pass-through converters excited by a constant current in the monitoring of moving current-conducting

articles. An analysis is made on the basis of accurate computations of improper integrals.)

V.A. Sandovskii, *Calculating the Tangential Component of the Magnetic Field Intensity Due to Eddy Currents Generated by an Inductive Transducer,* Defektoskopiya, Vol. 8, No. 3, pp. 90-93, May-June 1972.

V.V. Vlasov and V.A. Komarov, *Interaction of the Magnetic Field of a Long Single-Turn Loop with a Conducting Ferromagnetic Cylinder,* Defektoskopiya, Vol. 8, No. 4, pp. 64-73, July/August 1972.

G.A. Burtsev, *Straight-Through Eddy-Current Converters for Monitoring Ferromagnetic Articles of Finite Length,* Defektoskopiya, Vol. 9, No. 4, pp. 110-117, July/August, 1973.

N.L. Bondarenko, Yu. M. Shkarlet, and A.F. Chub, *Reflection and Screening of the Nonstationary Field of a Turn by a Conductive Medium,* Defektoskopiya, Vol. 9, No. 4, pp. 118-124, July/August, 1975.

A.A. Kabasheva and V.K. Popov, *Calculation of Multilayer Transformer Eddy Current Sensors,* Defektoskopiya, Vol. 9, No. 5, pp. 17-23, September/October, 1973.

Yu. M. Shkarlet, *Theoretical Principles of Electromagnetic and Electroacoustic Nondestructive Test Methods,* Defektoskopiya, Vol 10, No. 1, pp. 11-17, January/February, 1974.

V.V. Klyuev and M.L. Faingoiz, *Inspecting Moving Parts with Applied and Applied-Screen Eddy-Current Transducers,* Defektoskopiya, Vol. 10, No. 1, pp. 18-24, January/February, 1974.

V.V. Klyuev and M.L. Faingoiz, *Inspection of Moving, Ferromagnetic Components with Through Eddy Current Converters,* Defektoskopiya, Vol. 10, No. 2, pp. 106-110, March/April, 1974.

G.A. Burtsev and É.É. Fedorishcheva, *Simple Approximation for the Magnetostatic Fields of Surface Defects and Inhomogeneities,* Defektoskopiya, Vol. 10, No. 2, pp. 111-118, March/April, 1974.

V.V. Klyuev and M.L. Faingoiz, *Inspection of a Moving Metal Strip with an Off-Axial Shielded Contact Transducer,* Defektoskopiya, Vol. 10, No. 3, pp. 24-29, May/June, 1974.

V.F. Avduevskii, *Calculating the Response of Eddy-Current Transducers,* Defektoskopiya, Vol. 11, No. 5, pp. 27-30, September/October, 1975.

V.P. Zuev and V.N. Novikov, *Electrostatic Defectoscopy of Cylindrical Specimens with Axial Ducts,* Defektoskopiya, Vol. 11, No. 5, pp. 31-36, September/October, 1975.

V.P. Kurozaev, Yu. I. Steblev, and V.E. Shaternikov, *Influence of Part Geometry on the Results of Their Inspection by Eddy-Current Transducers,*

Defektoskopiya, Vol. 12, No. 1, pp. 115-123, January/February, 1976.

(Consideration is given to the effect of part geometry ["boundary effect"] on the effectiveness of electromagnetic inspection of thickness, specific electrical conductivity, and gaps. Recommendations are given for suppressing the boundary effect in measuring these values. An analysis is made on the basis of a solution of the electrodynamic boundary problem for an applied eddy-current transducer located above an electrically conducting ellipse of rotation.)

N.P. Rtishcheva and V.V. Sukhorukov, *Simulating the Operating Conditions of a Through-Type Eddy-Current Transducer When Inspecting Ferromagnetic Rods*, Defektoskopiya, Vol. 12, No. 1, pp. 109-114, January/February, 1976.

(By means of a nonlinear network model of the RC-type voltage-variable capacitors (varicaps) together with experiments a study was made of the conditions during eddy-current flaw detection in ferromagnetic rods which are subjected simultaneously to alternating and constant magnetic fields from a through-type transducer. The effect on the signal-to-noise ratio of a constant magnetic biasing field is shown and recommendations are made for choosing the optimal conditions when inspecting structural steels.)

B.N. Domashevskii and A.I. Geiser, *Polarization of Cracks When Magnetized in a Longitudinal Alternating Field*, Defektoskopiya, Vol. 12, No. 2, pp. 89-94, March/April, 1976.

(The field due to a crack in metal can be likened to a ribbon dipole with a density of surface magnetic charges which falls off exponentially with depth into the sample. The theoretical calculations are compared with experimental data.)

V.A. Sandovskii, *Calculating the Resistance Introduced by Cracks in an Applied Transducer*, Defektoskopiya, Vol 12, No. 2, pp. 95-101, March/April 1976.

(The impedance injected into an applied transducer by a crack is found by approximation in the form of the product of three functions depending on a generalized eddy-current parameter. A holograph is plotted for small and large openings of cracks.)

B.I. Kolodii and A. Ya. Teterko, *Determination of the Transverse Magnetostatic Field of a Cylinder with an Eccentric Cylindrical Inclusion*, Defektoskopiya, Vol. 12, No. 3, pp. 44-50, May/June 1976.

(Using the method of the vector potential in bipolar coordinates, the magnetostatic field of an infinite cylinder with an eccentric cylindrical inclusion situated in a transverse field is determined. Special attention is paid to the field of a semi-infinite solid with a cylindrical inclusion parallell to the surface. For the case of an eccentric cavity

a quantitative analysis is made of the field in relation to the size and depth of the cavity and the magnetic permeability of the parent material.)

V.V. Panasyuk, B.I. Kolodii, and A.A. Orlovskii, *Electromagnetic Control of Electrically Conducting Spherical Specimens*, Defektoskopiya, Vol. 12, No. 5, pp. 129-130, September/October, 1976.

A.S. Popov and L.I. Trakhtenberg, *Effect of the Section Shape of a Nonmagnetic Electrically Conducting Rod on the Parameters of an Eddy-Current Transducer with a Uniform Field*, Defektoskopiya, Vol. 12, No. 5, pp. 94-101, September/October 1976.

(Expressions for both the resistive and the reactive voltage induced in the measuring coil of an eddy-current transducer by a nonmagnetic conducting long rectangular prismatic rod in a uniform longitudinal field are derived here from the well-known solution to the problem concerning the distribution of the magnetic field intensity over the cross section of such a rod. The effects which rods in the shapes of a regular triangular prism, a regular hexagonal prism, and a circular cylinder cut by two planes parallel to and equidistant from its axis have on the transducer output signal have been studied experimentally. It is estimated here, on the basis of the results, how the parameters of the transducer output signal are affected by changes in the shape of the rod cross section.)

Yu. K. Fedosenko, *A Metallic Cylinder in the Field of a Noncoaxial Coil*, Defektoskopiya, Vol. 12, No. 6, pp. 43-52, November/December, 1976.

(The problem of calculating the electromagnetic field of a coil, carrying an alternating current, that encloses a metallic infinitely long cylinder arranged noncoaxially with respect to the coil is considered. The problem is solved by using scalar functions that enable separation of variables in cylindrical functions. The problem is reduced to finite expressions defining the induced emf of a feedthrough transducer. The effect of displacement ρ_o on the induced emf is analyzed. The author shows that the amplitude-phase method can be used to compensate for the influence of ρ_o when monitoring any of the parameters μ, σ, or R. The attenuation of the ρ_o is not measured in the differential method.)

V.E. Shcherbinin and M.L. Shur, *Calculating the Effect of the Boundaries of a Product on the Field of a Cylindrical Defect*, Defektoskopiya, Vol. 12, No. 6, pp. 30-35, November/December, 1976.

(Calculations are made of the defect field in the form of an infinite cylinder, taking magnetic reflections from the spatial boundaries and the boundaries of the defect into consideration. The authors show that taking the last factor into account leads to a quantitative and qualitative change in the calculated values of the defect field.)

V.F. Khrebtishchev and N.S. Savorovskii, *Effect of Surface Flaws in Thin-Walled Cylinders*, Defektoskopiya, Vol. 13, No. 2, pp. 154-157, March/April, 1977.

V.E. Shaternikov, *Interaction of Electromagnetic-Transducer Fields with Conducting Bodies of Complex Shape*, Defektoskopiya, Vol. 13, No. 2, pp. 162-167, March/April, 1977.

M.L. Shur and V.E. Shcherbinin, *Magnetostatic Field of a Defect Inside a Plane-Parallel Plate*, Defektoskopiya, Vol. 13, No. 3, pp. 92-96, May/June, 1977.

V.A. Sandovskii and M. Ya. Khalikov, *Two-Channel Eddy Current Inspection Unit for Inspecting Cylindrical Parts*, Defektoskopiya, Vol. 13, No. 4, pp. 94-98, July/August, 1977.

D.O. Thompson, *ARPA/AFML Review of Progress in Quantitative NDE*, (Rockwell International) September 1977.

K.F. Bainton, *Characterizing Defects by Determining Magnetic Leakage Fields*, NDT International, pp. 253-257, October 1977.

(Harwell's computerised ndt literature store was used to identify papers discussing magnetic flux leakage detection of defects. The following survey deals with those papers which deal at least in part with the characterization of defects rather than purely defect detection. The papers covered used magnetic particle, magnetographic or magnetometric detection techniques and various theoretical models were proposed. It would appear that there is a measure of agreement between theoretical models and experimental data if one chooses to work with specific flaw forms and materials, testing of material in automatic plant being a practical consequence. It is important to know the magnetic history of some materials in order to work at a suitable magnetization level. For the general case it has been suggested that one may be able to characterize surface opening cracks, but not sub-surface flaws, by an equivalent depth width and angle. Experimentally improvements in tapes, microprobes, methods of magnetization, lift off control and use of electronic tailoring have led to imporved signal-to-noise, sensitivity and resolution.)

D.A. Hill and J.R. Wait, *Analysis of Alternating Current Excitation of a Wire Rope by a Toroidal Coil*, Journal of Applied Physics, Vol. 48, No. 12, pp. 4893-4897, December, 1977.

(An idealized magnetic sheet current model for a toroidal coil which encircles a conducting ferromagnetic rope is analyzed. This configuration is suitable for the nondestructive testing of wire ropes and cables. Numerical results for the axial electric current density induced in the rope reveal that low frequencies on the order of 10 Hz are required to produce a uniform current in a typical rope. For a toroidal coil which does not completely encircle the rope, the azimuthal symmetry is lost and harmonics in ϕ are produced. These harmonics are large but decay rapidly away from the source.)

James R. Wait, *Electromagnetic Induction in an Anisotropic Cylinder*, Preliminary Report to U.S. Bureau of Mines on Contract No. H0155008, pp. 1-14, 8 February, 1978.

(The electromagnetic theory of an infinitely long cylinder is presented for the case when the electrical conductivity and the magnetic permeability are uni-axial tensors. This is an idealized yet relevant model for a stranded wire rope or cable that is to be excited by an external alternating-current source. The general and special forms of the solution are discussed in the context of non-destructive testing (NDT) of the rope. The method of deducing the electromagnetic response for a finite source is described in the special case where azimuthal symmetry prevails.)

D.A. Hill and J.R. Wait, *Scattering by a Slender Void in a Homogeneous Conducting Wire Rope*, Applied Physics, Vol. 16, pp. 391-398, 1978.

(A thin prolate spheroidal void in an infinite conducting circular cylinder is used to model a broken strand in a wire rope. The rope is excited by an azimuthal magnetic line current which is a model for a thin toroidal coil. The anomalous external fields are computed from the induced electric and magnetic dipole moments of the void. The results have applications to nondestructive testing of wire ropes.)

Jean-Luc Boulnois and Jean-Luc Giovachini, *The Fundamental Solution in the Theory of Eddy Currents and Forces for Conductors in Steady Motion*, Journal of Applied Physics, Vol. 49, No. 4, pp. 2241-2249, April, 1978.

(A closed-form solution to the central problem of the steady linear motion of an arbitrary current distribution past materials of constant permeability is presented. The application of the Green's function technique to the field equations yields integral representations of the induction, eddy currents, and electromagnetic forces. Due to interface coupling of the boundary conditions along the surface of the conductor, Green's functions are shown to satisfy integral equations. In the case of a conducting slab, explicit solutions for the Green's functions are derived. Application to magnetic levitation and the calculations of forces on moving coils are developed. Results are compared with experimental drag measurements.)

D.A. Hill and J.R. Wait, *Electromagnetic Field Perturbation by an Internal Void in a Conducting Cylinder Excited by a Wire Loop*, Preliminary Report to U.S. Bureau of Mines on Contract No. H0155008, pp. 1-55, 14 July, 1978.

(A thin prolate spheroidal void in an infinite conducting circular cylinder is used to model an internal flaw in a wire rope. The rope is excited by an electric ring current which is a model for a thin solenoid or multi-turn wire loop. The anomalous external fields are computed from the induced electric and magnetic dipole moments of the void. Computer plots of the scattered fields are generated to illustrate the effects of various

parameters. The results have application to nondestructive testing of wire ropes.)

David A. Hill and James R. Wait, *Theory of Electromagnetic Methods for Nondestructive Testing of Wire Ropes*, Proceedings of the Fourth West Virginia University Conference on Coal Mine Electrotechnology, pp. 16-1 to 16-13, August 2-4, 1978.

(Past and current techniques for electromagnetic nondestructive testing of wire ropes are briefly reviewed. Recent theoretical work is also discussed. In particular, we mention prolate spheroidal void model for a broken strand or individual wire. Here we assume the wire rope is excited by an electric current loop. This primary field, in turn, induces both electric and magnetic dipole moments in the small void. The resulting external scattered field is then derived and numerical results are presented which suggest an effective configuration of sensing coils. The dual source of a magnetic current loop which is a model for a toroidal coil is also considered.)

B.G. Marchent, *An Instrument for the Non-Destructive Testing of Wire Ropes*, Systems Technology, No. 29, pp. 26-32, August, 1978.

(The safety and security of a number of mechanical systems and equipment depends on the strength of a wire rope. This article describes an instrument developed by Plessey, under the terms of a contract placed by the Safety in Mines Research Establishment, to test wire ropes in situ and to provide an indication of any deterioration in the rope. A magnetic method of non-destructive testing (n.d.t.) is used in which the rope is magnetized by means of either an electromagnet or permanent magnet and magnetic sensors are used to detect anomaious magnetic fields due to wear, corrosion or broken wires in the rope. A prototype instrument has been produced for testing stranded haulage ropes used in mines and the technique can, in principle, be extended to test other types of wire ropes, for example general stranded ropes of any diameter, locked coil hoisting ropes, and large mooring cables for offshore structures.)

James R. Wait, *The Electromagnetic Basis for Nondestructive Testing of Cylindrical Conductors*, IEEE Transactions on Instrumentation and Measurement, Vol. IM-27, No. 3, pp. 235-238, September 1978.

(Using an idealized model, we deduce the impedance per unit length of long solenoid of many turns that contains a cylindrical sample. The sample with a specified conductivity and magnetic permeability need not be centrally located within the solenoid provided all transverse dimensions are small compared with the free-space wavelength. The derivation is relatively straightforward and it provides a justification for earlier use of the impedance formula. The dual problem, where the solenoid is replaced by a toroidal coil is also considered.

It is shown that both excitation methods have merit in non-destructive testing procedures.)

Robert L. Gardner, *Late Time Response of a Cylindrical Wire Rope Model to a Solenoid,* Preliminary Report to U.S. Bureau of Mines on Contract No. H0155008, pp. 1-12, 19 December 1978.

(Using an idealized model we consider the transient response when a step function voltage is applied to an infinite solenoid encircling a homogeneous cylinder. Previous early time results are extended to late time. The data showing the sensitivity of the response to changes in conductivity and permeability can be used in non-destructive testing of wire ropes and other cylindrical structures.)

James R. Wait, *Electromagnetic Response of an Anisotropic Conducting Cylinder to an External Source,* Radio Science, Vol. 13, No. 5, pp. 789-792, September/October 1978.

(A novel analytical solution is obtained for the boundary value problem of a circular cylinder of infinite length that is excited by a prescribed external field. The cylinder is anisotropic in the sense that the complex conductivity and magnetic permeability are diagonal uniaxial tensors with generally unequal elements. The solution involves Bessel functions of non-integral order. Known special cases are recovered.)

James R. Wait and David A. Hill, *Electromagnetic Interaction Between a Conducting Cylinder and a Solenoid in Relative Motion,* Preliminary Report to U.S. Bureau of Mines on Contract No. H0155008, pp. 1-17, January 9, 1979.

(An analysis is presented for the mutual impedance between two solenoids that are coaxial with a conducting cylinder in relative motion. The formulation is based on the first order Lorentz transformation and the results obtained are sufficiently general to encompass any such situation that could arise in nondestructive testing schemes. A numerical example, relevant to steel wire ropes of 2 cm radius used in mine hoists indicates that, even with relative velocities as high as 10 m/s, the mutual impedance at 10 Hz differs little from that calculated for zero velocity. However, the non-reciprocal effects could be significant for higher velocities and/or for more highly conducting and larger ropes.)

SECTION 3

Electromagnetic Induction of an Anisotropic Cylinder

JAMES R. WAIT

Abstract-The electromagnetic theory of an infinitely long cylinder is presented for the case when the electrical conductivity and the magnetic permeability are uni-axial tensors. This is an idealized yet relevant model for a stranded wire rope or cable that is to be excited by an external alternating-current source. The general and special forms of the solution are discussed in the context of non-destructive testing (NDT) of the rope. The method of deducing the electromagnetic response for a finite source is described in the special case where azimuthal symmetry prevails.

INTRODUCTION

There is a rapidly growing interest in the non-destructive testing of materials using electromagnetic fields [1]. The basic idea is to induce currents into the target and then observe the secondary response. The material properties are then deduced from the measured data. At least this is the objective which is seldom attained.

A particularly important example of non-destructive testing deals with the examination of metallic cables or stranded wire ropes [2]. Both the electric and magnetic properties may be an indicator of the mechanical condition of the material. For example, internal breaks in the

strands will decrease the longitudinal component of both the effective conductivity and permeability of the cable. Also, internal corrosion will tend to inhibit azimuthal and radial current flow so the effective transverse component of the conductivity would be mainly affected.

STATEMENT OF PROBLEM

Our purpose here is to set forth a general analysis for the electromagnetic fields that can be induced in an anisotropic cylindrical structure of infinite length with a circular cross section. The procedure to be employed bears some similarity to the analyses of isotropic cylindrical structures [3]. We simplify the problem to some extent by choosing uni-axial forms for the conductivity and permeability tensors with their principal axes to be taken parallel to the axis of the cylinder. In spite of the seemingly simplified description, the resulting field solution does not seem to be available.

FORMULATION

To be specific, we chose a cylindrical coordinate system (ρ,ϕ,z) such that the surface of the cylinder is $\rho = a$ where a is the radius. The external region $\rho > a$ will contain the sources but for the time being we will restrict our attention to the internal region $\rho < a$.

Maxwell's equations for the internal region, for a time factor $\exp(i\omega t)$, are

$$(\sigma)\vec{E} = \text{curl } \vec{H} \tag{1}$$

$$-i\omega(\mu)\vec{H} = \text{curl } \vec{E} \tag{2}$$

where $\vec{E}$ and $\vec{H}$ are the vector electric and magnetic fields respectively, and (σ) and (μ) are the tensor conductivity and permeability, respectively. In view of our stated assumptions, we may write

$$(\sigma) = \begin{pmatrix} \sigma_\rho & 0 & 0 \\ 0 & \sigma_\phi & 0 \\ 0 & 0 & \sigma_z \end{pmatrix} \tag{3}$$

and

$$(\mu) = \begin{pmatrix} \mu_\rho & 0 & 0 \\ 0 & \mu_\phi & 0 \\ 0 & 0 & \mu_z \end{pmatrix} \tag{4}$$

Here it should be noted that σ_ρ, σ_ϕ and σ_z are scalar complex conductivities; thus, for example, $\sigma_\rho = g_\rho + i\omega\varepsilon_\rho$ where g_ρ and ε_ρ are the real conductivity and the real permittivity, respectively, in the ρ direction. Similarly, we could write $\mu_\rho = \mu'_\rho - i\mu''_\rho$ where μ'_ρ and μ''_ρ are both positive real. However, for virtually all applications in NDT, the elements of (σ) and (μ) can be regarded as real since the imaginary parts are entirely negligible. A more important limitation is that we restrict attention to time harmonic fields of sufficiently small magnitude that the elements of (σ) and (μ) do not vary with the field magnitude (i.e. we are within the linear regime).

Equations (1) and (2), expressed in cylindrical coordinates, are

$$\frac{1}{\rho}\frac{\partial E_z}{\partial \phi} - \frac{\partial E_\phi}{\partial z} = -i\omega\mu_\rho H_\rho \quad (5); \qquad \frac{1}{\rho}\frac{\partial H_z}{\partial \phi} - \frac{\partial H_\phi}{\partial z} = \sigma_\rho E_\rho \quad (8)$$

$$\frac{\partial E_\rho}{\partial z} - \frac{\partial E_z}{\partial \rho} = -i\omega\mu_\phi H_\phi \quad (6); \qquad \frac{\partial H_\rho}{\partial z} - \frac{\partial H_z}{\partial \rho} = \sigma_\phi E_\phi \quad (9)$$

$$\frac{1}{\rho}\frac{\partial}{\partial \rho}(\rho E_\phi) - \frac{1}{\rho}\frac{\partial E_\rho}{\partial \phi} = -i\omega\mu_z H_z \quad (7); \qquad \frac{1}{\rho}\frac{\partial}{\partial \rho}(\rho H_\phi) - \frac{1}{\rho}\frac{\partial H_\rho}{\partial \phi} = \sigma_z E_z \quad (10)$$

Leading up to later developments, we now assume that the field components vary according to $\exp(-im\phi)\exp(-i\lambda z)$. For single-valuedness, m is restricted to positive or negative integers including zero. The parameter

λ, as yet, is unrestricted. Maxwell's equations are now simplified to

$$-\frac{im}{\rho}E_z + i\lambda E_\rho = -i\omega\mu_\rho H_\phi \quad (11); \qquad -\frac{im}{\rho}H_z + i\lambda H_\phi = \sigma_\rho E_\rho \quad (14)$$

$$-i\lambda E_\rho - \frac{\partial E_z}{\partial \rho} = -i\omega\mu_\phi H_\phi \quad (12); \qquad -i\lambda H_\rho - \frac{\partial H_z}{\partial \rho} = \sigma_\phi E_\phi \quad (15)$$

$$\frac{1}{\rho}\frac{\partial}{\partial \rho}(\rho E_\phi) + \frac{im}{\rho}E_\rho = -i\omega\mu_z H_z \quad (13); \qquad \frac{1}{\rho}\frac{\partial}{\partial \rho}(\rho H_\phi) + \frac{im}{\rho}E_\rho = \sigma_z E_z \quad (16)$$

To proceed further, we can now decompose or decouple the above set of equations into two cases. In the first case, we set $H_z = 0$ whence it is a simple matter to deduce that E_z satisfies

$$\frac{1}{\rho}\frac{\partial}{\partial \rho}\rho\frac{\partial}{\partial \rho}E_z - \frac{\sigma_\phi}{\sigma_\rho}\frac{m^2}{\rho^2}\frac{\lambda^2 + i\sigma_\rho\mu_\phi\omega}{\lambda^2 + i\sigma_\phi\mu_\rho\omega}E_z - (\lambda^2 + i\sigma_\rho\mu_\phi\omega)\frac{\sigma_z}{\sigma_\rho}E_z = 0 \quad (17)$$

The other case is when we set $E_z = 0$ whence H_z is found to satisfy

$$\frac{1}{\rho}\frac{\partial}{\partial \rho}\rho\frac{\partial}{\partial \rho}H_z - \frac{\mu_\phi}{\mu_\rho}\frac{m^2}{\rho^2}\frac{\lambda^2 + i\sigma_\phi\mu_\rho\omega}{\lambda^2 + i\sigma_\rho\mu_\phi\omega}H_z - (\lambda^2 + i\sigma_\phi\mu_\rho\omega)\frac{\mu_z}{\mu_\rho}H_z = 0 \quad (18)$$

Now clearly the total field is the superposition of these two cases. In fact, it is not difficult to show that

$$E_\rho = \frac{1}{(\lambda^2 + i\sigma_\rho\mu_\phi\omega)}\left[i\lambda\frac{\partial E_z}{\partial \rho} + \frac{m\omega\mu_\phi}{\rho}H_z\right] \quad (19)$$

$$E_\phi = \frac{1}{(\lambda^2 + i\sigma_\phi\mu_\rho\omega)}\left[\frac{\lambda m}{\rho}E_z - i\omega\mu_\rho\frac{\partial H_z}{\partial \rho}\right] \quad (20)$$

$$H_\rho = \frac{1}{(\lambda^2 + i\sigma_\phi\mu_\rho\omega)}\left[im\sigma_\phi E_z + i\lambda\frac{\partial H_z}{\partial \rho}\right] \quad (21)$$

$$H_\phi = \frac{1}{(\lambda^2 + i\sigma_\rho\mu_\phi\omega)}\left[\sigma_\rho\frac{\partial E_z}{\partial \rho} + \frac{\lambda m}{\rho}H_z\right] \quad (22)$$

GENERAL SOLUTION AND ITS PROPERTIES

Solutions of (17) and (18) are modified Bessel functions. In fact, for fields that are finite at $\rho = 0$, we can verify that

$$E_z = f_{e,m}(\lambda) I_{\alpha_m}(u\rho) e^{-im\phi} e^{-i\lambda z} \tag{23}$$

$$H_z = f_{h,m}(\lambda) I_{\beta_m}(v\rho) e^{-im\phi} e^{-i\lambda z} \tag{24}$$

where

$$u^2 = (\lambda^2 + i\sigma_\rho \mu_\phi \omega)\sigma_z/\sigma_\rho \tag{25}$$

$$v^2 = (\lambda^2 + i\mu_\rho \sigma_\phi \omega)\mu_z/\mu_\rho \tag{26}$$

$$\alpha_m^2 = m^2 \frac{\sigma_\phi}{\sigma_\rho} \frac{\lambda^2 + i\sigma_\rho \mu_\phi \omega}{\lambda^2 + i\sigma_\phi \mu_\rho \omega} \tag{27}$$

$$\beta_m^2 = m^2 \frac{\mu_\phi}{\mu_\rho} \frac{\lambda^2 + i\sigma_\phi \mu_\rho \omega}{\lambda^2 + i\sigma_\rho \mu_\phi \omega} \tag{28}$$

and where $f_{e,m}(\lambda)$ and $f_{h,m}(\lambda)$ are unspecified functions of λ and m.

Without actually solving anything, we can at this stage draw a number of important inferences about the eddy current testing of wire ropes and cables. When we impress an axial electric current, we expect, of course, that the axial electric field in the cable will be dominant. In fact, if the axial variation of the field is small (i.e. λ is small), the forms of the solutions simplify. Then

$$E_z \simeq f_{e,m}(\lambda) I_{\hat{m}}(\hat{u}\rho) e^{-im\phi} \tag{29}$$

where $\hat{u} \simeq (i\sigma_z \mu_\phi \omega)^{\frac{1}{2}}$ and $\hat{m} = m(\mu_\phi/\mu_\rho)^{\frac{1}{2}}$. Furthermore, since H_z is negligible in such cases, E_ρ and E_ϕ are also small. The induced currents and the secondary external fields are thus predominantly a function of the axial electrical conductivity σ_z and the azimuthal magnetic permeability

μ_ϕ. However, the higher-order harmonics (i.e. $m > 0$) are influenced to some extent by the radial magnetic permeability μ_ρ.

Another comparable situation is when the impressed magnetic field is axial and uniform. Then

$$H_z \simeq f_{h,m}(\lambda) I_{\bar{m}}(\bar{v}\rho) e^{-im\phi} \tag{30}$$

where $\bar{v} \simeq (i\mu_z \sigma_\phi \omega)^{\frac{1}{2}}$ and $\bar{m} = m(\sigma_\phi/\sigma_\rho)^{\frac{1}{2}}$. Now the significant induced currents are azimuthal and driven by the azimuthal electric field

$$E_\phi \simeq -\frac{1}{\sigma_\phi} \frac{\partial H_z}{\partial \rho} \tag{31}$$

Clearly, in this case, the secondary fields are mainly a function of the axial magnetic permeability μ_z and the azimuthal electric conductivity σ_ϕ. Analogously, the higher order harmonics are influenced by the radial electric conductivity σ_ρ.

The two cases considered above can be described as the E-field or the H-field method of excitation. Actually, it is the latter H-field configuration that is the basis for nearly all existing methods of eddy current testing of cables and wire ropes. In the case of the so-called DC technique, the external excitation is a solenoid that carries a large azimuthal current. The secondary H-field is then heavily influenced by the axial magnetic permeability. On the other hand, in the so-called AC method, the secondary field results from the induced eddy currents in the cable. These are primarily a function of the azimuthal conductivity σ_ϕ in addition to the axial magnetic permeability μ_z.

The E-field configuration would arise if the cable were excited by a toroidal or doughnut shaped coil [4]. The resulting induced currents now flow principally in the axial direction. In general, in this case, the finite value of λ needs to be considered. Nevertheless, the

secondary fields are now mainly a function of the axial conductivity σ_z and the azimuthal permeability μ_ϕ.

The situation generally becomes quite complicated when the effects of the non-zero values of λ and m are considered. The resulting fields then become hybrid [3] being neither purely E or H. In such cases, the secondary fields will depend, in general, on all tensor elements of the conductivity and permeability. Then it appears that quantitative calculations must be resorted to in order to gather further insight.

CASE OF AXIAL SYMMETRY

In the following discussion we will restrict attention to azimuthally uniform excitation such that all the harmonics for $m \neq 0$ may be discarded. We will consider, however, fields that have a significant variation in the axial direction. Now the field components are decomposed into two sets. For the E-field type,

$$E_z = f_e(\lambda) I_o(u\rho) e^{-i\lambda z} \tag{32}$$

$$H_\phi = \frac{\sigma_\rho u f_e(\lambda)}{\lambda^2 + i\omega\sigma_\rho\mu_\phi} I_1(u\rho) e^{-i\lambda z} \tag{33}$$

and

$$E_\rho = (i\lambda/\sigma_\rho) H_\phi \tag{34}$$

For the H-field type, we would have

$$H_z = f_h(\lambda) I_o(v\rho) e^{-i\lambda z} \tag{35}$$

$$E_\phi = \frac{-i\omega\mu_\rho v f_h(\lambda)}{\lambda^2 + i\omega\mu_\rho\sigma_\phi} I_1(v\rho) e^{-i\lambda z} \tag{36}$$

and

$$H_\rho = [-\lambda/(\mu_\rho\omega)] E_\phi \tag{37}$$

Two important physical parameters are the axial series impedance $Z_s(\lambda)$ and the axial series admittance $Y_s(\lambda)$ of the cable. These are defined and given as follows:

$$Z_s(\lambda) = \left.\frac{E_z}{2\pi a H_\phi}\right]_{\rho=a} = \frac{(\lambda^2 + i\omega\sigma_\rho\mu_\phi)I_o(ua)}{2\pi a\sigma_\rho u I_1(ua)} \tag{38}$$

and

$$Y_s(\lambda) = -\left.\frac{H_z}{2\pi a E_\phi}\right]_{\rho=a} = \frac{(\lambda^2 + i\omega\mu_\rho\sigma_\phi)I_o(va)}{2\pi a i\omega\mu_\rho v I_1(va)} \tag{39}$$

Two limiting cases follow immediately: (1), $|ua|$ and $|va| \ll 1$, then we obtain the static forms

$$Z_s(\lambda) \simeq 1/(\pi a^2\sigma_z) \tag{40}$$

and

$$Y_s(\lambda) \simeq 1/(\pi a^2 i\omega\mu_z) \tag{41}$$

(2), $|ua|$ and $|va| \gg 1$, then we obtain the asymptotic high frequency forms

$$Z_s(\lambda) \simeq \left(\frac{i\omega\mu_\phi}{\sigma_z}\right)^{1/2} \frac{1}{2\pi a} \tag{42}$$

and

$$Y_s(\lambda) \simeq \left(\frac{\sigma_\phi}{i\omega\mu_z}\right)^{1/2} \frac{1}{2\pi a} \tag{43}$$

These limiting cases have the expected dependencies on the electric properties. Not surprisingly, the static impedance (i.e. resistance) depends only on the axial conductivity. The analogue admittance depends in the same on the axial permeability.

THE EXCITATION PROBLEM

We now consider the excitation problem. The external source is taken to be a solenoid of radius b of finite axial extent that is concentric with the cable. The situation is illustrated in Fig. 1. The surface electric current density in the solenoid, in the present idealization, has both an axial and an azimuthal current density defined by

$$\left.\begin{aligned} j_z(z) &= j_o \sin\psi \\ \text{and} \qquad j_\phi(z) &= j_o \cos\psi \end{aligned}\right\} \quad \text{for } -\frac{\ell}{2} < z < \frac{\ell}{2} \tag{44}$$

(45)

where ψ is a pitch angle of the current flow. Here one should note that $\psi = 0$ corresponds to purely azimuthal current flow which is the condition approached in a solenoid of many turns. In general, for a pitched winding, the axial component of the current flow should also be accounted for. The corresponding boundary or initial conditions for the tangential magnetic fields, according to Ampere's law, must be

$$H_z(b^-,z) - H_z(b^+,z) = j_\phi(z) \tag{46}$$

and

$$H_\phi(b^-,z) - H_\phi(b^+,z) = -j_z(z) \tag{47}$$

where $b^{\pm}$ = limit of $b \pm \Delta$ when the positive quantity Δ tends to zero.

For the same excitation, we also have continuity of the tangential electric field. Thus

$$E_z(b^-,z) - E_z(b^+,z) = 0 \tag{48}$$

$$E_\phi(b^-,z) - E_\phi(b^+,z) = 0 \tag{49}$$

We now use the Fourier integral representation

$$j_\phi(z) = \int_{-\infty}^{+\infty} f(\lambda) e^{-i\lambda z} d\lambda \tag{50}$$

where it follows that

$$\begin{aligned} f(\lambda) &= \frac{1}{2\pi} \int_{-\infty}^{+\infty} j_\phi(z) e^{i\lambda z} d\lambda = \frac{1}{2\pi} (j_o \cos\psi) \int_{-\ell/2}^{\ell/2} e^{i\lambda z} d\lambda \\ &= (j_o \cos\psi)(\pi\lambda)^{-1} \sin(\lambda\ell/2) \end{aligned} \tag{51}$$

The desired representations are thus

$$j_\phi(z) = \frac{j_o \cos\psi}{\pi} \int_{-\infty}^{+\infty} \frac{\sin(\lambda\ell/2)}{\lambda} e^{-i\lambda z} d\lambda \tag{52}$$

and

$$j_z(z) = \frac{j_o \sin\psi}{\pi} \int_{-\infty}^{+\infty} \frac{\sin(\lambda\ell/2)}{\lambda} e^{-i\lambda z} d\lambda \tag{53}$$

In the free space region $\rho > a$, it is convenient to derive the fields from electric and magnetic Hertz vectors [3] that have only z components U and V, respectively. The fields are thus obtained from

$$E_\rho = \frac{\partial^2 U}{\partial\rho\partial z} \tag{54}$$

$$H_\rho = \frac{\partial^2 V}{\partial\rho\partial z} \tag{55}$$

$$E_z = \left(k_o^2 + \frac{\partial^2}{\partial z^2}\right) U \tag{56}$$

$$H_z = \left(k_o^2 + \frac{\partial^2}{\partial z^2}\right) V \tag{57}$$

$$H_\phi = -i\varepsilon_o \omega \frac{\partial U}{\partial\rho} \tag{58}$$

$$E_\phi = i\mu_o \omega \frac{\partial V}{\partial\rho} \tag{59}$$

where $k_o^2 = \varepsilon_o \mu_o \omega^2$.

To be compatible with the selected source fields, we assume the respective forms, for $a < \rho < b$,

$$U = \int_{-\infty}^{+\infty} A^e(\lambda)[I_o(\beta\rho) + \delta_e(\lambda) K_o(\beta\rho)] e^{-i\lambda z} d\lambda \tag{60}$$

and

$$V = \int_{-\infty}^{+\infty} A^h(\lambda)[I_o(\beta\rho) + \delta_h(\lambda)K_o(\beta\rho)]e^{-i\lambda z}d\lambda \tag{61}$$

where $\beta^2 = \lambda^2 - k_o^2$ and A^e and A^h are function of λ yet to be determined. Now the functions δ_e and δ_h can be determined immediately by imposing the impedance and admittance conditions at $\rho = a$ that are specified by (38) and (39). Then, using (56), (57), (58), and (59), it is easy to show that

$$\delta_e(\lambda) = -\left[\frac{\beta I_o(\beta a) - 2\pi a Z_s(\lambda) i\varepsilon_o \omega I_1(\beta a)}{\beta K_o(\beta a) + 2\pi a Z_s(\lambda) i\varepsilon_o \omega K_1(\beta a)}\right] \tag{62}$$

and

$$\delta_h(\lambda) = -\left[\frac{\beta I_o(\beta a) - 2\pi a Y_s(\lambda) i\mu_o \omega I_1(\beta a)}{\beta K_o(\beta a) + 2\pi a Y_s(\lambda) i\mu_o \omega K_1(\beta a)}\right] \tag{63}$$

Now in the outer region $\rho > b$ the appropriate forms for the Hertz potentials are

$$U = \int_{-\infty}^{+\infty} C^e(\lambda)K_o(\beta\rho)e^{-i\lambda z}d\lambda \tag{64}$$

and

$$V = \int_{-\infty}^{+\infty} C^h(\lambda)K_o(\beta\rho)e^{-i\lambda z}d\lambda \tag{65}$$

because the fields must be non-infinite as $\rho \to \infty$.

The source conditions specified by (46) and (47) can now be applied to yield

$$A^e(\lambda) = \frac{+(j_o/\pi\lambda)\sin\psi \sin(\lambda\ell/2)}{i\varepsilon_o\omega\beta[I_1 - (\delta_e + R_e)K_1]} \tag{66}$$

and

$$A^h(\lambda) = \frac{-(j_o/\pi\lambda)\cos\psi \sin(\lambda\ell/2)}{\beta^2[I_o + (\delta_h - R_h)K_o]} \tag{67}$$

where

$$R^e = C^e/A^e = (I_o + \delta K_o)/K_o \tag{68}$$

and

$$R^h = C^h/A^h = -(I_1 - \delta_h K_1)/K_1 \tag{69}$$

In the above four equations, the indicated modified Bessel functions are all functions of βb.

CONCLUDING REMARKS

In principle, we have now solved the problem since the resultant fields are now given in terms of the source current. The next step would be to deduce the pick up voltage in a sensor such as a small loop or electric probe. This is a straight forward process once we have specified the source and sensor configuration.

The method of obtaining the field expressions for the concentric current sheet is illustrative of the procedure to use in more general situations. For example, if the exciting current distribution is no longer azimuthally symmetric, we would require that higher harmonics of order m be included. This would tend to complicate the calculation for anisotropic cylinders because the modified Bessel functions are not of integer order. Nevertheless, this would be worthwhile.

A particularly important extension would be to consider the uniaxial tensors (3) and (4) to be directed along equi-angular spirals. This would correspond to the basic structure of stranded wire ropes. Analytically, this does not seem to be a trivial extension, since the axial E and H fields would then be solutions of coupled second order equations.

Further work on this subject is underway. The present preliminary report is intended as a guide to the analytical procedure that will be needed.

REFERENCES

[1] H.L. Libby, *Introduction to Electromagnetic Nondestructive Testing Methods.* New York: Wiley Interscience, 1971.

[2] J.P. Morgan, "Investigations of wire ropes in mine hoisting systems", *Australian Inst. Mining and Metal Proc.*, Vol. 215, pp. 59-85, 1965.

[3] J.R. Wait, *Electromagnetic Radiation From Cylindrical Structures.* Oxford: Pergamon Press, 1959.

[4] D.A. Hill and J.R. Wait, "Excitation of a wire rope by an azimuthal magnetic current sheet", *Report to U.S. Bureau of Mines on Contract No. H0155008*, 31 May 1977.

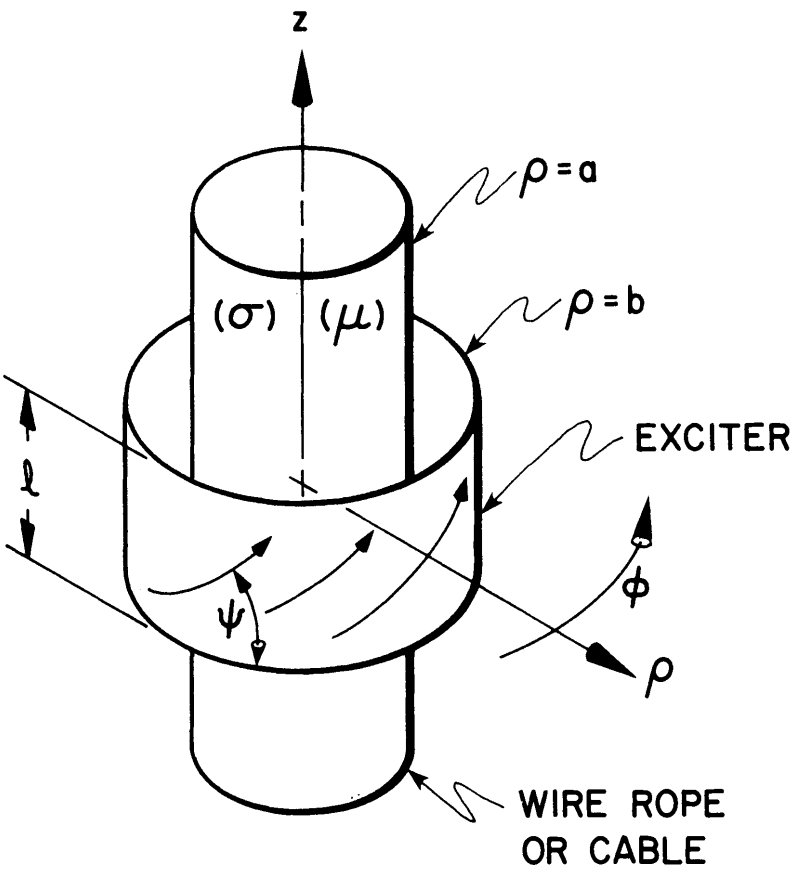

Fig. 1 ANISOTROPIC WIRE ROPE OR CABLE EXCITED BY A CONCENTRIC CURRENT SHEET OF FINITE AXIAL EXTENT.

Section 4

Electromagnetic Response of an Anisotropic Shell

JAMES R. WAIT

A remarkably simple and novel solution is obtained for the fields induced in an anisotropic cylindrical shell that is located coaxially within a long solenoid. This could be the basis of a non-destructive measuring scheme for stranded wire rope.

The non-destructive testing of wire ropes and cables exploits the electromagnetic response characteristics of cylindrical conductors. If the operating frequency is sufficiently low, the primary field can penetrate effectively to the interior of the sample and respond to internal imperfections such as fissures and voids. A straight-forward scheme to achieve this objective is to insert the sample into a long solenoid and measure the series impedance of the latter at a number of frequencies[1,2]. The electromagnetic basis of this method was discussed in an earlier paper[3] where the sample was idealized as a homogeneous cylinder with a specified conductivity and permeability.

It could be argued that a stranded wire rope is a cylindrical conductor but, because of the complicated spiral structure, it would not be isotropic. To shed some light on this problem, we examined the response of cylindrical conductors that were characterized by uni-axial conductivity and permeability tensors[4]. To facilitate the boundary value solution, the axes of these tensors were taken to be coaxial with the cylinder. A

rigorous solution for general anisotropy would be worthwhile but it appears this leads to coupled second order equations for the wave functions that are not immediately solvable by analytical methods[5]. As an interim approach, we adopt here a very simple model that consists of a thin shell whose conductivity along orthogonal spirals is different. The remarkable simplicity of the quasi-static form of the solution is justification for studying this problem in its own right.

We consider a thin cylindrical shell of thickness d and radius a that is encircled by a solenoid of radius b. The shell is characterized by a conductivity σ_s along spirals with a pitch angle of ψ; the conductivity in the transverse direction is σ_t. The nature of the idealizations will be evident in the formulation of the problem. The objective is to obtain an expression for the series impedance of the solenoid.

To be more specific, a cylindrical coordinate system (ρ,ϕ,z) is chosen and the shell of assumed infinite length is defined by $\rho = a$. The encircling solenoid of negligible thickness is at $\rho = b$. The impressed azimuthal current density in the solenoid is j amps./m. The region inside and outside the cylindrical shell is homogeneous with intrinsic propagation constant γ and intrinsic characteristic impedance η. For free space conditions, of course, $\gamma = i(\varepsilon_o\mu_o)^{1/2}\omega$ and $\eta = (\mu_o/\varepsilon_o)^{1/2}$ for a harmonic time factor $\exp(i\omega t)$.

Leaving aside many elementary details, we can now write down appropriate expressions for the axial fields and circumferential fields in the various regions:

$\rho<a$ (1)	$a<\rho<b$ (2)	$\rho>b$ (3)
$E_z = AI_o(\gamma\rho)$	$E_z = BK_o(\gamma\rho)$	$E_z = DK_o(\gamma\rho)$
$H_z = A^*I_o(\gamma\rho)$	$H_z = B^*K_o(\gamma\rho) + C^*I_o(\gamma\rho)$	$H_z = D^*K_o(\gamma\rho)$
$H_\phi = A\eta^{-1}I_1(\gamma\rho)$	$H_\phi = -B\eta^{-1}K_1(\gamma\rho)$	$H_\phi = -D\eta^{-1}K_1(\gamma\rho)$
$E_\phi = -A^*\eta I_1(\gamma\rho)$	$E_\phi = B^*\eta K_1(\gamma\rho) - C^*\eta I_1(\gamma\rho)$	$E_\phi = D^*\eta K_1(\gamma\rho)$

Here I_o, I_1, K_o, and K_1 are modified Bessel functions in conventional notation while A, A^*, B, B^*, C^*, D, and D^* are unknown coefficients.

By Ampere's law we can write $H_z(b+0) - H_z(b-0) = -j$ which is merely a statement that the tangential magnetic field is discontinuous at the solenoid by the amount of current it carries. Also, with the same idealization, E_z , E_ϕ and H_ϕ are continuous at $\rho = b$. This tells us that $D = B$ and $C^* = \gamma bK_1(\gamma b)\cdot j$ where we have made use of the Wronskian $I_o(x)K_1(x) + I_1(x)K_o(x) = 1/x$. Thus we think of C^* as the driving term.

Now we must deal with boundary conditions at the surface of the anisotropic shell. A direct application of Ampere's law requires that

$$H_s(a+0) - H_s(a-0) = -\sigma_t dE_t(a) \tag{4}$$

and

$$H_t(a+0) - H_t(a-0) = \sigma_s dE_s(a) \tag{5}$$

where the subscript s or t designates that field component is in the direction of the spiral or transverse to it. Also, for this model, E_s and E_t are continuous through the shell so we do not need to distinguish between the two values on each side. Now we note that

$$H_z(a\pm0) = H_s(a\pm0)\cdot C_o - H_t(a\pm0)\cdot S_o \tag{6}$$

and

$$H_\phi(a\pm0) = H_s(a\pm0)\cdot S_o + H_t(a\pm0)\cdot C_o \tag{7}$$

where $C_o = \cos\psi$ and $S_o = \sin\psi$ in terms of the pitch angle ψ. It is now a simple matter to rewrite (4) and (5) in the form

$$H_z(a+0) - H_z(a-0) = \sigma_t d(E_z S_o - E_\phi C_o)C_o - \sigma_s d(E_z C_o + E_\phi S_o)S_o \tag{8}$$

and

$$H_\phi(a+0) - H_\phi(a-0) = \sigma_t d(E_z S_o - E_\phi C_o)S_o + \sigma_s d(E_z C_o + E_\phi S_o)C_o \tag{9}$$

where it is understood that the E_ϕ and the E_z components are evaluated at $\rho = a$.

We can apply (8) and (9) to general forms given by (1), (2), and (3). Then, bearing in mind that $E_\phi(a+0) = E_\phi(a-0)$ and $E_z(a+0) = E_z(a-0)$, we can deduce that

$$\frac{B^*}{C^*} = \frac{\begin{vmatrix} (\sigma_t C_o^2 + \sigma_s S_o^2)d\eta I_1 , & -(\sigma_t - \sigma_s)dC_o S_o K_o \\ (\sigma_t - \sigma_s)dC_o S_o \eta I_1 , & \frac{-1}{\eta\gamma a I_o} + (\sigma_t S_o^2 + \sigma_s C^2)dK_o \end{vmatrix}}{\begin{vmatrix} \frac{1}{\gamma a I_1} + (\sigma_t C^2 + \sigma_s S^2)d\eta K_1 , & -(\sigma_t - \sigma_s)dC_o S_o K_o \\ (\sigma_t - \sigma_s)dC_o S_o \eta K_1 , & \frac{-1}{\eta\gamma a I_o} + (\sigma_t S^2 + \sigma_s C^2)dK_o \end{vmatrix}}$$

where all the Bessel functions in the elements of the determinants have common argument γa.

The series impedance Z per unit length of the solenoid can be obtained from its basic definition $Z = E_\phi(\rho=b)/j$. But what is most meaningful is the ratio Z/Z_o where Z_o is the corresponding series impedance of the solenoid in the absence of the core sample. It easily follows that

$$Z/Z_o = 1 - (B^*/C^*)K_1(\gamma b)/I_1(\gamma b)$$

Algebraically, this seems rather complicated but a great simplification ensues if we invoke the quasi-static approximation where $|\gamma b| << 1$. Then, using the small argument approximation for all the modified Bessel

functions, it follows that

$$Z/Z_o \simeq 1 - (a/b)^2 iq(1+iq)^{-1}$$

where

$$iq = (\gamma a/2)(\sigma_t C_o^2 + \sigma_s S_o^2)\eta d$$

When the ambient medium is free space, then $\gamma = i2\pi/\lambda_o$ where λ_o is the free space wavelength and $\eta = 120\pi$. Then we find that $q = 240\pi^2(a/\lambda_o) \times (\sigma_t C_o^2 + \sigma_s S_o^2)d$. This shows that the effective conductance of the shell is $(\sigma_t C_o^2 + \sigma_s S_o^2)d$ which is a remarkably simple result. Also, at sufficiently low frequencies (i.e. $q << 1$), $Z/Z_o \simeq 1 - iq(a/b)^2$ which indicates that the inductance of the solenoid is not modified by the presence of the sample. However, at relatively high frequencies (i.e. $q >> 1$), we see that $Z/Z_o \simeq 1 - (a/b)^2$ which shows that the solenoid inductance is reduced.

The pitch angle ψ enters into the general expressions via S_o and C_o. If the spiral is wound so that the wires are nearly axial (i.e. $S_o = \sin\psi << 1$), we see that the effective conductance of the shell is $\sigma_t d$. Conversely, if the pitch angle ψ is near 90° (i.e. wires almost circumferential so that $C_o = \cos\psi << 1$), the effective conductance is $\sigma_s d$.

More complicated models could be constructed by employing several concentric shells possibly in combination with intermediate regions of finite isotropic properties. This could lead to a more flexible yet still tractable model to describe the salient current flow pattern in a stranded wire rope. Work on the subject continues.

REFERENCES

1 LIBBY, H.L.: 'Introduction to electromagnetic non-destructive test methods', (John Wiley & Sons, 1971), Sec. 5.2, pp. 135-150).

2 FORSTER, F., AND STAMBKE, K.:'Theoretische und experimentelle Grundlagen der zerstörungfreien Werkstoffprufung mit Wirbelstromverfahren', Pt. III., *Zeits. Metallkde*, 1954, 45, pp. 166-179.

3 WAIT, J.R.: 'Electromagnetic basis for non-destructive testing of cylindrical conductors', *IEEE Trans.*, 1978, IM-27, pp. 235-238.

4 WAIT, J.R.: 'Electromagnetic response of an anisotropic conducting cylinder to an external source', *Radio Sci.*, 1978, 13,

5 WAIT, J.R.: 'Electromagnetics and plasmas', (Holt, Rinehart and Winston, 1968).

Section 5

ELECTROMAGNETIC NON-DESTRUCTIVE TESTING OF CYLINDRICALLY LAYERED CONDUCTORS

James R. Wait

and

Robert L. Gardner

Abstract-We extend a previous analysis for the series impedance of a long solenoid to allow for the cylindrical layering of the encircled conductor. The results are discussed in the context of non-destructive testing of steel ropes that may have external or internal corrosion. It is shown that even an internal layer of reduced conductivity and permeability will be detectable if the frequency is sufficiently low to permit penetration of the primary field.

INTRODUCTION AND FORMULATION

In an earlier paper [1], we had described the electromagnetic basis for the non-destructive testing of cylindrical conductors. The model was highly idealized; it consisted of a long solenoid that encircled the homogeneous cylindrical sample. Here we wish to generalize the theory to account for concentric layering within the sample. This is a possible model to account for the effect of internal and external corrosion that can occur in cables or wire ropes.

The derivation is given in outline only since the method is well documented elsewhere [2,3]. We deal specifically with a cylindrical sample that has an outer radius a_1 and a core of radius a_3. There is an intermediate annular region bounded by cylindrical surfaces of radii a_2 and a_3. The three

regions have electrical properties σ_j, ε_j, and μ_j where j = 1,2,3. For example, the outer layer has conductivity σ_1, permittivity ε_1 and permeability μ_1, the intermediate layer has properties σ_2, ε_2 and μ_2 and the core has properties σ_3, ε_2 and μ_3.

The sample is located within a solenoid of radius b but it need not be centrally located provided the free-space wavelength is much greater than b. Then, proceeding in the same manner as in the previous paper [1], we can derive an expression for the series impedance Z of the solenoid per unit length in the form

$$\frac{Z}{Z_o} = 1 - \frac{a_1^2}{b^2} + Z_c \frac{2a_1}{i\mu_o \omega b^2} \tag{1}$$

where Z_o is the series impedance when the solenoid is free of the sample. Here Z_c is the inwards looking wave impedance at the sample. For example, if the latter were homogeneous with electrical properties σ_1, ε_1, and μ_1, we would have

$$Z_c = \frac{i\mu_1 \omega}{\gamma_1} \frac{I_1(\gamma_1 a_1)}{I_o(\gamma_1 a_1)} \tag{2}$$

where $\gamma_1 = [i\mu_1\omega(\sigma_1 + i\varepsilon_1\omega)]^{1/2}$ is the intrinsic propagation constant of the sample. Here I_o and I_1 are modified Bessel functions of the first kind. This special case was derived in detail in the earlier paper [1].

THE GENERAL WAVE IMPEDANCE

To account for the concentric layering of the sample, we need to employ the appropriate expression for the radial wave impedance Z_c. This can be obtained in a rather prosaic manner by setting up wave function in each of the homogeneous regions and determining the unknown coefficients by matching tangential fields at the concentric interfaces. A more physically meaningful approach is to employ non-uniform transmission line theory as so elegantly

promulated by Sergei Schellkunoff [2]. The method has been applied to cylindrically layered plasma regions [3] so we can, in effect, write down the answer here in terms of wave impedances, transmission factors, and reflection coefficients. Thus, we find that

$$Z_c = \eta_1 \frac{I_1(\gamma_1 a_1)}{I_o(\gamma_1 a_1)} \frac{\left[1 + r \frac{I_1(\gamma_1 a_2)K_1(\gamma_1 a_1)}{I_1(\gamma_1 a_1)K_1(\gamma_1 a_2)}\right]}{\left[1 + R \frac{I_o(\gamma_1 a_2)K_o(\gamma_1 a_1)}{I_o(\gamma_1 a_1)K_o(\gamma_1 a_2)}\right]} \tag{3}$$

where

$$R = \left[\frac{\eta_1 I_1(\gamma_1 a_2)}{I_o(\gamma_1 a_2)} - \hat{Z}_c\right]\left[\frac{\eta_1 K_1(\gamma_1 a_2)}{K_o(\gamma_1 a_2)} + \hat{Z}_c\right]^{-1} \tag{4}$$

and

$$r = \left[\frac{I_o(\gamma_1 a_2)}{\eta_1 I_1(\gamma_1 a_2)} - \frac{1}{\hat{Z}_c}\right]\left[\frac{K_o(\gamma_1 a_2)}{\eta_1 K_1(\gamma_1 a_2)} + \frac{1}{\hat{Z}_c}\right]^{-1} \tag{5}$$

Here K_o and K_1 are modified Bessel functions of the second type and $\eta_1 = i\mu_1\omega/\gamma_1$. The inward looking wave impedance $\hat{Z}_c$ at the cylindrical interface of radius a_2 is given by an analogous form:

$$\hat{Z}_c = \eta_2 \frac{I_1(\gamma_2 a_2)}{I_o(\gamma_2 a_2)} \frac{\left[1 + \hat{r} \frac{I_1(\gamma_2 a_3)K_1(\gamma_2 a_2)}{I_1(\gamma_2 a_2)K_1(\gamma_2 a_3)}\right]}{\left[1 + \hat{R} \frac{I_o(\gamma_2 a_3)K_o(\gamma_2 a_2)}{I_o(\gamma_2 a_2)K_o(\gamma_2 a_3)}\right]} \tag{6}$$

where

$$\hat{R} = \left[\frac{\eta_2 I_1(\gamma_2 a_3)}{I_o(\gamma_2 a_3)} - \frac{\eta_3 I_1(\gamma_3 a_3)}{I_o(\gamma_3 a_3)}\right]\left[\frac{\eta_2 K_1(\gamma_2 a_3)}{K_o(\gamma_2 a_3)} + \frac{\eta_3 I_1(\gamma_3 a_3)}{I_o(\gamma_3 a_3)}\right]^{-1} \tag{7}$$

and

$$\hat{r} = \left[\frac{I_o(\gamma_2 a_3)}{\eta_2 I_1(\gamma_2 a_3)} - \frac{I_o(\gamma_3 a_3)}{\eta_3 I_1(\gamma_3 a_3)}\right]\left[\frac{K_o(\gamma_2 a_3)}{\eta_2 K_1(\gamma_2 a_3)} + \frac{I_o(\gamma_3 a_3)}{\eta_3 I_1(\gamma_3 a_3)}\right]^{-1} \tag{8}$$

where $\gamma_j = [i\mu_j\omega(\sigma_j + i\varepsilon_j\omega)]^{1/2}$ and $\eta_j = i\mu_j\omega/\gamma_i$ for $j = 1,2,3$.

Actually, subject to such assumptions as axial and azimuthal uniformity, the expressions for Z_c and Z_c are exact. For computation, however, we can

neglect displacement currents in the various layers. Thus, if $\varepsilon_j\omega << \sigma_j$, we see that $\gamma_j \simeq (i\sigma_j\mu_j\omega)^{1/2} = |\gamma_j| \exp(i\pi/4)$ whence all the modified Bessel functions have arguments with phase angles of 45°. The final results can then be written in terms of the tabulated Kelvin functions [4] via

$$I_o(\alpha i^{1/2}) = ber(\alpha) + ibei(\alpha)$$

$$iI_1(\alpha i^{1/2}) = ber_1(\alpha) + ibei_1(\alpha)$$

$$K_o(\alpha i^{1/2}) = ker(\alpha) + ikei(\alpha)$$

$$-iK_1(\alpha i^{1/2}) = ker_1(\alpha) + ikei_1(\alpha)$$

where α is a real parameter.

NUMERICAL EXAMPLES

Computations have been carried out for the complex quantity Z/Z_o for several specific conditions of practical interest. First of all, to provide a reference case, we let the sample be homogeneous with properties σ_1 and μ_1 and radius a_1. This, of course, corresponds to the general case under the condition $a_2 = a_3 = 0$. As indicated in the inset in Fig. 1, the sample is also located centrally within the solenoid of radius b. To be definite, we also choose the sample radius a_1 to be 2 cm which is kept fixed in all that follows. Also, the conductivity of the (uncorroded) sample is taken to be 1.1×10^6 mhos/m and its relative permeability $\mu_{rel} = \mu_1/\mu_o = 200$. These are typical values for steel. The corresponding series impedance $Z = R + iX$ of the solenoid is shown plotted in Fig. 1 in an Argand diagram. The abscissa and ordinate are actually $R/X_o\mu_{rel}$ and $X/X_o\mu_{rel}$, respectively, where we have assumed that the impedance of the same empty solenoid is $Z = iX_o$ being purely inductive. Various fill factors $F = a_1^2/b^2$ are shown and the operating frequencies are indicated. As expected, at sufficiently low

frequencies, R tends to zero and X approaches $X_o \times \mu_{rel} \times F$. Not surprisingly, the series impedance of the solenoid is sensitive to the diameter of the sample.

We now consider an external rust or corrosion layer of thickness ℓ at the outside of the sample as indicated in the inset in Fig. 2. This is a special case of the general analysis when $a_3 = 0$. The uncorroded region of radius a_2 has the same properties as before (i.e. $\sigma_2 = 1.1 \times 10^6$ mhos/m and $\mu_{rel} = \mu_2/\mu_o = 200$) but the external layer now assumes the values $\sigma_1 = 1$ mho/m and $\mu_1 = \mu_o$. The results are shown in Fig. 2 where we have taken the fill factor F to be 1 (i.e. $a_1 = b$). Different values of ℓ, the thickness of the rust layer, are shown. Not surprisingly, the effect of an external rust layer is to reduce the effective radius of the cylindrical steel sample.

Finally, we consider an internal corrosion layer. As indicated in Fig. 3, this corresponds to the case where the full formula for Z_c, as given by (3), is needed but we set $\sigma_1 = \sigma_3 = 1.1$ mhos/m and $\mu_1/\mu_o = \mu_3/\mu_o = \mu_{rel} = 200$ which are the "uncorroded" regions. In the central annular "corroded" region, we choose $\mu_2 = \mu_o$ and $\sigma_2 = 1.0$ mho/m. For the results shown in Fig. 3, we have also chosen the radius a_3 of the core to be $0.3a_1$ but the value of ℓ ranges from being zero (i.e. no rust layer) to a value of $0.3a_1$. As seen in Fig. 3, the series impedance of the solenoid is still markedly affected by the presence of the corrosion layer, even though it would not be visible to an outside observer. Of course, the frequency must be sufficiently low so that the primary fields of the solenoid can penetrate to the interior of the sample without significant dissipation.

CONCLUDING REMARKS

The present calculations, while based on a highly idealized model, indicate the potential of non-destructive schemes using electromagnetic waves [5]. More sophisticated models based on the layered cylinder formulations can easily be implemented. Actually, three dimensional models that allow for the finite extent of the primary field and the internal anomaly have been examined elsewhere [6,7].

Certainly, the sensitivity of such devices to the electrical, magnetic, and geometrical properties needs further study. Here we have only indicated a few examples that might promote further developments in this area.

REFERENCES

[1] J.R. Wait, "Electromagnetic basis for non-destructive testing of cylindrical conductors", *IEEE Trans. Instrumentation & Measurement*, Vol. IM-27, No. 3, 235-238, September 1978.

[2] S.A. Schelkunoff, *Electromagnetic Waves*. New York: Van Nostrand Co. Inc., 1943, p. 205.

[3] J.R. Wait, *Electromagnetic Waves in Stratified Media*. New York: Pergamon, 1970, 2nd Ed., p. 534.

[4] N.W. McLachlan, *Bessel Functions for Engineers*. London: Oxford University Press, (corrected 2nd Ed.), 1961, p. 211.

[5] H. Hochschild, "Electromagnetic methods of testing metals", *Progress in Non-Destructive Testing*, Vol. I, pp. 58-109, (ed. E.G. Stanford and J.H. Fearon), New York: The Macmillan Co., 1959.

[6] D.A. Hill and J.R. Wait, "Analysis of alternating current excitation of a wire rope by a toroidal coil", *J. Appl. Phys.*, Vol. 48, No. 12, pp. 4893-4897, 1977.

[7] D.A. Hill and J.R. Wait, "Scattering by a slender void in a homogeneous conducting wire rope", *Appl. Phys.* (Springer-Verlag), Vol. 16, pp. 391-398, 1978.

FIGURE CAPTIONS

Fig. 1. Normalized series impedance of solenoid of radius b for a concentric homogeneous cylindrical sample of radius a_1 for various fill factors $F = a_1^2/b^2$.

Fig. 2. Normalized series impedance of solenoid of radius $b = a_1$ for a sample with an external rust layer of thickness ℓ.

Fig. 3. Normalized series impedance of solenoid of radius $b = a_1$ for a sample of an interior rust layer of thickness ℓ.

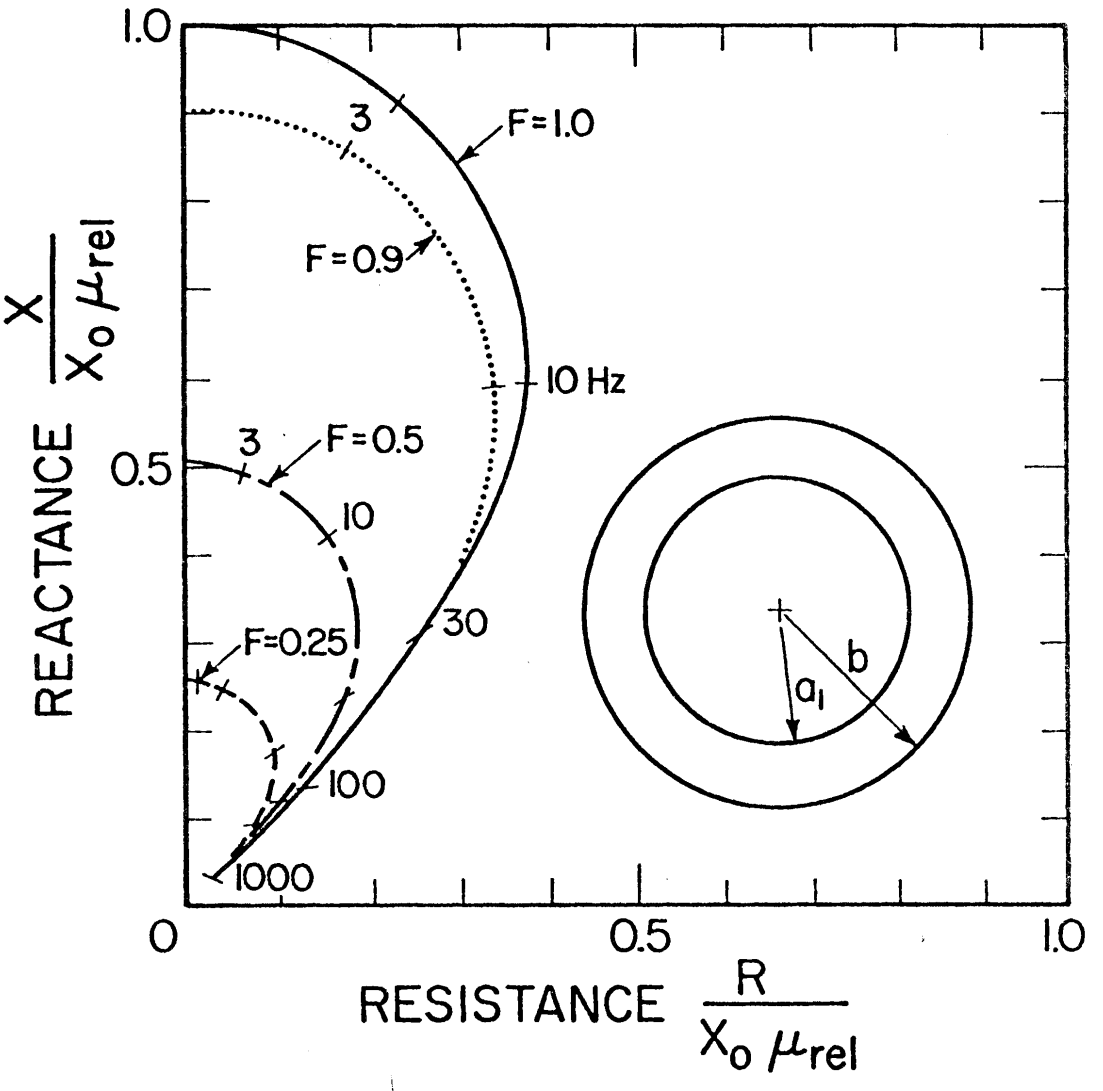

Fig. 1. Normalized series impedance of solenoid of radius b for a concentric homogeneous cylindrical sample of radius a_1 for various fill factors $F = a_1^2/b^2$.

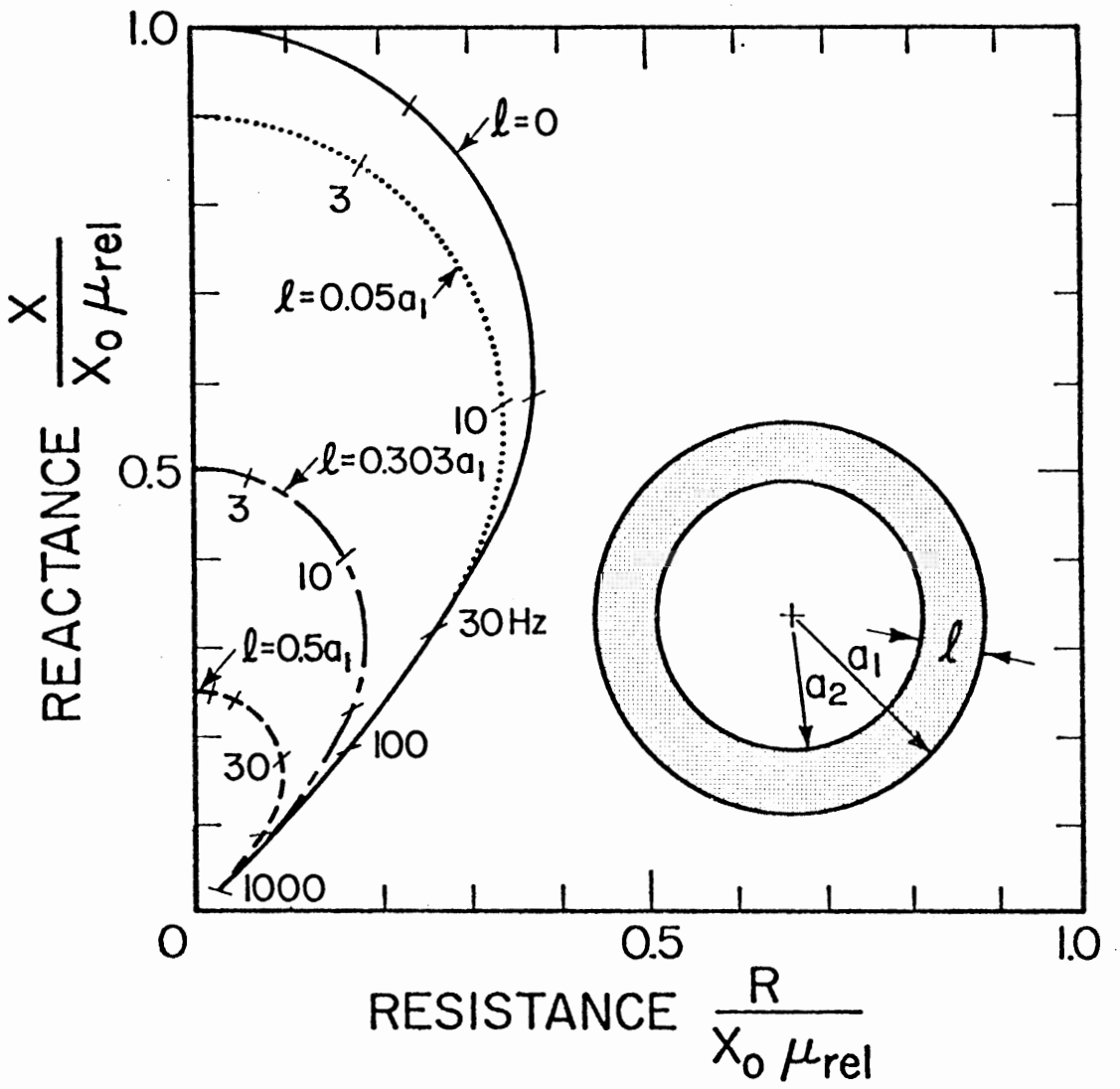

Fig. 2. Normalized series impedance of solenoid of radius b = a_1 for a sample with an external rust layer of thickness ℓ.

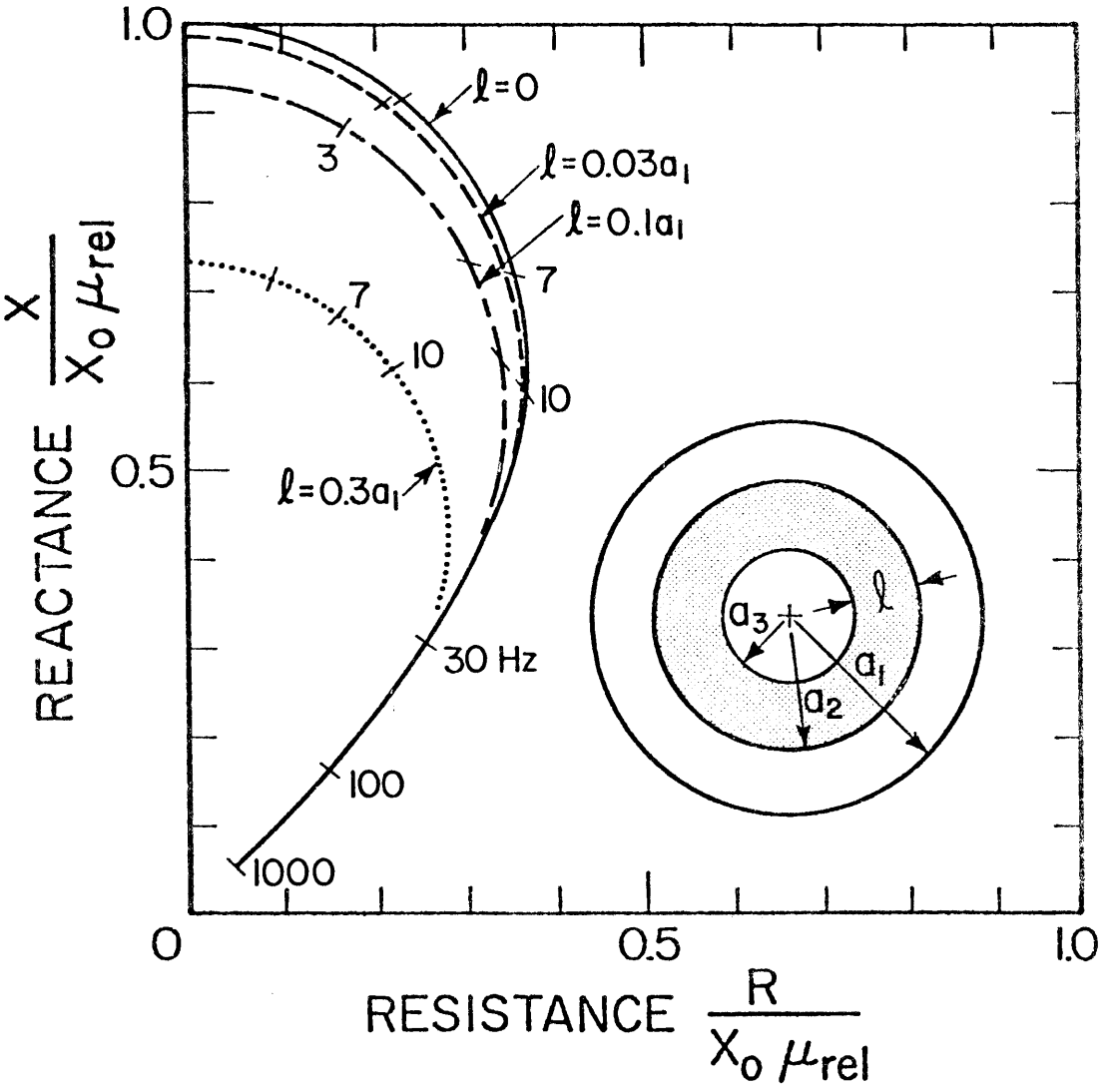

Fig. 3. Normalized series impedance of solenoid of radius b = a_1 for a sample of an interior rust layer of thickness ℓ.

Section 6

Non-Destructive Testing of a Cylindrical Conductor with an Internal Anomaly - A Two Dimensional Model

JAMES R. WAIT

and

Robert L. Gardner

Abstract-A self contained analysis is presented for the impedance of a solenoid that encircles a conducting cylinder that has an internal flaw or anomaly that is also cylindrical in form. A perturbation method is used to obtain an expression for the fractional change of the impedance as a function of the size and location of the anomaly.

INTRODUCTION

There is a need to evaluate the internal structure of wire ropes and similar cylindrical conductors. This has led to an extensive technology called non-destructuve testing (NDT). A good survey of the electromagnetic methods are given by Libby [1]. One of the basic configurations is a solenoidal coil that tightly encircles the wire rope specimen. As indicated in a two-dimensional analysis [2], the impedance of the solenoid can be related uniquely to the conductivity and permeability of the wire rope if it can be assumed homogeneous. It is the purpose of the present analysis to examine the effect of an internal flaw. While more complicated cases [3] can be treated, we consider here an idealized two-dimensional anomaly or cylindrical flaw of radius c that is contained within the otherwise homogeneous cylinder of radius a. The situation is illustrated in Fig. 1 which we will describe in more detail below.

Even for the assumed two-dimensionality, a rigorous solution is complicated. However, since we are interested in the threshold of the detectability of an internal anomaly, a perturbation approach is quite permissible. Here the anomaly is assumed to be "excited" by the field that would exist if the anomaly or flaw were not present. This primary field actually induces a monopole, dipole, and higher order multipoles. In the case where the wire rope is encircled by an idealized uniform solenoid [1,2], the primary magnetic field has only an axial component and the primary electric field is entirely azimuthal. These excite, respectively, a line magnetic monopole and a line electric dipole within the anomaly. If the transverse dimensions of the cylindrical flaw are small (in terms of skin depth of the wire rope material), the higher order multipoles are negligible. The secondary fields of the induced monopole and the dipole are the external observables. In the simplest case, they manifest themselves as a modification of the impedance of the encircling solenoid.

A preliminary problem that we need to consider is the excitation of a cylindrical flaw by a known form of primary field. In this manner, the polarizabilities or strengths of the induced monopole and dipole can be ascertained. We then use these results in the composite problem where the exciting field is produced by the encircling solenoid. Finally, some numerical results are presented to illustrate the fractional change of the solenoid impedance as a function of the dimensions and location of the anomaly.

PROTOTYPE PROBLEM

As indicated above, it is useful to consider the following prototype solution. A circular cylinder of conductivity σ_a and permeability μ_a with radius c is excited by an electric line source of strength M at a radial

separation ρ_1. The situation is illustrated in Fig. 2 with respect to cylindrical coordinates (ρ,ϕ,z) centered at the external line source and (ρ_a,ϕ_a,z) centered at the cylinder. The medium external to the cylinder has conductivity σ and permeability μ. In all cases, displacement currents are ignored. Their effect can be included by merely replacing σ by $\sigma + i\varepsilon\omega$ where ε is the permittivity; the time factor $\exp(i\omega t)$ being understood.

The primary field of the line source can be written as

$$H_z = -(\sigma M/2\pi)K_o(\gamma\rho) \tag{1}$$

where $\gamma = (i\sigma\mu\omega)^{\frac{1}{2}}$ and K_o is the modified Bessel function of the second kind of order zero. This can be checked by noting that

$$E_\phi = -\sigma^{-1}\partial H_z/\partial\rho = (\gamma M/2\pi)K_1(\gamma\rho) \tag{2}$$

As $\rho \to 0$ we see that $E_\phi \to M/(2\pi\rho)$ which has the required form.

Using an addition theorem [4], we know that

$$K_o(\gamma\rho) = \sum_{m=0}^{\infty} \varepsilon_m \cos m\phi_a \begin{cases} I_m(\gamma\rho_a)K_m(\gamma\rho_1); & \rho_1 > \rho_a \\ K_m(\gamma\rho_1)I_m(\gamma\rho_a); & \rho_a > \rho_1 \end{cases} \tag{3}$$

where the modified Bessel functions on the right hand side are of order m. It is then a simple matter [5] to show that the resultant field external to the cylinder is

$$H_z = -\frac{\sigma M}{2\pi}\{K_o(\gamma\rho) + \sum_{m=0}^{\infty} \varepsilon_m K_m(\gamma\rho_1)K_m(\gamma\rho_a)\frac{I_m(\gamma c)}{K_m(\gamma c)} R_m \cos\phi_a m\} \tag{4}$$

where

$$R_m = \frac{[\eta I_m'(\gamma c)/I_m(\gamma c)] - Z_{am}}{-[\eta K_m'(\gamma c)/K_m(\gamma c)] + Z_{am}} \tag{5}$$

$$Z_{am} = \eta_a I_m'(\gamma_a c)/I_m(\gamma_a c) \tag{6}$$

$\eta = i\mu\omega/\gamma$, $\eta_a = i\mu_a\omega/\gamma_a$ and $\gamma_a = (i\mu_a\sigma_a\omega)^{\frac{1}{2}}$.

From (4) we see that the first two terms of the secondary field can be written

$$H_z^s = H_z^{app}[I_o(\gamma c)/K_o(\gamma c)]R_o K_o(\gamma\rho_a)$$

$$-2(H_z^{app})'[I_1(\gamma c)/K_1(\gamma c)]R_1 K_1(\gamma\rho_a)\cos\phi_a \tag{7}$$

where

$$H_z^{app} = -(\sigma M/2\pi)K_o(\gamma\rho_1) \tag{8}$$

and

$$(H_z^{app})' = [\partial/\partial(\gamma\rho_1)]H_z^{app} = (\sigma M/2\pi)K_1(\gamma\rho_1) \tag{9}$$

Here it is useful to observe that the terms proportional to H_z^{app} and $(H_z^{app})'$ are the induced monopole and line dipole, respectively. By invoking the small argument approximations, we readily verify that

$$R_o \simeq -(i\omega/2)(\mu-\mu_a)\sigma c^2 \ell n(0.89c) \tag{10}$$

and

$$R_1 \simeq (\sigma_a-\sigma)/(\sigma_a+\sigma) \tag{11}$$

COMPOSITE PROBLEM

Now in the composite problem indicated in Fig. 1, we have

$$H_z^{app} = AI_o(\gamma\rho) \tag{12}$$

and

$$H_z^{app'} = AI_1(\gamma\rho) \tag{13}$$

or

$$E_\phi^{app} = -A\eta I_1(\gamma\rho) \tag{14}$$

which would be the fields inside the homogeneous cylinder (i.e. $\rho<a$) if there was no internal anomaly or flaw. These applied fields excite or induce the monopole, dipole, and multipoles within the cylindrical flaw. These in turn produce secondary fields that are observable outside the main cylindrical conductor. In what follows, we actually assume that $a - \rho_1 >> c$.

In order to deal with the interaction of the above secondary fields with the wall boundary at $\rho = a$, we need to translate back to the (ρ,ϕ,z) coordinates. First of all, we may employ the same addition theorem as used in the prototype problem:

$$K_o(\gamma\rho_a) = \sum_{n=-\infty}^{+\infty} K_n(\gamma\rho) I_n(\gamma\rho_1)\exp[in(\pi-\phi)] \tag{15}$$

where

$$\rho_a = [\rho^2 + \rho_1^2 + 2\rho_1\rho\cos\phi]^{\frac{1}{2}} \tag{16}$$

The other addition needed is obtained straight-forwardly by differentiating both sides of (15) with respect to ρ_1. Thus

$$K_1(\gamma\rho_a)\cos\phi_a = -\sum_{n=-\infty}^{\infty} K_n(\gamma\rho) I_n'(\gamma\rho_1)(-1)^n e^{-in\phi} \tag{17}$$

where we note that

$$\frac{\partial\rho_a}{\partial\rho_1} = \frac{\rho_1 + \rho_a\cos\phi}{\rho_a} = \cos\phi_a \tag{18}$$

It is now a simple matter to deal with the wall interaction. This amounts to replacing $K_n(\gamma\rho)$ in both (15) and (17) by $Z_n(\gamma\rho)$ where

$$Z_n(\gamma\rho) = K_n(\gamma\rho) + r_n \frac{K_n(\gamma a)}{I_n(\gamma a)} I_n(\gamma\rho) \tag{19}$$

where

$$r_n = \frac{[-\eta K_n'(\gamma a)/K_n(\gamma a)] - z_{an}}{[\eta I_n'(\gamma a)/I_n(\gamma a)] + z_{an}} \tag{21}$$

and

$$z_{an} = -\eta_o K_n'(\gamma_o a)/K_n(\gamma_o a) \tag{21}$$

This solution is entirely analogous to the earlier result but now the equivalent line source is inside the cylinder. Here z_{an} is the radial wave impedance looking outwards at $\rho = a$ into the external free space region.

Now we can write down the desired form for the secondary field. Clearly it is given by

$$H_z^s \simeq A \sum_{n=-\infty}^{+\infty} \{I_o(\gamma\rho_1) \frac{I_o(\gamma c)}{K_o(\gamma c)} R_o I_n(\gamma\rho_1) + 2I_1(\gamma\rho_1) \frac{I_1(\gamma c)}{K_1(\gamma c)} R_1 I_n'(\gamma\rho_1)\} \times (-1)^n Z_n(\gamma\rho) e^{-in\phi} \tag{22}$$

Actually, a quantity of special interest is the fractional change Δ of the impedance per unit length of an encircling solenoid at $\rho = a$. Under the usual assumptions [1,2], this can be obtained from

$$\Delta \simeq [\int_o^{2\pi} E_\phi^s(a,\phi)d\phi][\int_o^{2\pi} [E_\phi^{app}(a,\phi)d\phi]^{-1} \tag{23}$$

where

$$E_\phi^s(a,\phi) = -\eta\partial H_z^s/\partial(\gamma\rho) \tag{24}$$

The integration over ϕ removes all except the $n = 0$ term in the expressions for the secondary field. Thus we find that

$$\Delta \simeq \frac{1}{I_1(\gamma a)} \left[I_o^2(\gamma\rho_1) \frac{I_o(\gamma c)}{K_o(\gamma c)} R_o + 2I_1^2(\gamma\rho_1) \frac{I_1(\gamma c)}{K_1(\gamma c)} R_1 \right] Z_o'(\gamma a) \tag{25}$$

If $|\gamma a| << 1$, this reduces to the very simple result that

$$\Delta \simeq (\mu_a - \mu)c^2/(\mu a^2) \tag{26}$$

which is compatible with physical intuition. Here the contribution from the induced electric dipole term is of second order.

NUMERICAL RESULTS AND DISCUSSION

Some numerical results for the fractional impedance change $|\Delta|$ of the solenoid or sensor were obtained from (25) for the case where the wire rope conductivity $\sigma = 10^6$mho/m and the relative permeability $\mu/\mu_o = 44$. The wire rope radius a was 2.54cm (i.e. 2 inch diameter rope). The flaw or anomaly itself was assumed to be an air-filled void with free space properties (i.e. $\mu_o = 4\pi \times 10^{-7}$henries/m, $\sigma_a = 0$ and $\varepsilon_o = 8.854 \times 10^{-12}$farads/m).

The magnitude of Δ is shown plotted in Figs. 3, 4, 5, and 6 as a function of c/a where c is the radius of the anomaly. In each case the operating frequency is indicated. In Fig. 4, the anomaly is at the center of the main cylinder and, as indicated, the response for frequencies up to 10 Hz is essentially the same as that of DC or zero frequency. However, the 100 Hz response is reduced significantly due to the inability of the exciting field to penetrate to the center of the cylinder or wire rope. The corresponding response for 1000 Hz is off the scale for this example.

The effect of increasing the offset of the anomaly is illustrated in Figs. 5 and 6 where $\rho_1 = 0.5a$ and $0.8a$, respectively. The D.C. limit and the lower frequency response are not modified by changing the offset ρ_1 but for 100 Hz, and particularly for 1000 Hz, there is a marked change. Physically, this is not surprising since the energy even at 1000 Hz will penetrate to the outer region of the cylinder or wire rope with negligible attenuation.

Most of the curves shown in Figs. 3, 4, 5, and 6, on a log-log plot, differ imperceptibly from straight lines with a slope of two. In fact, for the D.C. limit, (26) tells us that $\Delta \propto (c/a)^2$. However, for the higher frequencies, the dipole term has a non-negligible contribution and the result is that the curves tend to be somewhat steeper.

REFERENCES

[1] H.L. Libby, *Introduction to Electromagnetic Nondestructive Test Methods*. New York: John Wiley & Sons, 1971.

[2] J.R. Wait, "The electromagnetic basis for non-destructive testing of cylindrical conductors", *Preliminary Report to U.S. Bureau of Mines on Contract No. HO155008*, 2 March 1978.

[3] D.A. Hill and J.R. Wait, "Scattering by a slender void in a homogeneous conducting wire rope", *Preliminary Report to U.S. Bureau of Mines on Contract No. HO155008*, 1 March 1978.

[4] A. Erdélyi (ed.), *Higher Transcendental Functions*. New York: McGraw-Hill Book Co., 1953, Vol. 2, p. 102.

[5] J.R. Wait, *Electromagnetic Radiation from Cylindrical Structures*. Oxford: Pergamon, 1959.

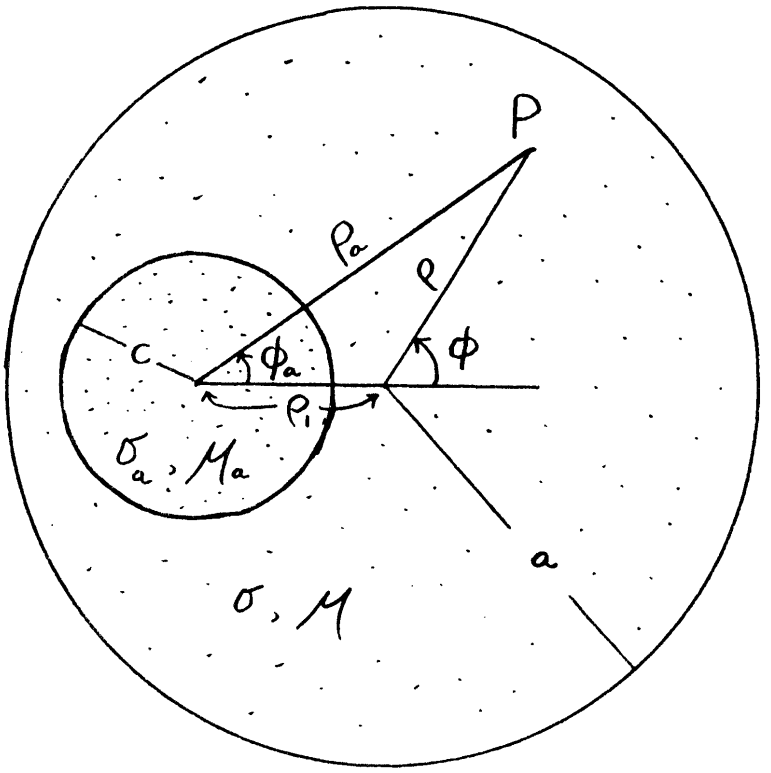

Fig. 1 : The composite problem

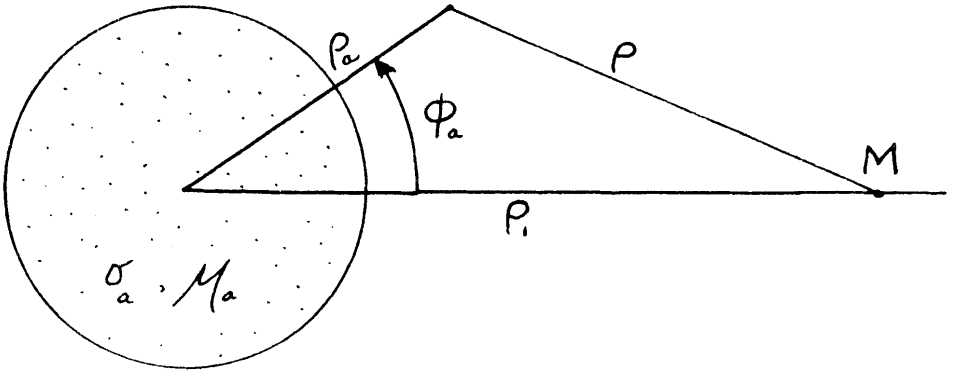

Fig 2: Prototype problem

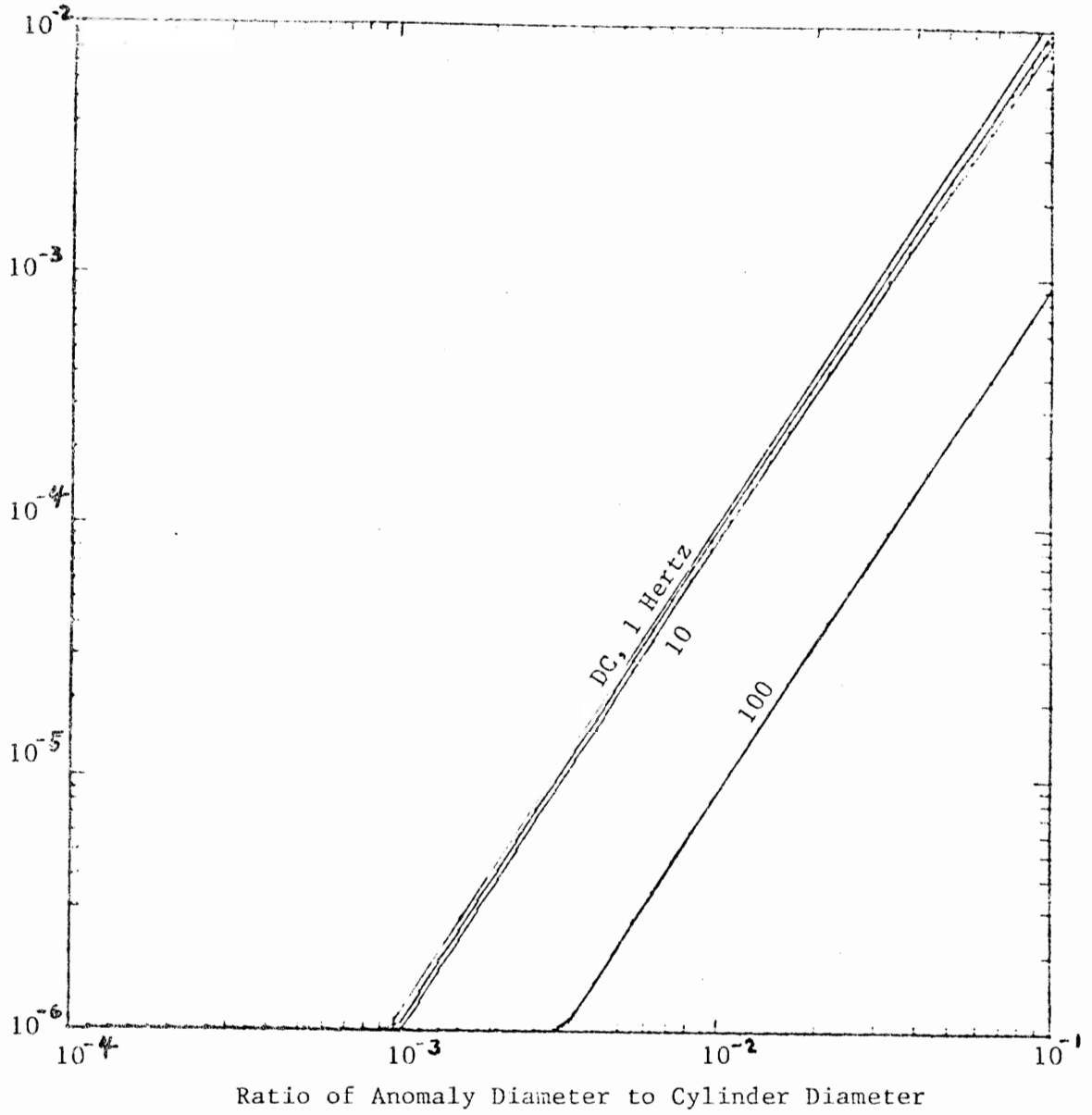

Figure 3 : Fractional Impedance Change for Sensor as a Function of Anomaly Size. The Anomaly is in the Center of the Cylinder.

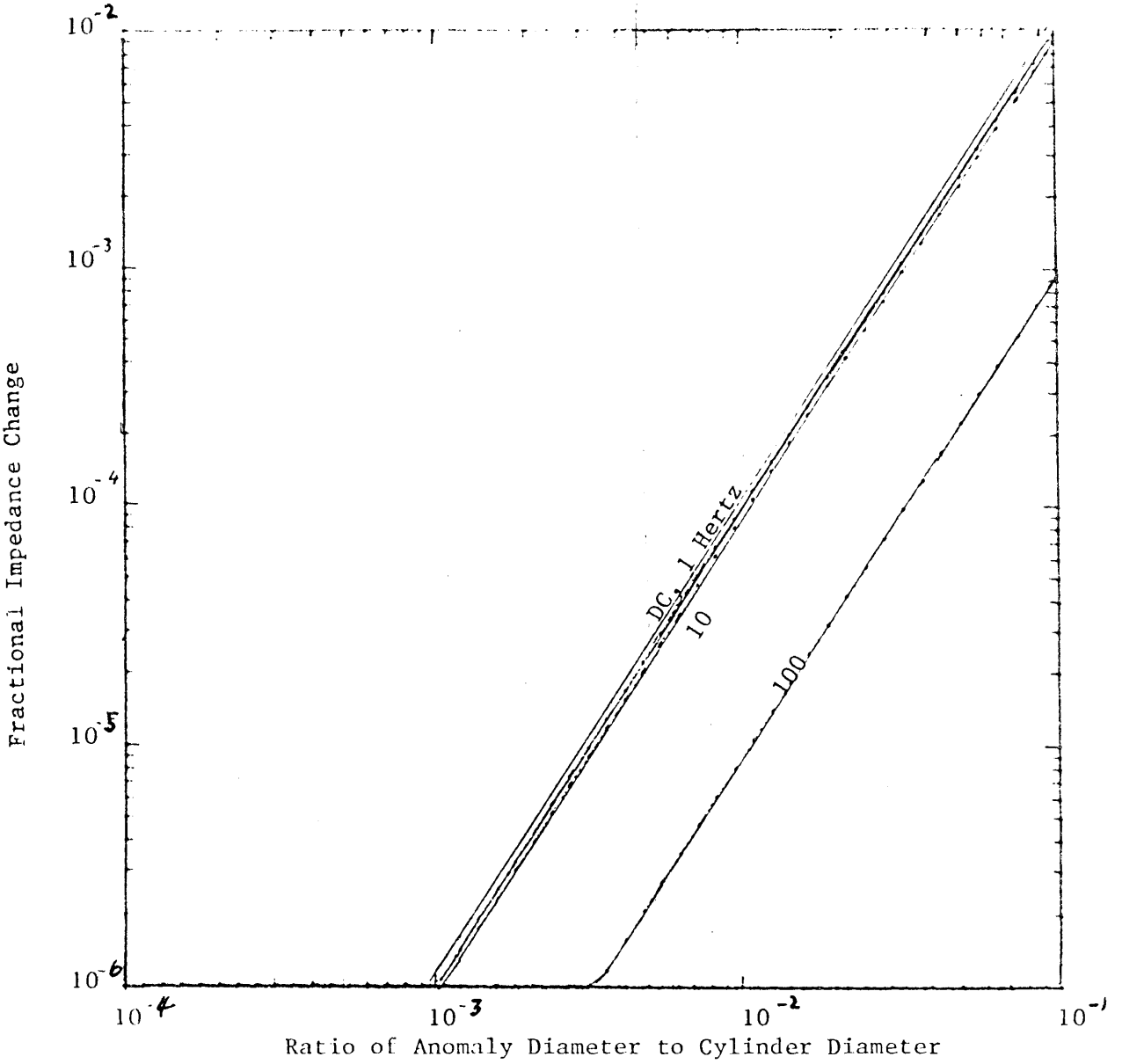

Figure 4 : Fractional Impedance Change for Sensor as a Function of Anomaly Size. The Anomaly is Slightly Offset from the Center of the Cylinder (ρ_1 = .1a).

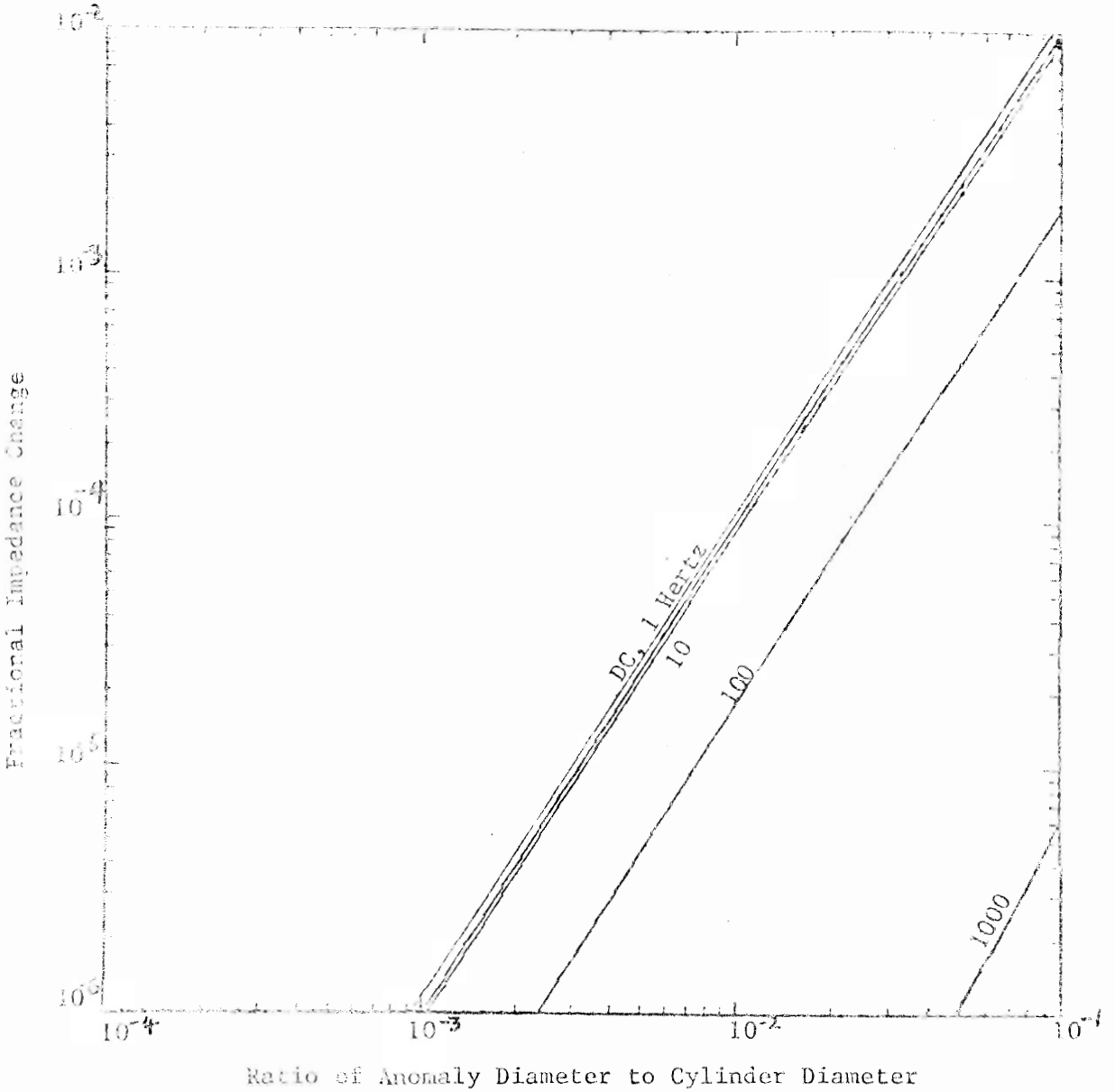

Figure 5 : Fractional Impedance Change for a Sensor as a Function of Anomaly Size. The Anomaly is Offset one-half the Cylinder Radius (ρ_1 = .5a).

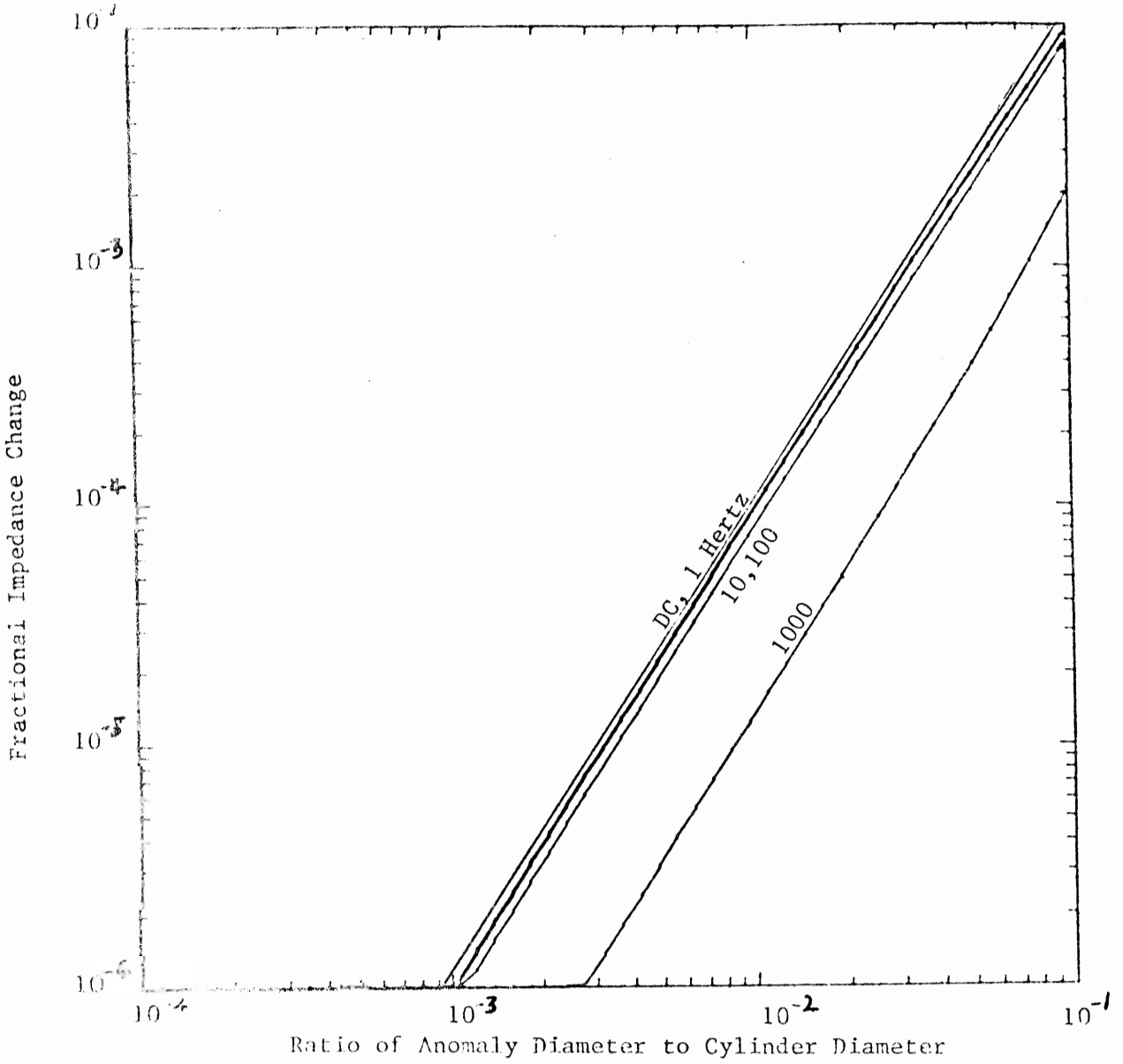

Figure 6 : Fractional Impedance Change for a Sensor as a Function of Anomaly Size. The Anomaly is Near the Cylinder Surface. (ρ_1 = .8a)

Section 7

Scattering by a Slender Void in a Homogeneous Conducting Wire Rope

DAVID A. HILL
and
JAMES R. WAIT

Abstract. A thin prolate spheroidal void in an infinite conducting circular cylinder is used to model a broken strand in a wire rope. The rope is excited by an azimuthal magnetic line current which is a model for a thin toroidal coil. The anomalous external fields are computed from the induced electric and magnetic dipole moments of the void. The results have applications to nondestructive testing of wire ropes.

Electromagnetic nondestructive testing is widely used in the metals industry to inspect and evaluate materials [1]. Both dc (direct current) and ac (alternating current) methods [2,3] are currently used for inspection of wire ropes [4] which are made of electrically conducting ferromagnetic material. In both methods, the magnetic field is applied along the axis of the rope, and rope irregularities produce magnetic field changes which induce voltages in the sensing coils.

An alternative ac method would excite the rope with an axial electric field rather than an axial magnetic field. Since axial electric currents would be induced, this method might be more sensitive to broken strands than the present ac method which induces only azimuthal currents which tend to flow normally to the strands. Such a method could also be used on electrical conductors which are not ferromagnetic.

An appropriate source for excitation of axial electric currents is a toridal coil which encircles the rope, and a magnetic current model for the toroidal source coil has been analyzed [5]. Expressions for both the interior and exterior fields were derived for a homogeneous wire rope.

In this paper we wish to allow for the presence of a small slender void within the rope. Such a void can be considered a model for a broken strand. The void is also allowed to be oriented at any arbitrary angle to the rope axis to account for the winding geometry of the wire rope. The induced electric and magnetic dipole moments are computed from the primary fields and the electric and magnetic polarizabilities of the void. We then obtain expressions for the external fields of electric and magnetic dipoles of arbitrary orientation. It is these external fields which are the observable quantities in any EM nondestructive testing method. The particular expressions, derived for the external fields of internal electric and magnetic dipoles, should be useful in future analyses of other types of small imperfections in wire ropes. Of course, in such cases, the electric and magnetic polarizabilities would be different.

Primary Field Excitation

In a previous analysis [5], we analyzed an azimuthal current sheet source which encircled the rope. The current sheet was allowed to have arbitrary width in the z or axial direction and arbitrary azimuthal extent. This source results in fairly complicated expressions for the electric and magnetic fields. Since, in this paper, we are primarily concerned with the fields scattered by the void, we take the simpler special case for the source shown in Fig. 1. Specifically, a magnetic current ring of strength K is located at a radius b in the plane $z = 0$. This is a model for a thin toroidal coil which completely encircles the rope. The adopted time dependence is $\exp(i\omega t)$ for all source and field quantities.

The rope is assumed to be infinitely long and has radius a. It has conductivity σ_w, permittivity ε_w, and permeability μ_w. The surrounding free space has permittivity ε_o and permeability μ_o. For now, we defer discussion of the void properties and consider only the homogeneous rope.

Because of the symmetry of the source and the rope, the fields are TM (transverse magnetic) and independent of ϕ. The magnetic field has only a nonzero azimuthal component H_ϕ^{pr}, and the electric field has only nonzero axial and radial components E_z^{pr} and E_ρ^{pr}. The superscript pr denotes the fields in the absence of the void. These primary fields have been derived previously [5], and the explicit forms both inside and outside the rope are given here in Appendix A. We note that E_ρ^{pr} and H_ϕ^{pr} are zero for $\rho = 0$. On the other hand, E_z^{pr} is nearly independent of ρ inside the rope for sufficiently low frequencies.

Induced Dipole Moments

We select a thin prolate spheroid of conductivity σ_v, permittivity ε_v, and permeability μ_v in order to model a broken strand. The prolate spheroidal shape is a convenient one because its electric and magnetic polarizabilities are known. However, we would not expect a significant difference for a thin circular cylinder of the same length and volume. To account for the winding geometry of the rope, we allow a rotation of the major axis of the spheroid about the ρ' axis by an angle α. Thus the major axis is oriented at an angle α to the unit vector $\hat{z}'$ and an angle $\pi/2 + \alpha$ to the unit vector $\hat{\phi}'$ as indicated in Fig. 1c.

Since the void has a contrast in both the electric and magnetic properties, both electric and magnetic dipole moments will be induced [6]. The electric polarizabilities for the incident electric field applied along the major axis, α_{maj}^e, or along the minor axis, α_{min}^e, are given by

$$\alpha^{e}_{maj} = -V(\sigma_w - \sigma_v) \tag{1}$$

and

$$\alpha^{e}_{min} = \frac{-2V(\sigma_w - \sigma_v)}{1 + \sigma_v/\sigma_w} \quad , \tag{2}$$

where V is the volume of the thin prolate spheroid. Since we anticipate the use of very low frequencies, we have neglected displacement currents. To include them, σ_w would be replaced by $\sigma_w + i\omega\varepsilon_w$ and σ_v would be replaced by $\sigma_v + i\omega\varepsilon_v$ in (1) and (2). The magnetic polarizabilities for the incident magnetic field applied along the major axis, α^{m}_{maj}, or along the minor axis, α^{m}_{min}, are similarly given by

$$\alpha^{m}_{maj} = -Vi\omega(\mu_w - \mu_v) \tag{3}$$

and

$$\alpha^{m}_{min} = \frac{-2Vi\omega(\mu_w - \mu_v)}{1 + \mu_v/\mu_w} \tag{4}$$

In order to compute the induced dipole moments, it is first necessary to resolve the incident electric and magnetic fields into components along the major and minor axes. The resultant induced dipole moments can then be resolved into the more convenient ρ, ϕ, and z components. When this is done, the induced electric dipole moments are found to be

$$(Ids)_z = E^{pr}_z(\alpha^{e}_{maj}\cos^2\alpha + \alpha^{e}_{min}\sin^2\alpha) \ , \tag{5}$$

$$(Ids)_\phi = E^{pr}_z(\alpha^{e}_{min} - \alpha^{e}_{maj})\sin\alpha\cos\alpha \ , \tag{6}$$

$$(Ids)_\rho = E^{pr}_\rho \alpha^{e}_{min} \tag{7}$$

In (5)-(7), the primary electric field components E^{pr}_z and E^{pr}_ρ are evaluated at ρ', ϕ', z'. Similarly, the induced magnetic dipole moments are found to be

$$(Kd\ell)_z = H^{pr}_\phi(\alpha^{m}_{min} - \alpha^{m}_{maj})\sin\alpha\cos\alpha \ , \tag{8}$$

$$(Kd\ell)_\phi = H^{pr}_\phi(\alpha^{m}_{min}\cos^2\alpha + \alpha^{m}_{maj}\sin^2\alpha) \ , \tag{9}$$

$$(Kd\ell)_\rho = 0 \ . \tag{10}$$

Note that the units of the induced electric dipole moments in (5)-(7) are ampere meters, and the units of the induced magnetic dipole moments in (8)-(10) are volt-meters.

These induced dipole moments are the sources of the scattered field. In the following section, the specific expressions for the scattered field are discussed.

External Scattered Fields

The scattered field external to the rope is the observable quantity in any NDT system. Since we anticipate the use of coils for sensors, we will consider primarily the scattered magnetic field components $H_\rho^{sc}(\rho,\phi,z)$, $H_\phi^{sc}(\rho,\phi,z)$, and $H_z^{sc}(\rho,\phi,z)$. Each of these components can be written as a superposition of the contributions from each of the six induced dipole sources. (Actually, there are only five nonzero sources since $(Kd\ell)_\rho$ is zero for the specific configuration considered here).

The three scattered field components can be compactly written in the following matrix form

$$\begin{bmatrix} H_\rho^{sc} \\ H_\phi^{sc} \\ H_z^{sc} \end{bmatrix} = \begin{bmatrix} G_{\rho\rho}^e & G_{\rho\phi}^e & G_{\rho z}^e \\ G_{\phi\rho}^e & G_{\phi\phi}^e & G_{\phi z}^e \\ G_{z\rho}^e & G_{z\phi}^e & G_{zz}^e \end{bmatrix} \cdot \begin{bmatrix} (Ids)_\rho \\ (Ids)_\phi \\ (Ids)_z \end{bmatrix} + \begin{bmatrix} G_{\rho\rho}^m & G_{\rho\phi}^m & G_{\rho z}^m \\ G_{\phi\rho}^m & G_{\phi\phi}^m & G_{\phi z}^m \\ G_{z\rho}^m & G_{z\phi}^m & G_{zz}^m \end{bmatrix} \cdot \begin{bmatrix} (Kd\ell)_\rho \\ (Kd\ell)_\phi \\ (Kd\ell)_z \end{bmatrix} \tag{11}$$

In the first 3 by 3 matrix, $G^e_{\rho\rho}$ is the ρ component of H at (ρ,ϕ,z) produced by a unit ρ-directed electric dipole at (ρ',ϕ',z'), $G^e_{\rho\phi}$ is the ρ component of H produced by a unit ϕ-directed electric dipole at (ρ',ϕ',z'), etc. The second 3 by 3 matrix is similar except that the G^m elements correspond to unit magnetic dipoles. We choose the above matrix notation rather than the elegant dyadic Green's function notation [7] because we are interested in the relative importance of each source and G term. Also, for the cylindrical geometry encountered here, all of the matrix elements can be derived in a systematic manner from z components of electric and magnetic Hertz vectors [8]. The specific expressions for the matrix elements are derived in Appendix B.

Numerical Results

The quantities of most interest in NDT are the external $(\rho>a)$ magnetic field components which are observed with the sensing coils. The primary magnetic field has only a ϕ component H^{pr}_{ϕ} which is given by (A-7) for $a < \rho < b$ or by (A-11) for $\rho > b$. The scattered magnetic field has all three components as given by (11). A computer program has been written to compute the external primary and scattered magnetic field components.

There are too many parameters to present a thorough parametric study here. For all numerical results shown the following parametric values remain fixed: $a = 1$ cm, $\sigma_w = 1.1 \times 10^6$mho/m, $\mu_w = 200\ \mu_o$, $b = 2$ cm, frequency = 10 Hz, $\rho = 2$ cm, $\sigma_v = 0$, and $\mu_v = \mu_o$. For this low frequency, the conduction currents dominate, and the permittivities ε_w and ε_v are unimportant. The above values of σ_w and μ_w are roughly representative of stainless steel [9], but the permeability of steel is quite variable [10]. For the above parameters, the radius a is approximately one skin depth.

In Figs. 2-9, we show the magnitude of the scattered magnetic field components normalized by VH_{ϕ}^{pr} as a function of $\phi - \phi'$. The reason for showing the $\phi - \phi'$ dependence is that, although the primary field is independent of ϕ, the scattered field varies considerably in ϕ. This variation might dictate the use of multiple sensing coils spaced in azimuth around the rope. The curves are normalized by the primary field because the anomalous scattered field is measured in the presence of the primary field and their ratio is thus of interest. We also normalize the results to the volume V of the void in order to make the curves more general. However, a typical value for V might be on the order of $10^{-8}m^3$ (= 1 cm × 1 mm × 1 mm).

In Figs. 2 and 3, we set $z = z' = 5a$ and $\alpha = 0°$. By symmetry, $H_z^{sc} \simeq 0$ for this case. H_{ρ}^{sc} and H_{ϕ}^{sc} are of approximately the same level, but H_{ρ}^{sc} is odd in $\phi - \phi'$ while H_{ϕ}^{sc} is even. Note the decrease in scattered field as the void is moved from the outer region $(\rho'/a = 0.9)$ toward the center $(\rho'/a = 0.1)$ of the rope.

In Figs. 4, 5, and 6, we retain $z = 5a$ and $\alpha = 0°$ but allow z' to vary. Also, we set $\rho'/a = 0.5$. Note that the level of H_{ρ}^{sc} and H_{ϕ}^{sc} increases as z' approaches z. However, H_z^{sc} is very small for $z' = z$, and its peak level is at about $z'/a = 3.75$. Since $\alpha = 0°$ in Figs. 2-6, only the axial and radial electric dipole moments, $(Ids)_z$ and $(Ids)_{\rho}$, and the azimuthal magnetic dipole, $(Kd\ell)_{\phi}$, are induced. Also, $(Ids)_{\rho}$ is very small because its exciting field E_{ρ}^{pr} is small. The calculations reveal that $(Ids)_z$ and $(Kd\ell)_{\phi}$ contribute approximately equally to the scattered field.

In Figs. 7-9, we have $z = z' = 5a$ and $\rho'/a = 0.5$, but we allow α to vary from 0° to 30°. Nonzero values of α allow two additional dipole moments, $(Ids)_{\phi}$ and $(Kd\ell)_z$ to be induced. The result is a decrease in the level of H_{ϕ}^{sc} and H_{ρ}^{sc} and an increase in the level of H_z^{sc}.

The phase of the scattered field was also computed, but was found to be of less interest. Also, the individual dipole contributions were computed, and they are of individual interest since they will be excited differently for other sources on other void configurations.

Concluding Remarks

An idealized model for a wire break in an infinite conducting rope has been analyzed. The thin prolate spheroidal void has been shown to produce a significant anomaly in the external magnetic field when the rope is excited by a thin toroidal coil. In general, all three components of the scattered magnetic field are nonzero, but the azimuthal dependence is fairly complicated and contains some deep nulls. This suggests that multiple sensing coils of various locations and orientations might be worthwhile.

Although we have generated numerical results for the specific case of a thin prolate spheroidal void, the formulation given here actually yields the external fields for arbitrary induced electric and magnetic dipole moments. Thus the formulation is useful for any type of rope imperfection that can be characterized by induced electric and magnetic dipole moments. This requires only that the rope imperfection be small in terms of the rope radius and the rope skin depth. Larger imperfections should have a similar qualitative behavior, but could probably be rigorously analyzed only by solving an integral equation for the fields in the imperfection.

Also, it is a simple matter to perform similar calculations for a solenoidal coil of the type used in present NDT systems [3]. The scattered field calculation remains unchanged, but the primary field would be $TE(E_z^{pr} = 0)$ rather than $TM(H_z^{pr} = 0)$. Some calculations for this case have been carried out by Burrows [11] for the special case where both exciting and sensing coils are coaxial with the tubular specimen.

APPENDIX A - Primary Fields

The previous analysis for the homogeneous rope excitation [5] can be reduced to the present thin current ring source by letting the thickness ℓ of the magnetic current source approach zero and by setting the azimuthal extent of the source equal to 2π. The resultant field expressions take different forms in the three regions, $\rho < a$, $a < \rho < b$, and $\rho > b$.

Inside the rope ($\rho < a$), we find

$$E_z^{pr} = -\int_{-\infty}^{\infty} w^2 a_o I_o(w\rho)\exp(-i\lambda z)d\lambda \ , \tag{A-1}$$

$$E_\rho^{pr} = -\int_{-\infty}^{\infty} i\lambda w a_o I_1(w\rho)\exp(-i\lambda z)d\lambda \ , \tag{A-2}$$

$$H_\phi^{pr} = -\int_{-\infty}^{\infty} i\omega\varepsilon_w w a_o I_1(w\rho)\exp(-i\lambda z)d\lambda \ , \tag{A-3}$$

where $w = (\lambda^2+\gamma_w^2)^{1/2}$, $\gamma_w^2 = i\omega\mu_w(\sigma_w+i\omega\varepsilon_w)$, $i\omega\hat{\varepsilon}_w = \sigma_w + i\omega\varepsilon_w$, and I_o and I_1 are zero and first order modified Bessel functions. The factor a_o is given by

$$a_o = \frac{-\gamma_o B_o}{w^2 a I_o(wa)K_o(ua)} \cdot \left[\frac{\gamma_o K_o'(ua)}{uK_o(ua)} - \eta_o y_o\right]^{-1} \ , \tag{A-4}$$

where

$$B_o = \frac{KbK_o'(ub)}{4\pi^2 u} \ , \quad u = (\lambda^2+\gamma_o^2)^{1/2}$$

$$\gamma_o = i\omega(\mu_o\varepsilon_o)^{1/2} \ , \quad \eta_o = (\mu_o/\varepsilon_o)^{1/2} \ ,$$

$$y_o = \frac{i\omega\hat{\varepsilon}_w}{w}\ \frac{I_1(wa)}{I_o(wa)} \ ,$$

K is the strength of the magnetic current ring, K_o is a zero order modified Bessel function, and prime ' denotes differentiation with respect to the argument.

In the region between the rope and the source ($a < \rho < b$), we find

$$E_z^{pr} = -\int_{-\infty}^{\infty} u^2[B_o I_o(u\rho) + C_o K_o(u\rho)]\exp(-i\lambda z)d\lambda \ , \tag{A-5}$$

$$E_\rho^{pr} = -\int_{-\infty}^{\infty} i\lambda u[B_o I_1(u\rho) - C_o K_1(u\rho)]\exp(-i\lambda z)d\lambda \ , \tag{A-6}$$

$$H_\phi^{pr} = -\int_{-\infty}^{\infty} i\omega\varepsilon_o u[B_o I_1(u\rho) - C_o K_1(u\rho)]\exp(-i\lambda z)d\lambda \ , \tag{A-7}$$

where

$$C_o = -\frac{I_o(ua)\left[\frac{\gamma_o}{u}\frac{I_o'(ua)}{I_o(ua)} - \eta_o y_o\right]}{K_o(ua)\left[\frac{\gamma_o}{u}\frac{K_o'(ua)}{K_o(ua)} - \eta_o y_o\right]} B_o \tag{A-8}$$

Outside the source ($\rho > b$), we find

$$E_z^{pr} = -\int_{-\infty}^{\infty} u^2 A_o K_o(u\rho)\exp(-i\lambda z)d\lambda \ , \tag{A-9}$$

$$E_\rho^{pr} = \int_{-\infty}^{\infty} i\lambda u A_o K_1(u\rho)\exp(-i\lambda z)d\lambda \ , \tag{A-10}$$

$$H_\phi^{pr} = \int_{-\infty}^{\infty} i\omega\varepsilon_o u A_o K_1(u\rho)\exp(-i\lambda z)d\lambda \ , \tag{A-11}$$

where

$$A_o = C_o - B_o I_1(ub)/K_1(ub) \ . \tag{A-12}$$

APPENDIX B - Dipole Fields

The derivation of the fields produced by a dipole source within a circular wire rope is analogous to that for a dipole source in a circular tunnel [8,9], and some of the details are excluded here. The fields within the wire rope for $\rho' < \rho < a$ can be obtained from U_w and V_w which are the z components of electric and magnetic Hertz vectors.

$$U_w = \Gamma[A_m(\lambda)K_m(w\rho) + P_m(\lambda)I_m(w\rho)] \quad , \tag{B-1}$$

$$V_w = \Gamma[B_m(\lambda)K_m(w\rho) + Q_m(\lambda)I_m(w\rho)] \quad , \tag{B-2}$$

where

$$\Gamma[\ \ ] = \int_{-\infty}^{\infty} \sum_{-\infty}^{\infty} [\ \ ] e^{-im(\phi-\phi')} e^{-i\lambda(z-z')} d\lambda \tag{B-3}$$

$A_m(\lambda)$ and $B_m(\lambda)$ are functions of the source dipole and will later be given for the six dipole types. P_m and Q_m are determined from the boundary conditions at $\rho = a$ and are given by

$$P_m = -\left\{ A_m \left[\left(\frac{m\lambda}{w^2 a} - \alpha_m \right)^2 + \left(\frac{\gamma_w K'_m}{wK_m} + \eta_w Y_m \right)\left(\frac{\gamma_w I'_m}{wI_m} + \frac{Z_m}{\eta_w} \right) \right] I_m K_m \right.$$
$$\left. + B_m \left(\frac{m\lambda}{w^2 a} - \alpha_m \right) \frac{i\omega\mu_w}{w^2 a} \right\} D_m^{-1} \quad , \tag{B-4}$$

$$Q_m = -\left\{ B_m \left[\left(\frac{m\lambda}{w^2 a} - \alpha_m \right)^2 + \left(\frac{\gamma_w I'_m}{wI_m} + \eta_w Y_m \right)\left(\frac{\gamma_w K'_m}{wK_m} + \frac{Z_m}{\eta_w} \right) \right] I_m K_m \right.$$
$$\left. - A_m \left(\frac{m\lambda}{w^2 a} - \alpha_m \right) \frac{i\omega\hat{\varepsilon}_w}{w^2 a} \right\} D_m^{-1} \quad , \tag{B-5}$$

where

$$D_m = \left[\left(\frac{m\lambda}{w^2 a} - \alpha_m \right)^2 + \left(\frac{\gamma_w I'_m}{wI_m} + \eta_w Y_m \right)\left(\frac{\gamma_w I'_m}{wI_m} + \frac{Z_m}{\eta_w} \right) \right] I_m^2 \quad ,$$

$$\alpha_m = \frac{m\lambda}{u^2 a} \quad , \quad Z_m = \frac{-i\omega\mu_o}{u} \frac{K'_m(ua)}{K_m(ua)} \quad ,$$

and

$$Y_m = \frac{-i\omega\varepsilon_o}{u} \frac{K_m'(ua)}{K_m(ua)} .$$

The argument of the modified Bessel functions I_m and K_m is wa unless indicated otherwise.

The external fields $(\rho > a)$ can be obtained from

$$U = \Gamma[U_m] \quad \text{and} \quad V = \Gamma[V_m] \tag{B-6}$$

where

$$U_m = S_m(\lambda)K_m(u\rho)$$

and

$$V_m = T_m(\lambda)K_m(u\rho)$$

Continuity of E_z and H_z at $\rho = a$ yields

$$S_m = \frac{w^2}{u^2}\left[\frac{A_m K_m(wa) + P_m I_m(wa)}{K_m(ua)}\right] \tag{B-7}$$

and

$$T_m = \frac{w^2}{u^2}\left[\frac{B_m K_m(wa) + Q_m I_m(wa)}{K_m(ua)}\right] \tag{B-8}$$

The external magnetic field components can be written

$$H_\rho = \Gamma[H_{\rho m}] , \quad H_\phi = \Gamma[H_{\phi m}] , \quad \text{and} \quad H_z = \Gamma[H_{zm}] \tag{B-9}$$

where

$$H_{\rho m} = -i\lambda \frac{\partial V_m}{\partial \rho} + \frac{\omega\varepsilon_o m}{\rho} U_m$$

$$= -i\lambda u T_m K_m'(u\rho) + \frac{\omega\varepsilon_o m}{\rho} S_m K_m(u\rho) , \tag{B-10}$$

$$H_{\phi m} = \frac{-m\lambda}{\rho} V_m - i\omega\varepsilon_o \frac{\partial U_m}{\partial \rho}$$

$$= \frac{-m\lambda}{\rho} T_m K_m(u\rho) - i\omega\varepsilon_o u S_m K_m'(u\rho) , \tag{B-11}$$

and

$$H_{zm} = -u^2 V_m = -u^2 T_m K_m(u\rho) . \tag{B-12}$$

Similar expressions are available for the electric field components.

Equations (B-1)-(B-12) yield the external magnetic field components in terms of A_m and B_m which are functions of the source dipole. We now tabulate A_m and B_m for the six dipole types [8].

For a radial electric dipole $(Ids)_\rho$, we have

$$A_m = (Ids)_\rho \cdot \frac{-i\lambda}{4\pi^2 i\omega\hat{\varepsilon}_w w} I'_m(w\rho') \tag{B-13}$$

and

$$B_m = (Ids)_\rho \cdot \frac{im}{4\pi^2 w^2 \rho'} I_m(w\rho') \tag{B-14}$$

For an azimuthal electric dipole $(Ids)_\phi$, we have

$$A_m = (Ids)_\phi \cdot \frac{m\lambda}{4\pi^2 i\omega\hat{\varepsilon}_w w^2 \rho'} I_m(w\rho') \tag{B-15}$$

and

$$B_m = (Ids)_\phi \cdot \frac{-1}{4\pi^2 w} I'_m(w\rho') \ . \tag{B-16}$$

For an axial electric dipole $(Ids)_z$, we have

$$A_m = (Ids)_z \cdot \frac{I_m(w\rho')}{4\pi^2 i\omega\hat{\varepsilon}_w} \tag{B-17}$$

and

$$B_m = 0 \ . \tag{B-18}$$

For a radial magnetic dipole $(Kd\ell)_\rho$, we have

$$A_m = (Kd\ell)_\rho \cdot \frac{im}{4\pi^2 w^2 \rho'} I_m(w\rho') \tag{B-19}$$

and

$$B_m = (Kd\ell)_\rho \cdot \frac{-i\lambda}{4\pi^2 w i\omega\mu_w} I'_m(w\rho') \tag{B-20}$$

For an azimuthal magnetic dipole $(Kd\ell)_\phi$, we have

$$A_m = (Kd\ell)_\phi \cdot \frac{-1}{4\pi^2 w^2} I'_m(w\rho') \tag{B-21}$$

and

$$B_m = (Kd\ell)_\phi \cdot \frac{m\lambda}{4\pi^2 w^2 i\omega\mu_w \rho'} I_m(w\rho') \tag{B-22}$$

For an axial mangetic dipole $(Kd\ell)_z$, we have

$$A_m = 0 \tag{B-23}$$

and

$$B_m = (Kd\ell)_z \cdot \frac{I_m(w\rho')}{4\pi^2 i\omega\mu_w} . \tag{B-24}$$

We are now able to define the matrix elements required in (11) in terms of H_ρ, H_ϕ, and H_z given in (B-9). For each of the six dipole types, we can define the required three elements in a column matrix as follows.

For a radial electric dipole $(Ids)_\rho$, we have

$$\begin{bmatrix} G^e_{\rho\rho} \\ G^e_{\phi\rho} \\ G^e_{z\rho} \end{bmatrix} = \frac{1}{(Ids)_\rho} \begin{bmatrix} H_\rho \\ H_\phi \\ H_z \end{bmatrix} \tag{B-25}$$

For an azimuthal electric dipole $(Ids)_\phi$, we have

$$\begin{bmatrix} G^e_{\rho\phi} \\ G^e_{\phi\phi} \\ G^e_{z\phi} \end{bmatrix} = \frac{1}{(Ids)_\phi} \begin{bmatrix} H_\rho \\ H_\phi \\ H_z \end{bmatrix} \tag{B-26}$$

For an axial electric dipole $(Ids)_z$, we have

$$\begin{bmatrix} G^e_{\rho z} \\ G^e_{\phi z} \\ G^e_{zz} \end{bmatrix} = \frac{1}{(Ids)_z} \begin{bmatrix} H_\rho \\ H_\phi \\ H_z \end{bmatrix} \tag{B-27}$$

For a radial magnetic dipole $(Kd\ell)_\rho$, we have

$$\begin{bmatrix} G^m_{\rho\rho} \\ G^m_{\phi\rho} \\ G^m_{z\rho} \end{bmatrix} = \frac{1}{(Kd\ell)_\rho} \begin{bmatrix} H_\rho \\ H_\phi \\ H_z \end{bmatrix} \tag{B-28}$$

For an azimuthal magnetic dipole $(Kd\ell)_\phi$, we have

$$\begin{bmatrix} G^m_{\rho\phi} \\ G^m_{\phi\phi} \\ G^m_{z\phi} \end{bmatrix} = \frac{1}{(Kd\ell)_\phi} \begin{bmatrix} H_\rho \\ H_\phi \\ H_z \end{bmatrix} \tag{B-29}$$

For an axial magnetic dipole $(Kd\ell)_z$, we have

$$\begin{bmatrix} G^m_{\rho z} \\ G^m_{\phi z} \\ G^m_{zz} \end{bmatrix} = \frac{1}{(Kd\ell)_z} \begin{bmatrix} H_\rho \\ H_\phi \\ H_z \end{bmatrix} \tag{B-30}$$

In order to numerically evaluate the G elements, we encounter the infinite summation and integration of the Γ operator as indicated by (B-9). However, all of the G elements are either even or odd in m and λ, and the summation and integration can be taken over positive values of m and λ to reduce the computation time by a factor of 4. Also, all G elements are calculated in parallel which means that the required modified Bessel are calculated only once resulting in a large time savings. In evaluating the λ integration, a variable step size integration is used to deal effectively with the rapid variation for small λ and the slower variation for large λ. Thus the subroutine which computes all 18 elements makes use of all these time saving features and is quite fast.

References

1. H.L. Libby: *Introduction to Electromagnetic Nondestructive Test Methods* (Wiley Interscience, New York 1971). [Gives numerous references].
2. C.H. Larsen, R.A. Egen, R.D. Jones, H.A. Cross: Report to the U.S. Bureau of Mines on Contract No. H0101741, June (1971).
3. J.G. Lang: The Canadian Mining and Metallurgical (CIM) Bulletin. 415 (1969).
4. E.R. Hoskins: Report to the U.S. Bureau of Mines on Contract No. H0346193 (South Dakota School of Mines & Technology) July (1975).
5. D.A. Hill, J.R. Wait: J. Appl. Phys 48, 4893 (1977).
6. W.R. Smythe: *Static and Dynamic Electricity* , Sec. 5.28, p. 171, 3rd ed. (McGraw-Hill Book Co., New York 1968).
7. C.T. Tai: *Dyadic Green's Functions in Electromagnetic Theory* (Scranton, Intext 1971).
8. J.R. Wait, D.A. Hill: Appl. Phys. 11, 351 (1976).
9. D.R.J. White: *Electromagnetic Shielding Material and Performance*, Sec. 2.1 (Don White Consultants, Inc., Germantown, MD 1975).
10. A.G. Kandoian: *Reference Data for Radio Engineers*, pp. 4-32 (ITT Corp., New York 1968).
11. M.L. Burrows: Ph.D Thesis (Dept. of Electrical Engrg., University of Michigan, Ann Arbor 1964).

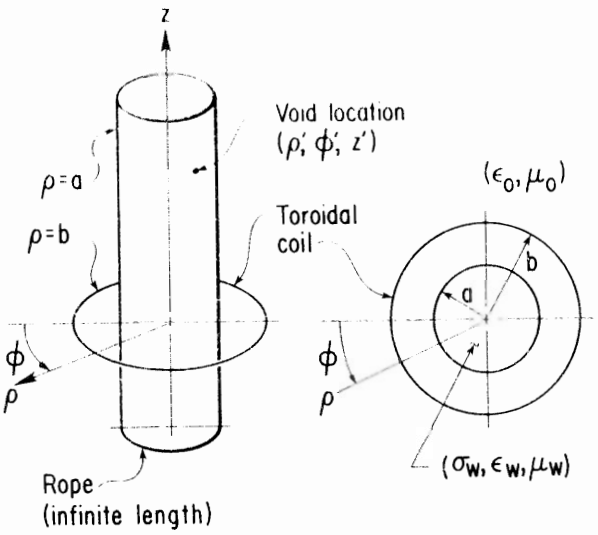

Fig. 1a Fig. 1b

Fig. 1. Thin toroidal coil surrounding a metal rope of infinite length.

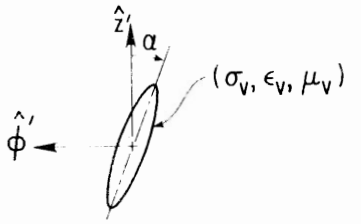

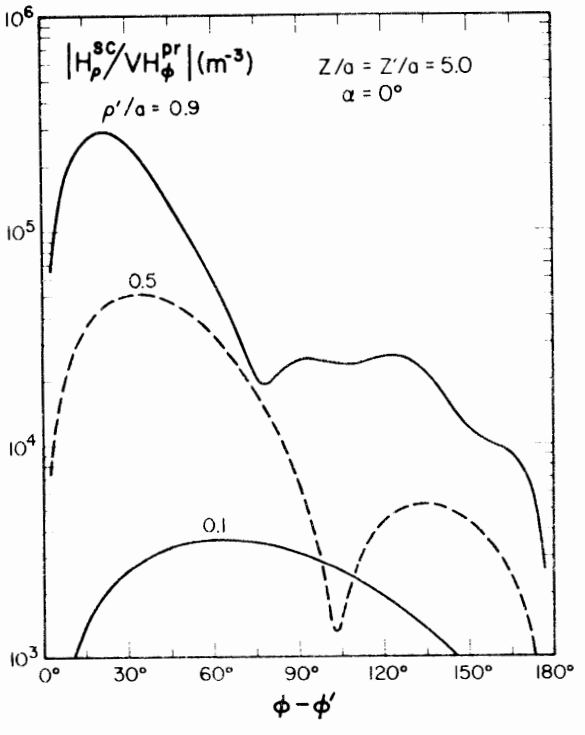

Fig. 2. The normalized magnitude of the scattered radial magnetic field for various void locations ρ'.

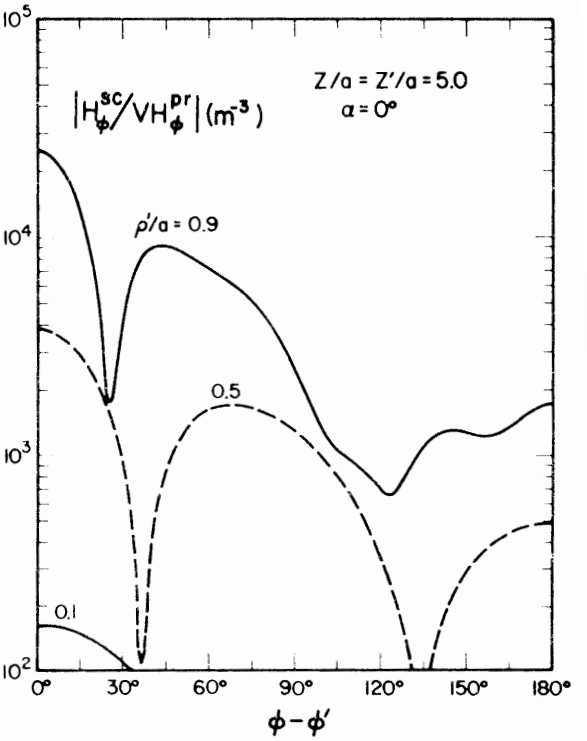

Fig. 3. The normalized magnitude of the scattered azimuthal magnetic field for various void locations ρ'.

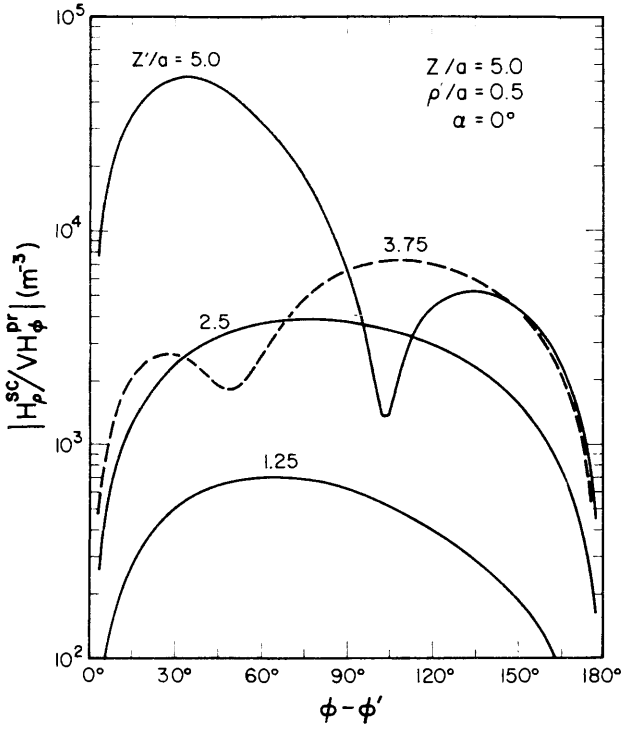

Fig. 4. The normalized magnitude of the scattered radial magnetic field for various void locations z'.

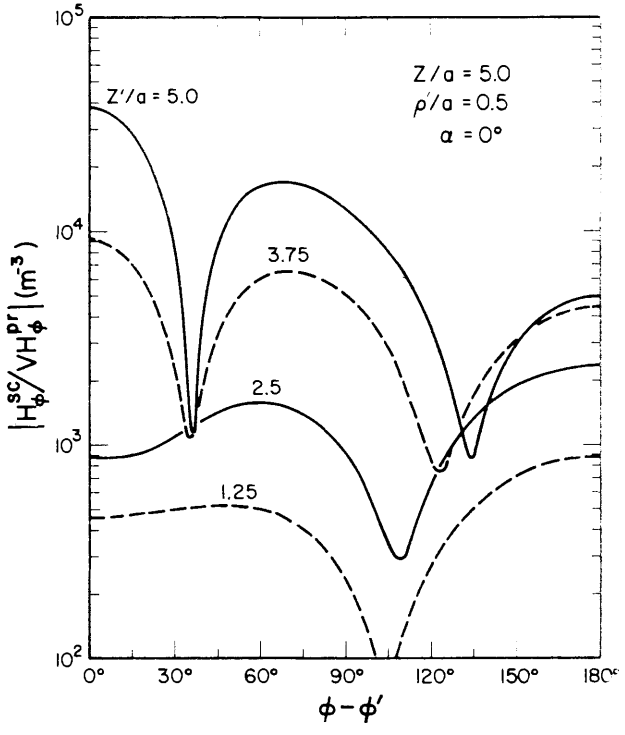

Fig. 5. The normalized magnitude of the scattered azimuthal magnetic field for various void locations z'.

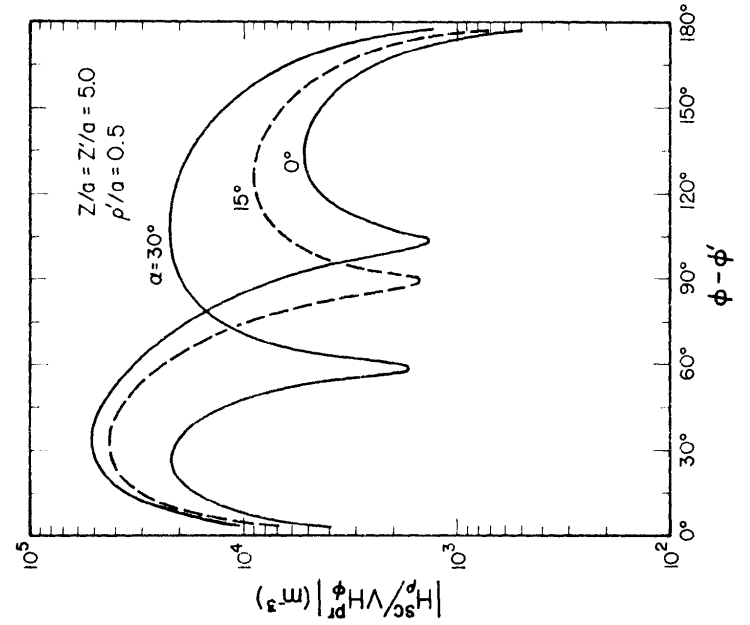

Fig. 7. The normalized magnitude of the scattered radial magnetic field for various void orientations α.

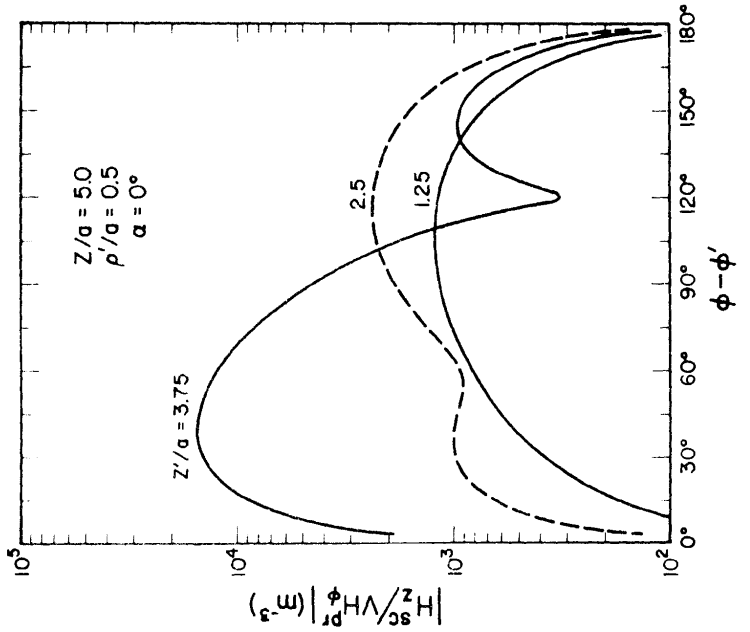

Fig. 6. The normalized magnitude of the scattered axial magnetic field for various void locations z'.

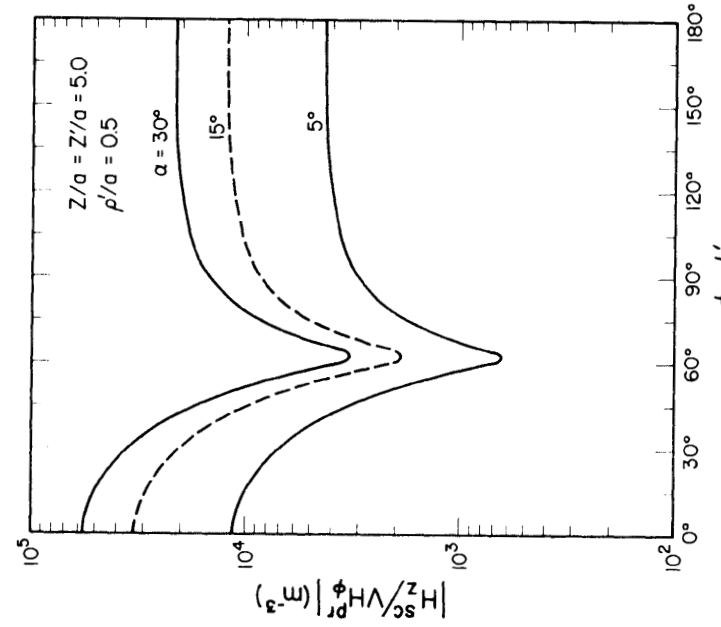

Fig. 9. The normalized magnitude of the scattered axial magnetic field for various void orientations α.

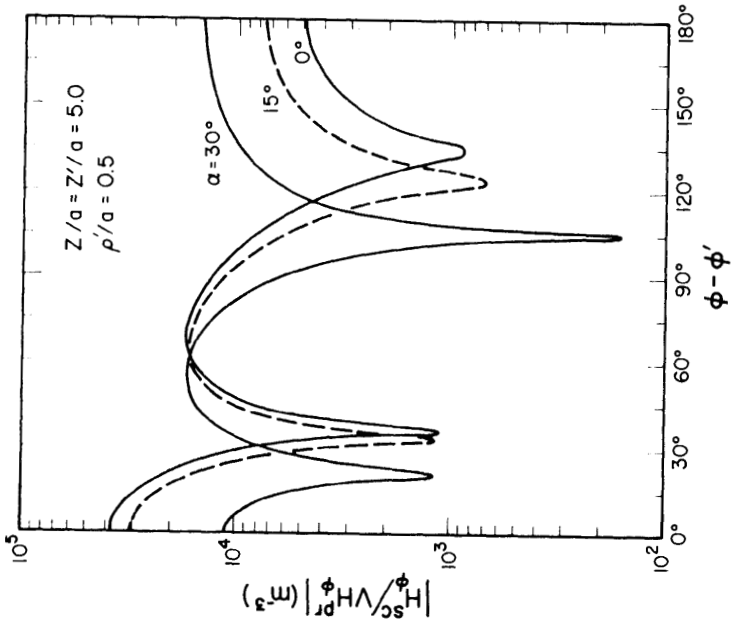

Fig. 8. The normalized magnitude of the scattered azimuthal magnetic field for various void orientations α.

Section 8

Electromagnetic Field Perturbation by an Internal Void in a Conducting Cylinder Excited by a Wire Loop

DAVID A. HILL
and
JAMES R. WAIT

Abstract. A thin prolate spheroidal void in an infinite conducting circular cylinder is used to model an internal flaw in a wire rope. The rope is excited by an electric ring current which is a model for a thin solenoid or multi-turn wire loop. The anomalous external fields are computed from the induced electric and magnetic dipole moments of the void. For this type of excitation, the induced axial magnetic dipole moment is the dominant contributor to the scattered field. The results have application to nondestructive testing of wire ropes.

Introduction

Electromagnetic NDT (Nondestructive Testing) is widely used for inspection and evaluation of metals [1], and electromagnetic methods in NDT of wire ropes [2] have recently been reviewed [3]. Both DC and AC methods [4,5] are currently in use. In both methods, the magnetic field is applied along the axis of the rope, and rope irregularities produce magnetic field changes which induce voltages in the sensing coils. A two-dimensional model of solenoidal (electric current ring) excitation of a homogeneous wire rope has now been analyzed fully [6]. The toroidal coil (magnetic current ring)

excitation was also treated by invoking the principle of duality. A further analysis deals with a two-dimensional model for a wire rope with an internal anomaly [7], and the resulting change in the input impedance of the surrounding solenoid.

Here we consider a three-dimensional model in which an electric current ring is used to model a thin solenoid or multi-turn wire loop. The analogous problem of a magnetic current ring has already been solved [8]; thus the needed primary field expressions can be obtained from the magnetic ring current solution by duality. We allow for the presence of a small slender void within the otherwise homogeneous rope. Such a void can be considered a model for a broken wire within the rope or similar internal flaw. The void is allowed to be oriented at any arbitrary angle to the rope axis to account for the winding geometry. Following a previous analysis [9], we compute the induced electric and magnetic dipole moments from the primary fields and the electric and magnetic polarizabilities of the void. The external fields of the induced dipole moments are then calculated using the previous formulation for dipoles of arbitrary orientation [9]. These external fields are the observable quantities in any nondestructive testing method.

The most common methods of wire rope testing detect the average or integrated value of the circumferential electric field with a receiving solenoid which completely encircles the rope. Usually this is done by making and measuring the change in the mutual impedance of two coaxial loops or similar arrangement. But, in addition, one should be able to probe the detailed structure of the external magnetic field components with small sensing coils. Because this possibility has not been well explored, we present here, in graphical form, the azimuthal dependence

of the three components of the external magnetic field for a significant range of the relevant parameters. These plots are intended to be an aid to the design of an effective configuration of sensing coils. Although the analysis is carried out for the AC case, DC excitation is included as a special case.

Primary Field Excitation

The geometry of the rope and the source are shown in Fig. 1. The rope is infinitely long and has radius a, conductivity σ_w, permittivity ϵ_w, and (magnetic) permeability μ_w. The surrounding free space has permittivity ϵ_o and permeability μ_o. For now, we defer discussion of the void properties and consider only the homogeneous rope.

The source is an electric current ring of strength I located at $\rho = b$ in the plane $z = 0$. This is a model for a thin and narrow solenoid which completely encircles the rope. This source is the dual of the magnetic current ring or thin toroidal coil which was considered previously [9]. The time dependence is $\exp(i\omega t)$ for all source and field quantities.

Due to the symmetry of the source and the rope, the fields are TE to z (Transverse Electric) and independent of ϕ. The electric field has only a nonzero azimuthal component E_ϕ^{pr}, and the magnetic field has only nonzero axial and radial components H_z^{pr} and H_ρ^{pr}. The superscript pr denotes the fields in the absence of the void. Since the dual problem of the magnetic ring source has already been solved [9], the fields of the electric ring source can be obtained by duality [10]. The resultant expressions for the primary fields both inside and outside the rope are given in Appendix A. The axial magnetic field H_z^{pr} is nearly independent of ρ inside the rope for sufficiently low frequencies. On the other hand, H_ρ^{pr} and E_ϕ^{pr} are zero at the rope center $\rho = 0$. For the D.C. limit (ω=0), E_ϕ^{pr} is zero everywhere.

Induced Dipole Moments

To allow comparison between the toroid [9] and solenoid excitation, we again select a thin prolate spheroid in order to model a broken strand. As indicated in Fig. 1c, the spheroid has conductivity σ_v, permittivity ε_v, and permeability μ_v. We also allow a rotation of the major axis of the spheroid about the ρ' axis by an angle α in order to account for the winding geometry of the rope. Consequently, the major axis is oriented at an angle α to the unit vector $\hat{z}'$ and an angle $\pi/2 + \alpha$ to the unit vector $\hat{\phi}'$.

The prolate spheroidal void model is a convenient one because the electric and magnetic polarizabilities are known [11]. The electric polarizabilities for the incident electric field applied along the major axis, α^e_{maj}, or along the minor axis, α^e_{min}, are given by

$$\alpha^e_{maj} = -V(\sigma_w - \sigma_v) \tag{1}$$

and

$$\alpha^e_{min} = \frac{-2V(\sigma_w - \sigma_v)}{1 + \sigma_v/\sigma_w} \quad , \tag{2}$$

where V is the volume of the thin prolate spheroid. Displacement currents have been neglected in (1) and (2), but they can be included merely by replacing σ_w by $\sigma_w + i\omega\varepsilon_w$ and σ_v by $\sigma_v + i\omega\varepsilon_v$. The magnetic polarizabilities for the incident magnetic field applied along the major axis, α^m_{maj}, or along the minor axis, α^m_{min}, are given by

$$\alpha^m_{maj} = -Vi\omega(\mu_w - \mu_v) \tag{3}$$

and

$$\alpha^m_{min} = \frac{-2Vi\omega(\mu_w - \mu_v)}{1 + \mu_v/\mu_w} \tag{4}$$

Although the polarizabilities in (1)-(4) are derived for a thin prolate spheroid, we would not expect a significant difference for a thin circular cylinder of the same length and volume.

In order to compute the induced dipole moments, it is necessary to first resolve the incident electric and magnetic fields into components along the major and minor axes. The resultant dipole moments can then be resolved into the more convenient ρ, ϕ, and z components. When this is done, the induced electric dipole moments are found to be

$$(Ids)_z = E_\phi^{pr}(\alpha_{min}^e - \alpha_{maj}^e)\sin\alpha\cos\alpha \quad , \tag{5}$$

$$(Ids)_\phi = E_\phi^{pr}(\alpha_{min}^e\cos^2\alpha + \alpha_{maj}^e\sin^2\alpha) \quad , \tag{6}$$

$$(Ids)_\rho = 0 \tag{7}$$

The induced magnetic dipole moments are found to be

$$(Kd\ell)_z = H_z^{pr}(\alpha_{maj}^m\cos^2\alpha + \alpha_{min}^m\sin^2\alpha) \quad , \tag{8}$$

$$(Kd\ell)_\phi = H_z^{pr}(\alpha_{min}^m - \alpha_{maj}^m)\sin\alpha\cos\alpha \quad , \tag{9}$$

$$(Kd\ell)_\rho = H_\rho^{pr}\alpha_{min}^m \quad . \tag{10}$$

In (5)-(7), the primary field components E_ϕ^{pr}, H_z^{pr}, and H_ρ^{pr} are evaluated at ρ', ϕ', z'.

External Scattered Field

The total scattered field can be written as a superposition of the contributions from each of the six induced dipole sources given in (5)-(10). (Actually, there are only five nonzero sources since $(Ids)_\rho$ is zero for the specific configuration considered here.) The scattered magnetic field components $H_\rho^{sc}(\rho,\phi,z)$, $H_\phi^{sc}(\rho,\phi,z)$, and $H_z^{sc}(\rho,\phi,z)$ are of particular interest when small coils are used as sensors. However, the scattered electric field components $E_\rho^{sc}(\rho,\phi,z)$, $E_\phi^{sc}(\rho,\phi,z)$, and $E_z^{sc}(\rho,\phi,z)$ can also be computed with little additional effort. The ϕ-averaged value of E_ϕ^{sc} is of

interest when a solenoid which completely encircles the rope is used as a sensor.

Both the magnetic and electric scattered fields can be compactly written in the following matrix form:

$$\begin{bmatrix} H_\rho^{sc} \\ H_\phi^{sc} \\ H_z^{sc} \end{bmatrix} = \begin{bmatrix} G_{\rho\rho}^e & G_{\rho\phi}^e & G_{\rho z}^e \\ G_{\phi\rho}^e & G_{\phi\phi}^e & G_{\phi z}^e \\ G_{z\rho}^e & G_{z\phi}^e & G_{zz}^e \end{bmatrix} \begin{bmatrix} (Ids)_\rho \\ (Ids)_\phi \\ (Ids)_z \end{bmatrix} + \begin{bmatrix} G_{\rho\rho}^m & G_{\rho\phi}^m & G_{\rho z}^m \\ G_{\phi\rho}^m & G_{\phi\phi}^m & G_{\phi z}^m \\ G_{z\rho}^m & G_{z\phi}^m & G_{zz}^m \end{bmatrix} \begin{bmatrix} (Kd\ell)_\rho \\ (Kd\ell)_\phi \\ (Kd\ell)_z \end{bmatrix} \tag{11}$$

and

$$\begin{bmatrix} E_\rho^{sc} \\ E_\phi^{sc} \\ E_z^{sc} \end{bmatrix} = \begin{bmatrix} F_{\rho\rho}^e & F_{\rho\phi}^e & F_{\rho z}^e \\ F_{\phi\rho}^e & F_{\phi\phi}^e & F_{\phi z}^e \\ F_{z\rho}^e & F_{z\phi}^e & F_{zz}^e \end{bmatrix} \begin{bmatrix} (Ids)_\rho \\ (Ids)_\phi \\ (Ids)_z \end{bmatrix} + \begin{bmatrix} F_{\rho\rho}^m & F_{\rho\phi}^m & F_{\rho z}^m \\ F_{\phi\rho}^m & F_{\phi\phi}^m & F_{\phi z}^m \\ F_{z\rho}^m & F_{z\phi}^m & F_{zz}^m \end{bmatrix} \begin{bmatrix} (Kd\ell)_\rho \\ (Kd\ell)_\phi \\ (Kd\ell)_z \end{bmatrix} \tag{12}$$

In the first 3 by 3 matrix, $G_{\rho\rho}^e$ is the ρ component of H at (ρ,ϕ,z) produced by a unit ρ-directed electric dipole at (ρ',ϕ',z'), $G_{\rho\phi}^e$ is the ρ component of H produced by a unit ϕ-directed electric dipole at (ρ',ϕ',z'), etc. The second 3 by 3 matrix is similar except that the G^m elements correspond to unit magnetic dipole sources. For the cylindrical geometry encountered here, all the matrix elements can be derived from z components of electric and magnetic Hertz vectors [12], and the specific expressions for the G elements have been given previously [9]. The expressions for the matrix elements in (12) are derived in Appendix B. The ϕ-averaged value of E_ϕ^{sc} which is of interest for solenoid reception is defined as

$$\overline{E_\phi^{sc}} = \frac{1}{2\pi} \int_0^{2\pi} E_\phi^{sc}(\rho,\phi,z)\,d\phi \quad . \tag{13}$$

The specific form of $\overline{E_\phi^{sc}}$ is also given in Appendix B. Of course, instead of (13), one could also obtain $\overline{E_\phi^{sc}}$ by integrating the flux over the area of the wire loop, but the present approach is simpler and more convenient.

Numerical Results

Numerically efficient computer programs have been written to evaluate the scattered fields as given by (11) and (12) and the primary fields as given by (A-5)-(A-7) for $a < \rho < b$ and by (A-9)-(A-11) for $\rho > b$.

In Figs. 2, 3, and 4 the magnitudes of the three scattered magnetic field components H_ρ^{sc}, H_ϕ^{sc}, and H_z^{sc} are shown plotted as a function of ϕ for a selected set of the parameters. The vertical scale is in per cent of the primary axial magnetic field H_z^{pr} running from 10^{-3}% to 1%. The volume of the small slender void V is taken to be 10^{-8} m^3(= 1mm × 1mm × 1cm) and the void itself is oriented in the axial direction (i.e. α=0°). Since the scattered fields are proportional to V, the curves are easily scaled to other values of V. Also, the constitutive parameters of the void are taken to be those of free space: $\epsilon_v = \epsilon_o$, $\sigma_v = 0$, and $\mu_v = \mu_o$. In these cases, ϕ' is taken to be zero, but for ϕ' not equal to zero, the horizontal axis can simply be replaced by $\phi - \phi'$. Other selected values of the parameters are: a = 1 cm, $\sigma_w = 1.1 \times 10^6$ mho/m, $\mu_w/\mu_o = 200$, b/a = 2, $\rho'/a = 0.5$, $z'/a = 3.75$, $\rho/a = 2$, $z/a = 5$, f = 10 Hz.

The magnitudes of the individual dipole contributions to the total scattered field are also shown for each component of H in Figs. 2, 3, and 4. Since α is zero, there are only three induced dipole moments $(Kd\ell)_z$, $(Kd\ell)_\rho$, and $(Ids)_\phi$. As expected, $(Kd\ell)_z$ is the major contributor. $(Kd\ell)_\rho$ is small because H_ρ^{pr} is very small inside the rope.

Actually, for solenoid reception, the value of $\overline{E_\phi^{sc}}$ is of primary importance. In Fig. 5, we also show the ϕ dependence of E_ϕ^{sc} for three values of ρ'/a for $z'/a = 5$. Of course, the greatest ϕ variation occurs for the void near the surface ($\rho'/a = 0.9$). In Table I the normalized averaged scattered azimuthal electric field $|\overline{E_\phi^{sc}}/E_\phi^{pr}|$ is shown for the same parameters which were

used in Figs. 2-4. This is the quantity which indicates the sensitivity of the solenoid sensor used in present systems. The values of $|\overline{E_\phi^{sc}}/E_\phi^{pr}|$ are typically rather small ($\simeq$ .01%). Note in Fig. 5 that $|E_\phi^{sc}/E_\phi^{pr}|$ has a comparable level for $\rho'/a = 0.1$, but a much larger level for $\rho'/a = 0.5$ or 0.9. This is due to the higher ϕ harmonics in E_ϕ^{sc} which do not contribute to $\overline{E_\phi^{sc}}$. It is also the case that the normalized scattered magnetic field components have a higher level because of the higher order harmonics in ϕ for $\rho'/a \neq 0$.

Concluding Remarks

Excitation of a wire rope containing a slender void has been analyzed for a thin solenoid source. The prolate spheroidal void has been shown to produce an anomaly in the external fields which is typically larger than that produced for the case of toroidal excitation [9]. Again, the external scattered magnetic field components (not shown here) have a rather complicated azimuthal dependence containing some peaks and nulls. This suggests that multiple sensing coils of various locations and orientations might be worthwhile.

The ϕ-averaged value of the scattered azimuthal electric field $\overline{E_\phi^{sc}}$ has also been examined. This is the quantity which is sensed by a solenoidal sensor which encircles the rope, and Burrows [15] has also examined this quantity. This scattered field is typically quite small compared to the primary field as indicated in Table 1. Of course, the solenoid sensor does not make any use of the higher harmonics in ϕ which can be considerably larger than the ϕ-averaged value. However, a possible advantage of the solenoid sensor is that $\overline{E_\phi^{sc}}$ is not highly dependent on the void location. Thus the anomaly is related more to the void's volume than location. A system which senses the scattered field directly without any ϕ averaging

will detect a greater anomaly when the void is located near the surface of the rope.

On the basis of calculations at other frequencies, one general conclusion is that 10 Hz is a good choice. Higher frequencies suffer from poor penetration of the rope. Also, the exciting solenoid and the sensors should be located as close to the rope as possible to maximize the relative scattered field.

The individual contributions of the various induced dipole moments to the scattered field are illustrated in Figs. 2-4. As expected for solenoidal excitation, the induced axial magnetic dipole moment is the dominant contributor to the scattered field. Actually, this dipole moment requires that the magnetic permeability of the rope be different from that of the void. In fact, calculations show that if the rope is nonmagnetic, the effect of the anomaly is quite small because only an electric dipole moment is induced.

A further worthwhile study would be to examine the response as a function of void location for a fixed geometry of the sensor. Some additional calculations, in a computer print-out format, that can give such information, may be obtained from the authors on request.

Although we have only examined the thin prolate spheroidal void, we have derived expressions which are useful for other shapes. The only requirement is that the imperfection be sufficiently small that its scattered fields can be represented by induced electric and magnetic dipole moments. Another convenient imperfection to treat would be an oblate spheroidal imperfection which could model a region of corrosion. Also, it might be possible to treat a rope model where the conductivity and permeability are tensors. This anisotropic feature of ropes is expected because of the winding geometry; the subject has been examined by Wait [16].

Appendix A - Primary Fields

The primary fields for excitation by a magnetic current ring of strength K have been derived previously [9]. By duality [10], the previous results hold for electric current ring excitation if we make the following transformations: $K \rightarrow I$, $H_\phi^{pr} \rightarrow E_\phi^{pr}$, $E_z^{pr} \rightarrow -H_z^{pr}$, $E_\rho^{pr} \rightarrow -H_\rho^{pr}$, $\mu_o \rightarrow \varepsilon_o$, $\varepsilon_o \rightarrow \mu_o$, $i\omega\mu_w \rightarrow \sigma_w + i\omega\varepsilon_w$, and $\sigma_w + i\omega\varepsilon_w \rightarrow i\omega\mu_w$. The resultant primary field expressions take different forms in the three regions, $\rho < a$, $a < \rho < b$, and $\rho > b$.

Inside the rope ($\rho < a$), we find

$$H_z^{pr} = -\int_{-\infty}^{\infty} w^2 a_o I_o(w\rho)\exp(-i\lambda z)d\lambda \ , \qquad \text{(A-1)}$$

$$H_\rho^{pr} = -\int_{-\infty}^{\infty} i\lambda w a_o I_1(w\rho)\exp(-i\lambda z)d\lambda \ , \qquad \text{(A-2)}$$

$$E_\phi^{pr} = i\omega\mu_w \int_{-\infty}^{\infty} w a_o I_1(w\rho)\exp(-i\lambda z)d\lambda \ , \qquad \text{(A-3)}$$

where $w = (\lambda^2+\gamma_w^2)^{1/2}$, $\gamma_w^2 = i\omega\mu_w(\sigma_w+i\omega\varepsilon_w)$, and I_o and I_1 are zero and first order modified Bessel functions. The factor a_o is given by

$$a_o = \frac{-\gamma_o B_o}{w^2 a I_o(wa)K_o(ua)}\left[\frac{\gamma_o K_o'(ua)}{uK_o(ua)} - \frac{z_o}{\eta_o}\right]^{-1} , \qquad \text{(A-4)}$$

where

$$B_o = \frac{IbK_o'(ub)}{2\pi u} \ , \quad u = (\lambda^2+\gamma_o^2)^{1/2} \ ,$$

$$\gamma_o = i\omega(\mu_o\varepsilon_o)^{1/2} \ , \quad \eta_o = (\mu_o/\varepsilon_o)^{1/2} \ ,$$

$$z_o = \frac{i\omega\mu_w}{w}\frac{I_1(wa)}{I_o(wa)} \ ,$$

K_o is a zero order modified Bessel function, and prime ' denotes differentiation with respect to the argument. (In the previous paper [9], the

expression for B_o should actually read $B_o = -KbK_o'(ub)/(2\pi u))$.

In the region between the rope and the source ($a < \rho < b$), we find

$$H_z^{pr} = - \int_{-\infty}^{\infty} u^2[B_o I_o(u\rho) + C_o K_o(u\rho)]\exp(-i\lambda z)d\lambda, \tag{A-5}$$

$$H_\rho^{pr} = - \int_{-\infty}^{\infty} i\lambda u[B_o I_1(u\rho) - C_o K_1(u\rho)]\exp(-i\lambda z)d\lambda \quad , \tag{A-6}$$

$$E_\phi^{pr} = i\omega\mu_o \int_{-\infty}^{\infty} u[B_o I_1(u\rho) - C_o K_1(u\rho)]\exp(-i\lambda z)d\lambda \quad , \tag{A-7}$$

where

$$C_o = - \frac{I_o(ua)\left[\frac{\gamma_o}{u}\frac{I_o'(ua)}{I_o(ua)} - \frac{z_o}{\eta_o}\right]}{K_o(ua)\left[\frac{\gamma_o}{u}\frac{K_o'(ua)}{K_o(ua)} - \frac{z_o}{\eta_o}\right]} B_o \, . \tag{A-8}$$

Outside the source ($\rho > b$), we find

$$H_z^{pr} = - \int_{-\infty}^{\infty} u^2 A_o K_o(u\rho)\exp(-i\lambda z)d\lambda \quad , \tag{A-9}$$

$$H_\rho^{pr} = \int_{-\infty}^{\infty} i\lambda u A_o K_1(u\rho)\exp(-i\lambda z)d\lambda \quad , \tag{A-10}$$

$$E_\phi^{pr} = i\omega\mu_o \int_{-\infty}^{\infty} u A_o K_1(u\rho)\exp(-i\lambda z)d\lambda \quad , \tag{A-11}$$

where

$$A_o = C_o - B_o I_1(ub)/K_1(ub). \tag{A-12}$$

Appendix B - Scattered Electric Fields

The derivation for the electric fields produced by a dipole source within a wire rope is a direct extension of the derivation of the magnetic field derivation given previously [9], and some of the details are excluded here. The external fields can be obtained from U and V which are the z components of electric and magnetic Hertz vectors

$$U = \Gamma[U_m] \quad \text{and} \quad V = \Gamma[V_m] \quad , \tag{B-1}$$

where

$$U_m = S_m(\lambda)K_m(u\rho), \quad V_m = T_m(\lambda)K_m(u\rho) \quad , \tag{B-2}$$

and

$$\Gamma[\ ] = \int_{-\infty}^{\infty} \sum_{-\infty}^{\infty} [\ ] e^{-im(\phi-\phi')} e^{-i\lambda(z-z')} d\lambda \quad . \tag{B-3}$$

The expressions for S_m and T_m have been given for each of the six dipole types [9].

The electric field components can be written

$$E_\rho = \Gamma[E_{\rho m}], \quad E_\phi = \Gamma[E_{\phi m}], \quad \text{and} \quad E_z = \Gamma[E_{zm}] \ , \tag{B-4}$$

where

$$E_{\rho m} = -i\lambda \frac{\partial U_m}{\partial \rho} - \frac{\omega\mu_o m}{\rho} V_m$$

$$= -i\lambda u S_m K_m'(u\rho) - \frac{\omega\mu_o m}{\rho} T_m K_m(u\rho) \quad , \tag{B-5}$$

$$E_{\phi m} = \frac{-m\lambda}{\rho} U_m + i\omega\mu_o \frac{\partial V_m}{\partial \rho}$$

$$= \frac{-m\lambda}{\rho} S_m K_m(u\rho) + i\omega\mu_o u T_m K_m'(u\rho) \quad , \tag{B-6}$$

and

$$E_{zm} = -u^2 U_m = -u^2 S_m K_m(u\rho) \ . \tag{B-7}$$

We are now able to define the matrix elements required in (12) in terms of E_ρ, E_ϕ, and E_z given in (B-4). For each of the six dipole types, we can define the required three matrix elements in a column matrix as follows.

For a radial electric dipole $(Ids)_\rho$, we have

$$\begin{bmatrix} F^e_{\rho\rho} \\ F^e_{\phi\rho} \\ F^e_{z\rho} \end{bmatrix} = \frac{1}{(Ids)_\rho} \begin{bmatrix} E_\rho \\ E_\phi \\ E_z \end{bmatrix} \tag{B-8}$$

For an azimuthal electric dipole $(Ids)_\phi$, we have

$$\begin{bmatrix} F^e_{\rho\phi} \\ F^e_{\phi\phi} \\ F^e_{z\phi} \end{bmatrix} = \frac{1}{(Ids)_\phi} \begin{bmatrix} E_\rho \\ E_\phi \\ E_z \end{bmatrix} \tag{B-9}$$

For an axial electric dipole $(Ids)_z$, we have

$$\begin{bmatrix} F^e_{\rho z} \\ F^e_{\phi z} \\ F^e_{zz} \end{bmatrix} = \frac{1}{(Ids)_z} \begin{bmatrix} E_\rho \\ E_\phi \\ E_z \end{bmatrix} \tag{B-10}$$

For a radial magnetic dipole $(Kd\ell)_\rho$, we have

$$\begin{bmatrix} F^m_{\rho\rho} \\ F^m_{\phi\rho} \\ F^m_{z\rho} \end{bmatrix} = \frac{1}{(Kd\ell)_\rho} \begin{bmatrix} E_\rho \\ E_\phi \\ E_z \end{bmatrix} \tag{B-11}$$

For an azimuthal magnetic dipole $(Kd\ell)_\phi$, we have

$$\begin{bmatrix} F^m_{\rho\phi} \\ F^m_{\phi\phi} \\ F^m_{z\phi} \end{bmatrix} = \frac{1}{(Kd\ell)_\phi} \begin{bmatrix} E_\rho \\ E_\phi \\ E_z \end{bmatrix} \tag{B-12}$$

For an axial magnetic dipole $(Kd\ell)_z$, we have

$$\begin{bmatrix} F^m_{z} \\ F^m_{z} \\ F^m_{zz} \end{bmatrix} = \frac{1}{(Kd\ell)_z} \begin{bmatrix} E_\rho \\ E_\phi \\ E_z \end{bmatrix} \tag{B-13}$$

The ϕ-averaged value of E_ϕ as given by (B-4) can be written

$$\overline{E}_\phi = \frac{1}{2\pi} \int_0^{2\pi} E_\phi d\phi = \Gamma_o[E_{\phi o}] \tag{B-14}$$

where

$$\Gamma_o[\ \ ] = \int_{-\infty}^{\infty} [\ \ ] e^{-i\lambda(z-z')} d\lambda$$

and

$$E_{\phi o} = i\omega\mu_o T_o K_o'(u\rho) \ .$$

As expected, only the m = 0 term of the electric Hertz vector contributes to $\overline{E}_\phi$.

References

1. H.L. Libby: *Introduction to Nondestructive Test Methods* (Wiley Interscience, New York, 1971).
2. E.R. Hoskins: Report to the U.S. Bureau of Mines on Contract No. H0346193, South Dakota School of Mines and Technology, (July 1975).
3. J.R. Wait: Review of electromagnetic methods in non-destructive testing of wire ropes, Preliminary Report to the U.S. Bureau of Mines on Contract No. H0155008, (March 1978).
4. C.H. Larsen, R.A. Egen, R.D. Jones, H.A. Cross: Report to the U.S. Bureau of Mines on Contract No. H0101741, (June 1971).
5. J.G. Lang: The Canadian Mining and Metalurgical (CIM) Bulletin, 415 (1969).
6. J.R. Wait: The electromagnetic basis for nondestructive testing of cylindrical conductors, IEEE Transactions on Instrumentation and Measurement, IM-27, 235 (September 1978).
7. J.R. Wait and R.L. Gardner: Non-destructive testing of a cylindrical conductor with an internal anomaly - A two-dimensional model, Preliminary Report to the U.S. Bureau of Mines on Contract No. H0155008, (May 1978).
8. D.A. Hill and J.R. Wait: J. Appl. Phys. 48, 4893 (December 1977).
9. D.A. Hill and J.R. Wait: Scattering by a slender void in a homogeneous conducting wire rope, Appl. Phys., 16, 391 (1978).
10. R.F. Harrington: *Time-Harmonic Electromagnetic Fields* (McGraw-Hill, New York, Sec. 3.2, 1961).
11. W.R. Smythe: *Static and Dynamic Electricity* (McGraw-Hill, Sec. 5.28, 1968).
12. J.R. Wait and D.A. Hill: Appl. Phys. 11, 351 (1976).
13. A.G. Kandoian: *Reference Data for Radio Engineers* (ITT Corp., New York, pp. 4-32, 1968).

14. D.R.J. White: *Electromagnetic Shielding Material and Performance* (Don White Consultants, Inc., Germantown, MD, Sec. 2.1, 1975).

15. M.L. Burrows: Ph.D. Thesis, Department of Electrical Engineering, University of Michigan, Ann Arbor (1964).

16. J.R. Wait: Electromagnetic induction in an anisotropic cylinder, Radio Science, 13, (September/October 1978).

Table 1 - Normalized $\overline{E_\phi^{sc}}$

Parameters*	$\lvert\overline{E_\phi^{sc}}/E_\phi^{pr}\rvert$ (%)
Same as Fig. 5	.01044
$\rho'/a = 0.1$	.00986
$\rho'/a = 0.9$	.01472
$z'/a = 1.25$	.01068
$z'/a = 2.5$	.01058
$z'/a = 3.75$	.01068
$\alpha = 15°$	.01107
$\alpha = 30°$	.01279
$f = 1$ Hz	.01025
$f = 100$ Hz	.00943
$f = 1000$ Hz	.00009
$\rho/a = 1.1$	.01229
$\rho/a = 1.5$	.01124
$\sigma_w = 10^5$ mho/m	.01025
$\sigma_w = 10^7$ mho/m	.00993
$\mu_w/\mu_o = 50$	.02046
$\mu_w/\mu_o = 10$	.03367
$\mu_w/\mu_o = 1$	.00003
$b/a = 3$	.01041
$b/a = 4$	.01039
$z/a = z'/a = 2.5$	.01049
$z/a = z'/a = 10$	.01039
$\rho/a = b/a = 1.1$	.01229
$\rho/a = b/a = 1.5$	.01125
$\rho/a = b/a = 3$	.00937
$\rho/a = b/a = 4$	.00851
$a = 2$ cm	.00143
$a = 2.5$ cm	.00073

*Parameters for each entry are the same as Fig. 5 except where noted.

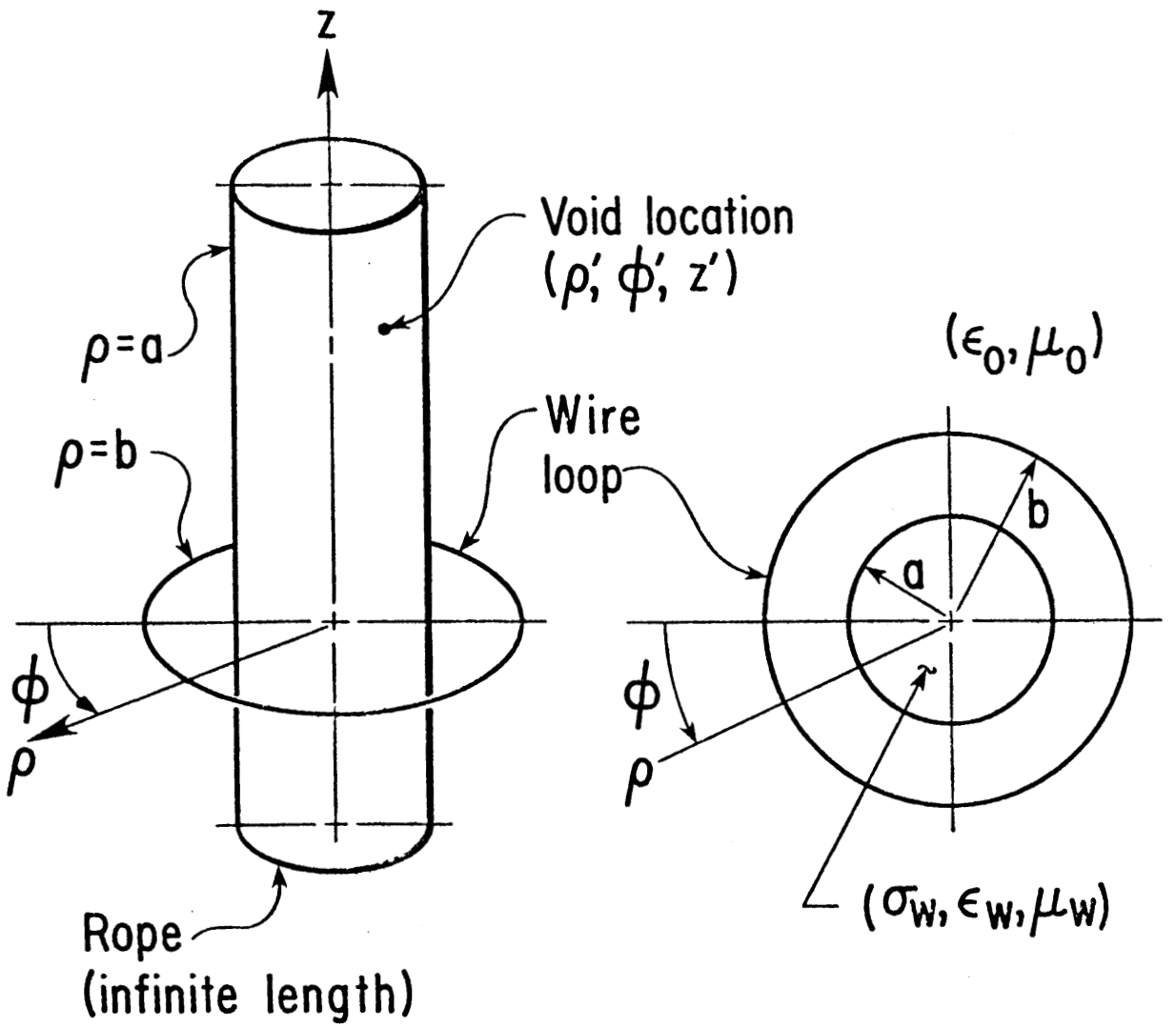

Fig. 1a
Perspective View

Fig. 1b
Top View

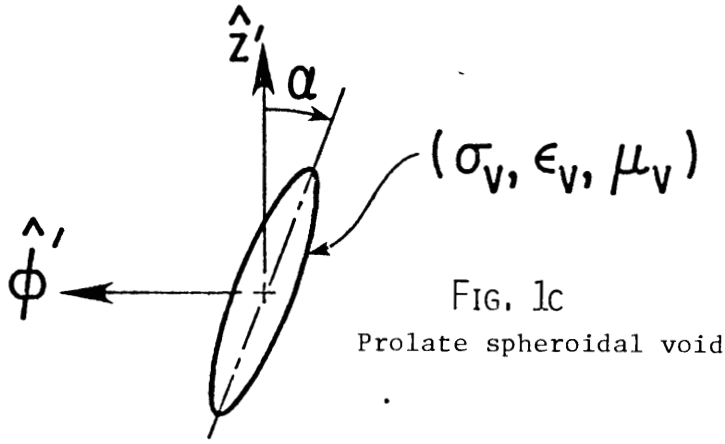

FIG. 1c
Prolate spheroidal void

Fig. 1. Thin solenoid surrounding a metal rope of infinite length.

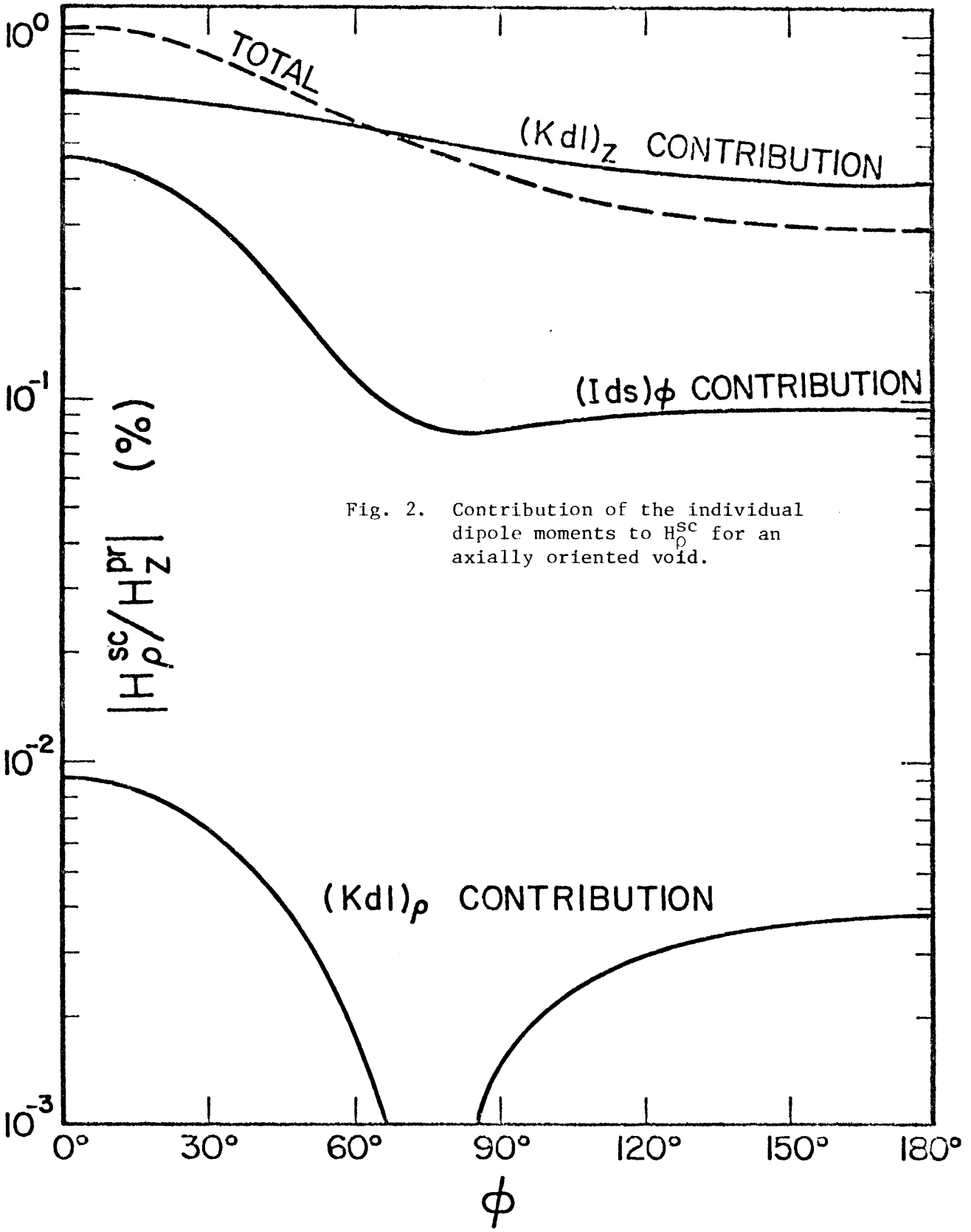

Fig. 2. Contribution of the individual dipole moments to H_ρ^{sc} for an axially oriented void.

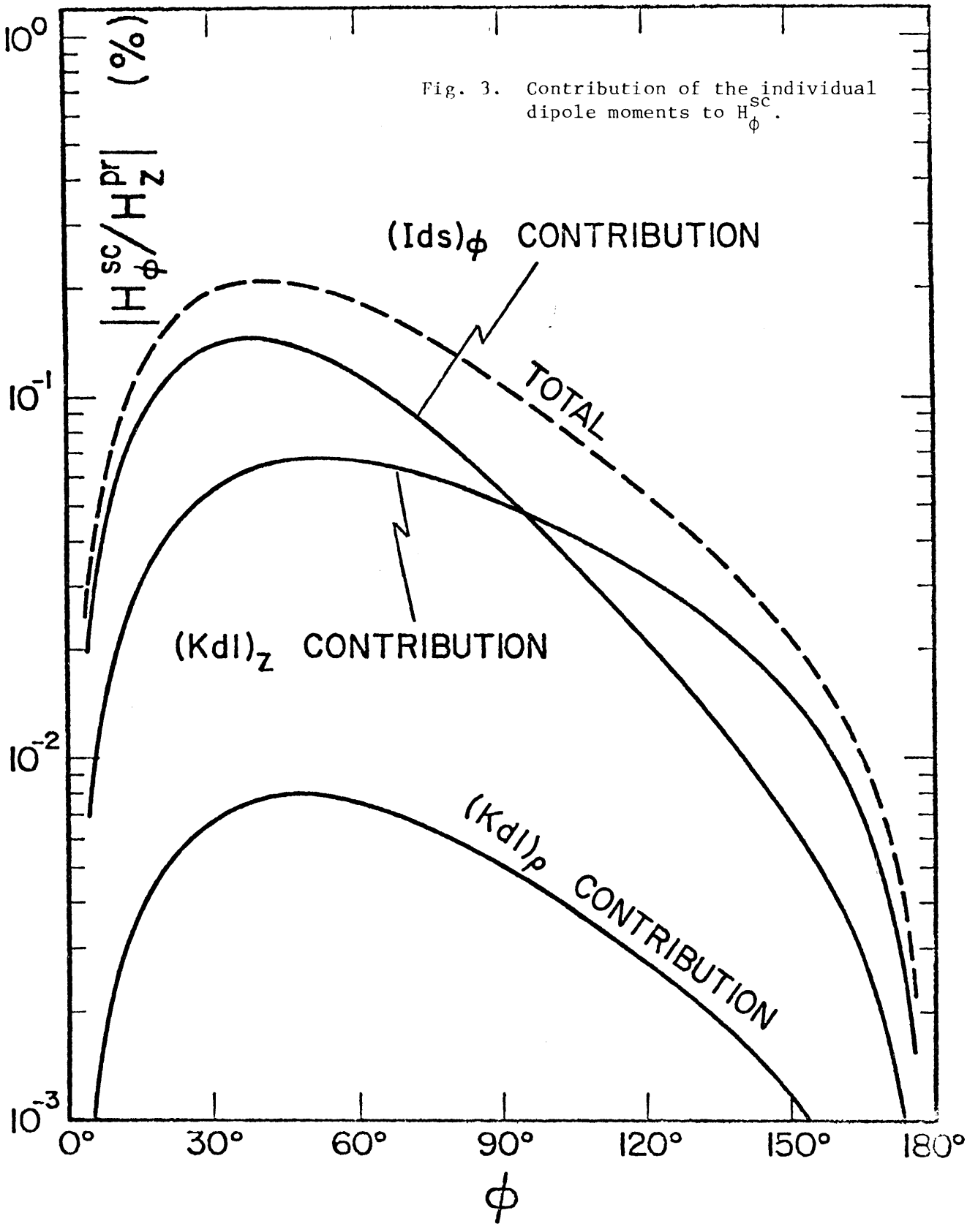

Fig. 3. Contribution of the individual dipole moments to H_ϕ^{sc}.

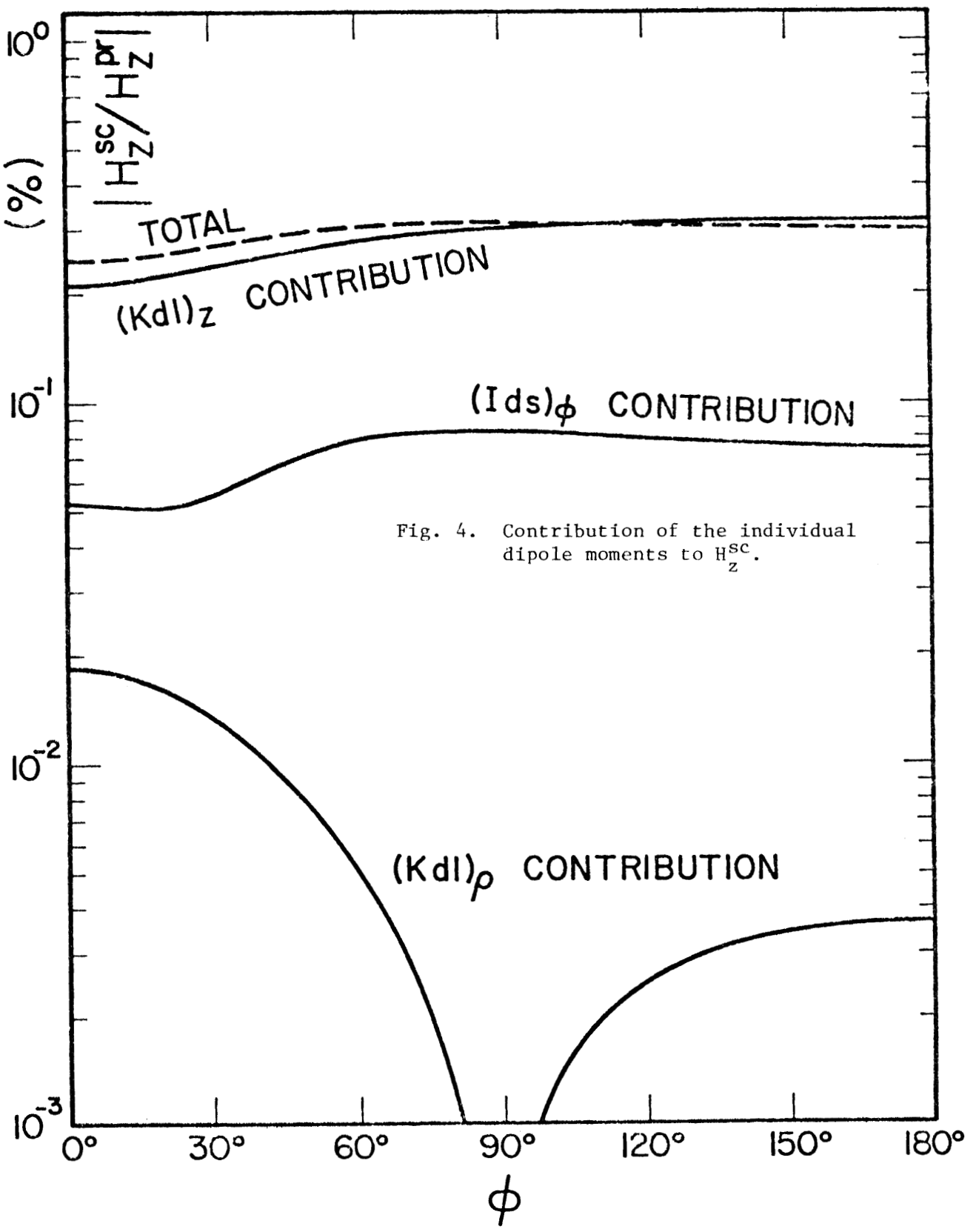

Fig. 4. Contribution of the individual dipole moments to H_z^{sc}.

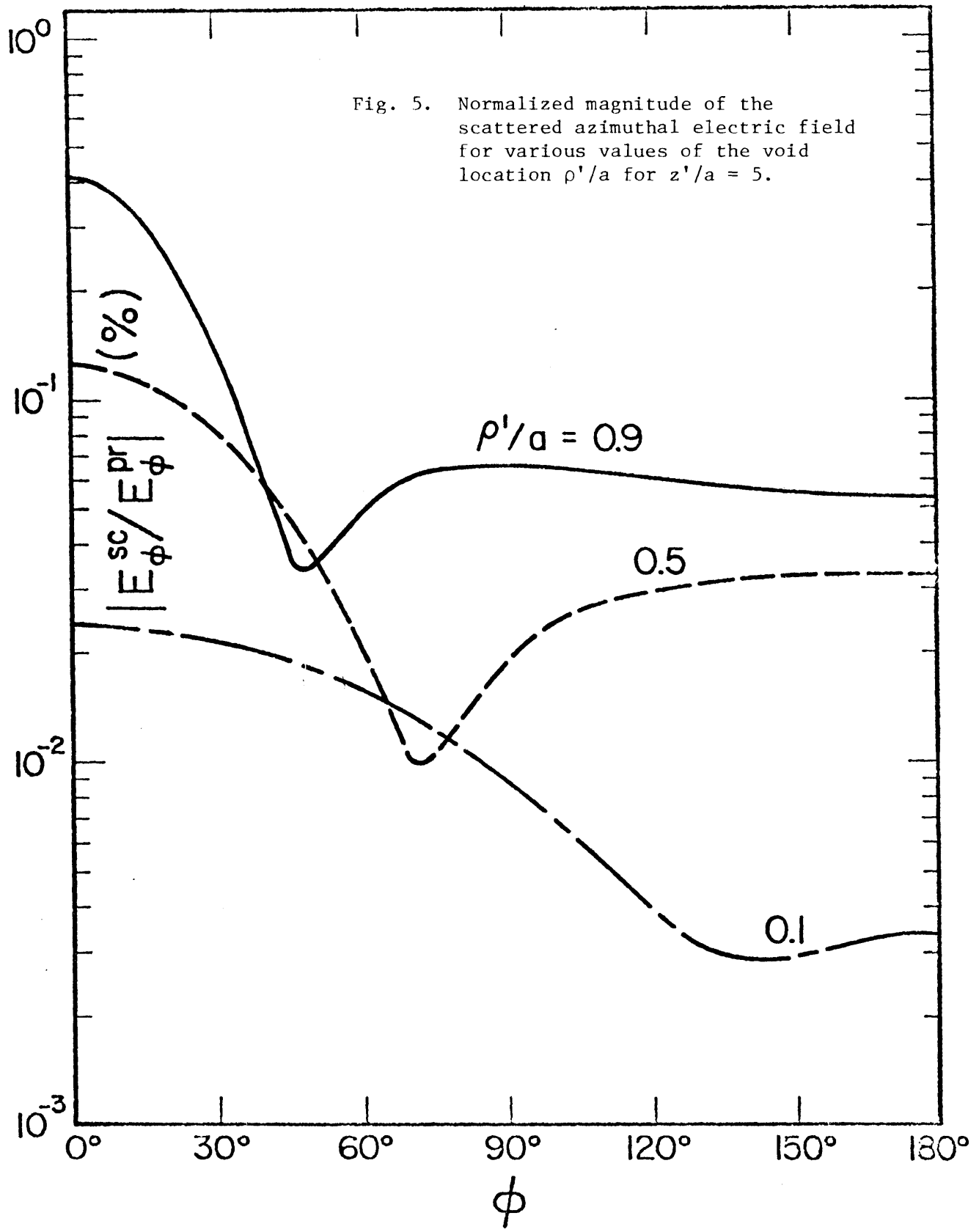

Fig. 5. Normalized magnitude of the scattered azimuthal electric field for various values of the void location ρ'/a for $z'/a = 5$.

Section 9

Dynamic Electromagnetic Response of a Homogeneous Conducting Cylinder for Symmetric Excitation

DAVID A. HILL
and
JAMES R. WAIT

Abstract-A stranded wire rope is idealized as a homogeneous conducting and permeable cylinder of circular cross section and of infinite length. The rope is excited by a coaxial solenoid or finite length multi-turn coil that carries an azimuthally directed alternating current. The rope and the enclosing solenoid may have a uniform velocity relative to each other. Using a non-relativistic analysis, the nature of this dynamic interaction is examined and numerical results are presented for parameter values that are relevant to both static and dynamic conditions in non-destructive testing of such cylindrical conductors. It is shown that even for motional velocities v as high as 10 m/s the dynamic interaction with the rope specimen is not appreciably modified from that for the static condition (i.e., for $v = 0$).

INTRODUCTION

The nondestructive testing of metallic structures often utilizes the interaction of electromagnetic fields with the specimen [1,2]. A particularly good example is a steel stranded wire rope such as is used in mine hoists. In this case it may be desirable to test the rope under dynamic conditions such

that the sensor and the rope have a uniform velocity relative to each other. It is the purpose of the present paper to examine the effect of the motional velocity on the nature of the electromagnetic fields excited by a coaxial solenoid or finite length coil that carries an alternating current. We also consider the mutual impedance between two solenoids that are both coaxial with the rope. Such a configuration is quite common in testing both solid and tubular conductors.

FORMULATION

We consider a simple model; the rope is treated as a uniform cylindrical structure of radius a. It is excited by a current-carrying concentric solenoid of radius b as indicated in Fig. 1. Cylindrical coordinates (ρ,ϕ,z) fixed within the rope are chosen such that the surface of the cylindrical conductor is $\rho = a$ while the solenoid is idealized as an azimuthal current sheet of axial length ℓ located at $\rho = b$. The solenoid is taken to be moving with a uniform velocity v in the positive z direction relative to the rope frame. (ρ,ϕ,z). Azimuthal variations of the fields are assumed to be negligible which is the case when the azimuthal current is constant and the rope is located concentrically within the solenoid.

The solenoid current surface density in amperes/meter at $\rho = b$ is specified to be

$$j_\phi(z,t) = \text{Real part of } (NI/\ell)\exp(i\omega t) \qquad (1)$$

for $(\ell/2) + vt > z > (-\ell/2) + vt$ and zero outside this interval. Here N is the total number of turns that are wound uniformly throughout the axial length ℓ of the solenoid. I is the magnitude of the current. The angular frequency is ω and t is the time. Now it is not difficult to show that

$$j_\phi(z,t) = \frac{NI}{2\pi}\int_{-\infty}^{+\infty} \frac{\sin(\lambda \ell/2)}{(\lambda \ell/2)}\, e^{-i\lambda z}\, e^{i\lambda vt}\, d\lambda\, e^{i\omega t} \qquad (2)$$

where it is understood here and in what follows that we take the real part of the indicated complex quantity.

We are now interested in the interaction of the fields from this primary current with the conducting cylinder. While the analysis can be carried through quite rigorously by using the full-blown Lorentz transformation [3,5], here we will use a nonrelativistic approach [6] that is justified when terms containing v^2/c^2 are negligibly small. This will certainly be the case in any practically realizable remote sensing scheme [e.g., even for a motional velocity v = 100 m/s, $v^2/c^2 \simeq 10^{-13}$ where $c = 3 \times 10^8$ m/s]. Also we will assume that the fields in the region external to the rope are quasi-static in nature. This is justified when the significant dimensions of the sensor and the rope diameter are small compared with the operating free-space wavelength λ_o [e.g., at a typical operating frequency of 10 Hz the $\lambda_o \simeq 3 \times 10^7$ m]. In this context it is worth pointing out that $|\lambda|^{-1}$, where λ is the axial wave number, should also be small compared with λ_o over the significant range of the integration variable λ.

EXTERNAL FIELDS

In view of our assumptions the fields in the region $\rho > a$ can be obtained from a magnetic type Hertz vector that has only a z component $\Pi_o(\rho,z,t)$ which satisfies Laplace's equation

$$\left(\frac{1}{\rho}\frac{\partial}{\partial\rho}\,\rho\,\frac{\partial}{\partial\rho} + \frac{\partial^2}{\partial z^2}\right)\Pi_o = 0 \qquad (3)$$

Taking a cue from (2) we construct the following appropriate integral form for Π as :

$$\Pi_o(\rho,z,t) = \int_{-\infty}^{+\infty} \hat{\Pi}_o(\lambda,\rho) e^{-i\lambda z} e^{i(\omega + \lambda v)t} d\lambda \tag{4}$$

where, in view of (3), $\hat{\Pi}_o$ must satisfy

$$\left(\frac{1}{\rho}\frac{\partial}{\partial\rho}\rho\frac{\partial}{\partial\rho} - \lambda^2\right)\hat{\Pi}_o = 0 \tag{5}$$

Suitable solutions are

$$\hat{\Pi}_o = B(\lambda)I_o(|\lambda|\rho) + C(\lambda)K_o(|\lambda|\rho) \text{ for } a < \rho < b \tag{6}$$

and

$$\hat{\Pi}_o = D(\lambda)K_o(|\lambda|\rho) \text{ for } \rho > b. \tag{7}$$

where I_o and K_o are modified Bessel functions. The particular form $K_o(|\lambda|\rho)$ is dictated in the region $\rho > b$ since it vanishes exponentially for all positive and negative real values of λ when $\rho \to \infty$. Then, to assure field matching for all λ, the other Bessel functions in the air region must have the same argument. The functions B, C and D are yet to be determined.

The field components in the region $\rho > b$ can be obtained from

$$H_{o\rho} = \partial^2\Pi_o/\partial\rho\partial z \tag{8}$$

$$E_{o\phi} = \mu_o\partial^2\Pi_o/\partial t\partial\rho \tag{9}$$

and

$$H_{oz} = \partial^2\Pi_o/\partial z^2 \tag{10}$$

The corresponding integral representations are

$$\begin{bmatrix} H_{o\rho} \\ E_{o\phi} \\ H_{oz} \end{bmatrix} = \int_{-\infty}^{+\infty} \begin{bmatrix} \hat{H}_{o\rho}(\lambda) \\ \hat{E}_{o\phi}(\lambda) \\ \hat{H}_{oz}(\lambda) \end{bmatrix} e^{-i\lambda z} e^{i(\omega + \lambda v)t} d\lambda \tag{11}$$

where

$$\hat{H}_{o\rho}(\lambda) = -i\lambda\partial\Pi_o/\partial\rho \tag{12}$$

$$\hat{E}_{o\phi}(\lambda) = i\mu_o(\omega + \lambda v)\partial\hat{\Pi}_o/\partial\rho \tag{13}$$

and

$$\hat{H}_{oz}(\lambda) = -\lambda^2 \hat{\Pi}_o. \tag{14}$$

We are now in the position to apply the source conditions

$$H_{oz}(b - 0) - H_{oz}(b + 0) = j_\phi(z,t) \tag{15}$$

$$E_{o\phi}(b - 0) - E_{o\phi}(b + 0) = 0 \tag{16}$$

and the impedance condition

$$\left[\hat{E}_{o\phi}(\lambda) = -Z(\lambda)\hat{H}_{oz}(\lambda)\right]_{\rho = a} \tag{17}$$

where $Z(\lambda)$ is discussed below. Thus we deduce that

$$B(\lambda) = -\frac{NIb}{2\pi|\lambda|}\frac{\sin(\lambda\ell/2)}{(\lambda\ell/2)} K_1(|\lambda|b) \tag{18}$$

$$\frac{B(\lambda)}{C(\lambda)} = \frac{i\mu_o(\omega + \lambda v)K_1(|\lambda|a) + |\lambda|Z(\lambda)K_o(|\lambda|a)}{i\mu_o(\omega + \lambda v)I_1(|\lambda|a) - |\lambda|Z(\lambda)I_o(|\lambda|a)} \tag{19}$$

and

$$D(\lambda) = C(\lambda) - B(\lambda)I_1(|\lambda|b)/K_1(|\lambda|b) \tag{20}$$

Here we have made use of the Wronskian relation

$$I_o(\chi)K_1(\chi) + I_1(\chi)K_o(\chi) = 1/\chi. \tag{21}$$

SOLUTION FOR INTERNAL FIELD

Now we must specify the internal structure of the cylinder in order to obtain an explicit expression for $Z(\lambda)$. For present purposes we will assume homogeneity with a conductivity σ and magnetic permeability μ. Displacement currents in the cylinder are also neglected.

The fields within the cylinder (i.e. $\rho < a$) can also be obtained from an azimuthally independent magnetic Hertz vector that has only an axial component Π. In the rope frame (ρ,ϕ,z), it satisfies the time dependent wave equation

$$\left(\frac{1}{\rho}\frac{\partial}{\partial\rho}\,\rho\,\frac{\partial}{\partial\rho} + \frac{\partial^2}{\partial z^2} - \sigma\mu\,\frac{\partial}{\partial t}\right)\Pi = 0 \tag{22}$$

The corresponding integral form is

$$\Pi(\rho,z,t) = \int_{-\infty}^{+\infty} \hat{\Pi}(\lambda,\rho)\, e^{-i\lambda z}\, e^{i(\omega + \lambda v)t}\, d\lambda \tag{23}$$

where $\hat{\Pi}$ satisfies

$$\left(\frac{1}{\rho}\frac{\partial}{\partial\rho}\,\rho\,\frac{\partial}{\partial\rho} - w^2\right)\hat{\Pi} = 0 \tag{24}$$

where

$$w = [\lambda^2 + i\sigma\mu(\omega + \lambda v)]^{\frac{1}{2}}$$

The field components in the region $\rho < a$ are obtained from

$$H_\rho = \partial^2\Pi/\partial\rho\partial z \tag{25}$$

$$E_\phi = \mu\partial^2\Pi/\partial t\partial\rho \tag{26}$$

and

$$H_z = \left(-\sigma\mu\,\frac{\partial}{\partial t} + \frac{\partial^2}{\partial z^2}\right)\Pi \tag{27}$$

The corresponding expressions for the field components are then

$$\begin{bmatrix} H_\rho \\ E_\phi \\ H_z \end{bmatrix} = \int_{-\infty}^{+\infty} \begin{bmatrix} \hat{H}_\rho(\lambda) \\ \hat{E}_\phi(\lambda) \\ \hat{H}_z(\lambda) \end{bmatrix} e^{-i\lambda z}\, e^{i(\omega + \lambda v)t}\, d\lambda \tag{28}$$

where

$$\hat{H}_\rho(\lambda) = -i\lambda\partial\hat{\Pi}/\partial\rho \tag{29}$$

$$\hat{E}_\phi(\lambda) = i\mu(\omega + \lambda v)\partial\hat{\Pi}/\partial\rho \tag{30}$$

$$\hat{H}_z(\lambda) = -w^2\hat{\Pi} \tag{31}$$

The appropriate solution of (24) that is finite at $\rho = 0$ is clearly

$$\hat{\Pi} = A(\lambda) I_o(w\rho) \tag{32}$$

where $A(\lambda)$ is determined below.

Thus, we readily deduce that

$$-\hat{E}_{\phi}(\lambda)/\hat{H}_{z}(\lambda) = Z(\lambda) = i\mu(\omega + \lambda v)I_{1}(wa)/I_{o}(wa) \tag{33}$$

This completes the specification of the ratio $B(\lambda)/C(\lambda)$ as given by (19). Also since $\hat{H}_{oz}$ and $\hat{H}_{z}$ are continuous at $\rho = a$, we ascertain from (4) and (31) that

$$A(\lambda) = (\lambda^2/w^2)[B(\lambda)I_{o}(|\lambda|a) + C(\lambda)K_{o}(|\lambda|a)]/I_{o}(wa) \tag{34}$$

The fields everywhere in the (ρ,ϕ,z) frame are now given in terms of the known parameters of the problem.

To express the fields $\vec{E}_{o}'$ and $\vec{H}_{o}'$ in the (ρ,ϕ,z') coordinates in the frame of the solenoid we need to apply the transformation law

$$\vec{E}_{o}' = \vec{E}_{o} + \mu_{o}v\vec{i}_{z} \times \vec{H}_{o} \tag{35}$$

and

$$\vec{H}_{o}' = \vec{H}_{o} - \varepsilon_{o}v\vec{i}_{z} \times \vec{E}_{o} \tag{36}$$

where $\vec{i}_{z}$ is a unit vector in the positive z direction. These forms are valid for the external region $\rho > a$; the corresponding forms for $\rho < a$ are similar. The important point is that the axial magnetic field is not changed as a result of the uniform axial motion.

RESULTS FOR INTERNAL FIELD

In any non-destructive testing scheme the internal field of the sample interacts with the material properties and, in turn, produces a secondary field that is detected in the external region [7]. Thus, it is of interest to examine the internal axial magnetic H_{z} at some fixed distance z' from the solenoid as indicated in Fig. 1.

The field in question is given by

$$H_{z} = -\int_{-\infty}^{+\infty} w^2 A(\lambda) e^{-i\lambda z}\, e^{i(\omega + \lambda v)t}\, d\lambda \tag{37}$$

Now $z = z' + vt$ if the solenoid is located at $z = 0$ at $t = 0$. Thus we have simply that

$$H_z = -\int_{-\infty}^{+\infty} w^2 A(\lambda) e^{-i\lambda z'} \, d\lambda \cdot e^{i\omega t} \tag{38}$$

The v dependence is contained entirely in $A(\lambda)$ that is defined by (34) where $B(\lambda)$ and $C(\lambda)$ are given explicitly by (18) and (19).

The integration over λ indicated by (38) is performed numerically using a variable step size in order to deal effectively with the relatively rapid variation for small values of $|\lambda|$. In general, at least for the case $v \neq 0$, the integrand is not an even function of λ so the integration must be carried out over the full range of λ from $-\infty$ to $+\infty$. Here we maintain the requirement that Re. $w > 0$ or that w tends to $|\lambda|$ as λ tends to $\pm\infty$. Some results for $|H_z|$ plotted as a function of z' are shown in Figs. 2 through 9 where the curves are normalized by choosing NI = 1 ampere as the total current in the solenoid. Positive values of z' correspond to points that are ahead of the solenoid in the sense that the solenoid is moving with a uniform velocity v in the positive z direction relative to the rope. Of course the results apply to the special case when the solenoid is fixed and the rope moves with a relative velocity v in the negative z direction.

In each of the curves for $|H_z|$ shown in Figs. 2 through 9, the rope radius $a = 2$ cm, the solenoid radius $b = 2.5$ cm, and the solenoid length $\ell = 2$ cm. We then choose various values and combinations of the following parameters: operating frequency $\omega/2\pi$, rope conductivity σ, rope magnetic permeability (relative to free space) μ/μ_o and the velocity v.

In Fig. 2 we consider the case of a solenoid that is stationary with respect to the rope (i.e., $v = 0$) and illustrate the effect of frequency on the field $|H_z|$ at the surface of the rope, $\rho = a$. Here $\mu/\mu_o = 200$ and

$\sigma = 10^6$ mho/m. As expected the curves are symmetrical about $z' = 0$. In each there is a pronounced peak within the region of the solenoid which again is not surprising. However, there is an enhancement of the peak for the A.C. cases (i.e., f = 10 and 100 Hz) over that for the D.C. case (i.e., f = 0). At 100 Hz this is particularly noticeable since the magnetic flux is being excluded from the interior of the rope. In Fig. 3 the corresponding curves are shown for $|H_z|$ at the center of the rope, $\rho = 0$. Here we can see that, particularly at 100 Hz, the field magnitude is much reduced which is consistent with our statement above.

In Fig. 4 we now illustrate the influence of the motional velocity on the field H_z at the surface $\rho = a$ for frequency $f = \omega/2\pi = 10$ Hz, rope conductivity $\sigma = 10^6$ mho/m and a relative permeability $\mu/\mu_o = 200$. The three cases shown are for rope velocities v = 0, 10 and 50 m/s. The corresponding results are shown in Fig. 5 for the internal field at the rope center $\rho = 0$ where there is a decided "delay" of the buildup of the field magnitude; this effect becomes quite appreciable at v = 50 m/s.

In Fig. 6 we show the influence of the relative permeability μ/μ_o for the case $\rho = 0$, f = 10 Hz, v = 0, and for $\sigma = 10^6$ mho/m. The curves are particularly peaked when $\mu/\mu_o = 1$ corresponding to a nonmagnetic metal but the maxima become smoothed out as μ/μ_o increases. Corresponding results are shown in Fig. 7 for v = 50 m/s. Again these show the pronounced "delay" of the maximum which we might describe as a *hydromagnetic drag*.

In Fig. 8 we illustrate the influence of the rope conductivity σ on the internal field for the case where v = 0, f = 10 Hz and $\mu/\mu_o = 200$. Not surprisingly there is a progressive decrease of the field magnitude as σ increases from 10^5, to 10^6, to 10^7 mho/m. In the latter case the attenuation is quite severe. The corresponding curves are shown in Fig. 9 for a motional

velocity v = 50 m/s. Again we have a good illustration of the hydromagnetic drag effect that is particularly evident for $\sigma = 10^6$ mho/m.

MUTUAL IMPEDANCE FOR COAXIAL SOLENOIDS

In various nondestructive testing schemes for wire ropes and similar tubular metal specimens the mutual impedance between two coaxial solenoids is measured. Such a configuration is depicted in Fig. 10 where we can specify that the bottom solenoid is excited by a current I and the induced voltage V' is measured in the upper solenoid. Both solenoids have a fixed separation s and they move in the upward direction with a velocity v relative to the cylindrical rope. For convenience we select both solenoids to have N turns uniformly spaced over a length ℓ. Clearly the voltage V' is to be obtained from

$$V' = -\frac{2\pi bN}{\ell}\int_{s-\ell/2}^{s+\ell/2} E'_{o\phi}(b,z',t)\,dz'$$

where

$$E'_{o\phi}(b,z',t) = E_{o\phi}(b,z',t) + v\mu_o H_{o\rho}(b,z',t)$$

Then if we define the mutual impedance Z'_m according to

$$Z'_m = V'/(Ie^{i\omega t})$$

it follows readily that

$$Z'_m = i\mu_o\omega b^2 N^2 \int_{-\infty}^{+\infty} \left[\frac{\sin(\lambda\ell/2)}{(\lambda\ell/2)}\right]^2 K_1(|\lambda|b)e^{-i\lambda s} \times [I_1(|\lambda|b) - (C/B)K_1(|\lambda|b)]d\lambda$$

where C/B is given explicitly by (19). In the limiting case where the rope is absent we have the simpler formula

$$Z'_m = iX_o = 2i\mu_o\omega b^2 N^2 \int_0^{\infty} \left[\frac{\sin(\lambda\ell/2)}{(\lambda\ell/2)}\right]^2 K_1(\lambda b)I_1(\lambda b)\cos\lambda s\,d\lambda$$

Here X_o is the free-space mutual reactance between the two solenoids.

The quantity we consider for the final numerical examples is the normalized response defined by the complex ratio $(Z'_m - iX_o)/X_o$. In Fig. 11 the real and imaginary parts are plotted as a function of frequency from 1 to 1000 Hz for the following parameters: $v = 0$, a rope radius $a = 2$ cm, radius of both solenoids $b = 2.5$ cm, rope conductivity $\sigma = 10^6$ mho/m, rope permeability $\mu/\mu_o = 200$. The two sets of curvesin Fig. 11 correspond to $s = 0$ and $s = 4$ cm. In the first case of zero separation we are dealing with the self impedance of one solenoid whereas in the second case the solenoids are distinctly separated. In both situations it is evident that the imaginary part considerably exceeds the real part at the lowermost frequencies. The corresponding results for a motional velocity of $v = 50$ m/s are shown in Fig. 12. Now we must distinguish between positive and negative values of s according to whether the "receiving" solenoid is above or below the "transmitting" solenoid, respectively. The marked changes between the curves in Figs. 11 and 12 are entirely due to the difference between motional velocity of zero and 50 m/s. It is particularly significant that in the latter case the reciprocity theorem is violated but such an effect is really not unexpected because of the lack of symmetry in the problem.

Finally, in Fig. 13, the normalized response at 10 Hz is plotted as a function of the motional velocity v from 1 to 1000 m/s for the three conditions $s = 0$, +4 and -4 cm. Otherwise the parameters are the same as before. These curves show very clearly that, for v somewhat less than 10 m/s, the influence of the relative motion is negligible. In fact if $v = 1$ m/s the curves have reached the $v = 0$ asymptotes.

CONCLUDING REMARKS

The electromagnetic fields induced in the cylindrical specimen or rope are seen to be influenced by the relative motion of the sensor. However, the effect is quite small unless the motional velocity is on the order of 10 m/s or higher. The same conclusion would apply to more complicated rope models if the average properties and geometrical dimensions are of the same order.

REFERENCES

[1] H.L. Libby, *Introduction to Electromagnetic Non Destructive Test Methods*, New York: Wiley Interscience, 1971.

[2] V.V. Klyuev and M.L. Faingoiz, "Non destructive testing of moving current conducting articles by means of pass-through converters using the constant field method," *Defektoskopiya*, Vol 8, No. 2, pp. 27-31, March/April 1972.

[3] H.N. Kritikos, K.S.H. Lee and C.H. Papas, "Electromagnetic reflectivity of nonuniform jet streams," *Radio Science*, Vol. 2, No. 9, pp. 991-995, Sept. 1967.

[4] R.H. Ott and G. Hufford, "Scattering by an arbitrarily shaped conductor in uniform motion relative to the source of an incident spherical wave," *Radio Science*, Vol. 3, No. 8 pp. 857-861, Aug. 1968.

[5] J.R. Wait and D.A. Hill, "Electromagnetic interaction between a conducting cylinder and a solenoid in relative motion," *Preliminary Report to U.S. Bureau of Mines on Contract No. H0155008*, 9 January 1979.

[6] L.D. Landau and E.M. Lifshitz, *Electrodynamics of Continuous Media*, Oxford: Pergamon Press, Sec. 4.9, pg. 205, 1960.

[7] D.A. Hill and J.R. Wait, "Scattering by a slender void in a homogeneous conducting wire rope," *Applied Physics*, Vol. 16, pp. 391-398, 1978.

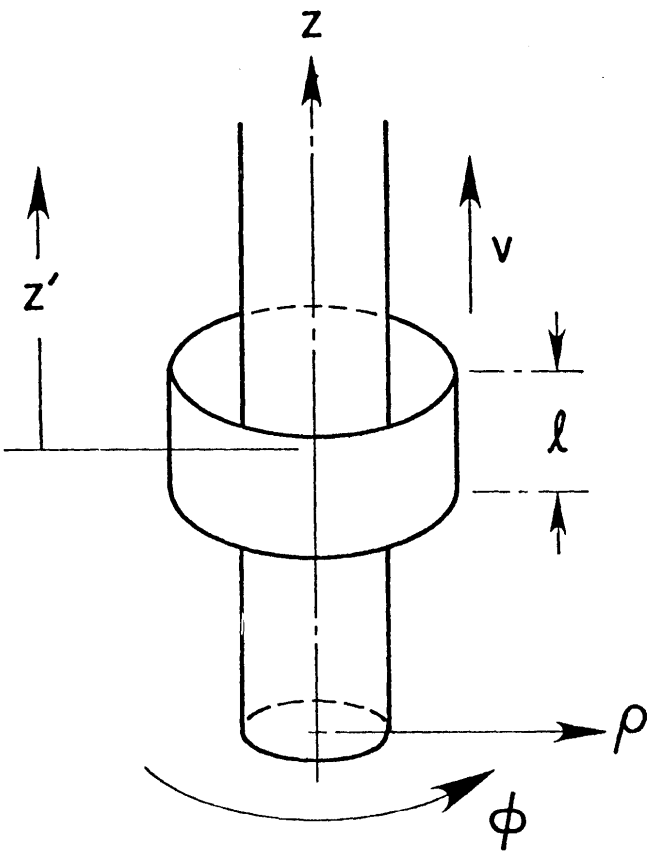

Fig. 1. Cylindrical Conductor of radius a excited by a concentric solenoid of radius b that has a velocity v relative to conductor. In examples that follow, a = 2 cm, b = 2.5 cm and ℓ = 2 cm.

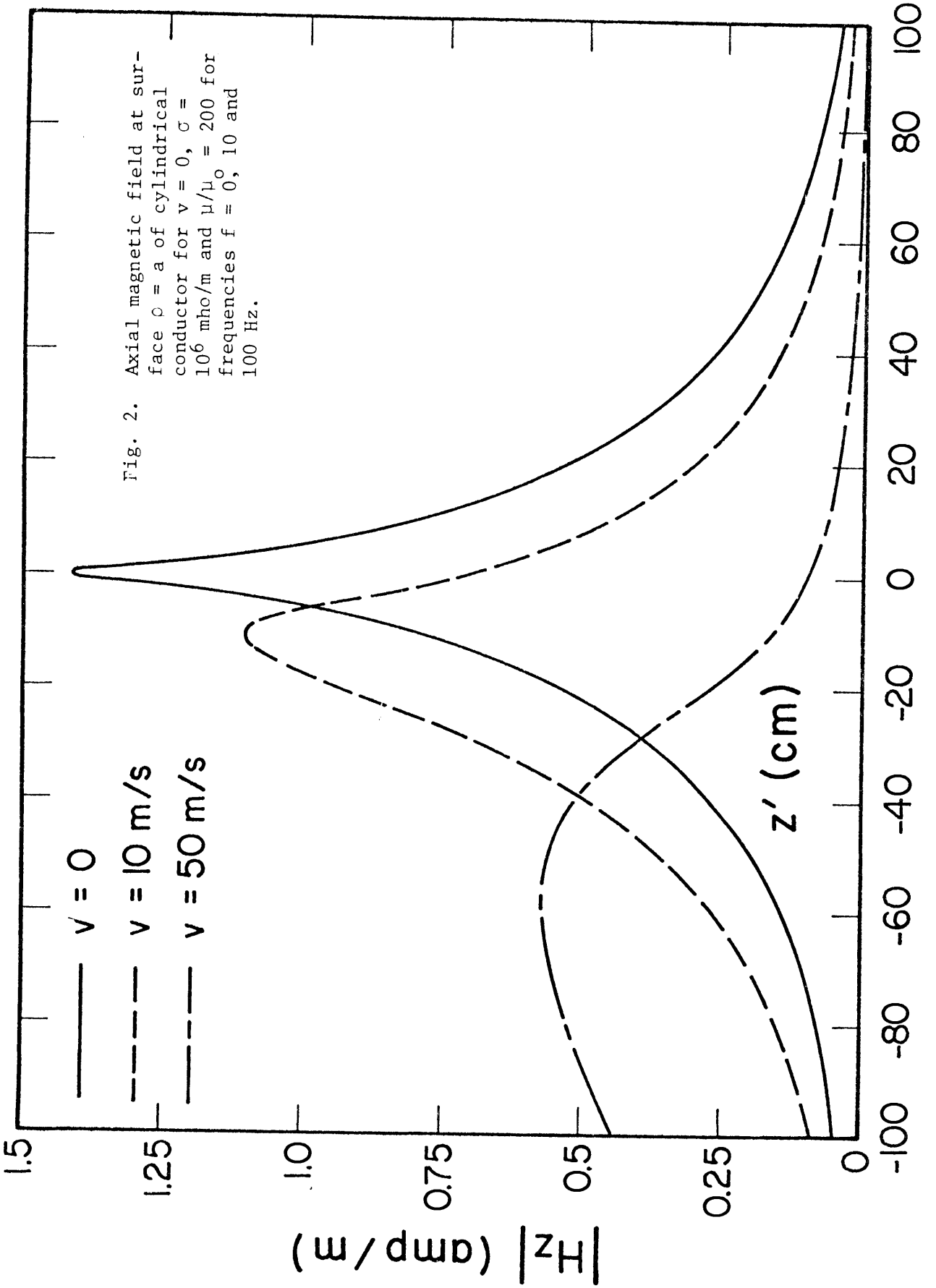

Fig. 2. Axial magnetic field at surface $\rho = a$ of cylindrical conductor for $v = 0$, $\sigma = 10^6$ mho/m and $\mu/\mu_o = 200$ for frequencies $f = 0$, 10 and 100 Hz.

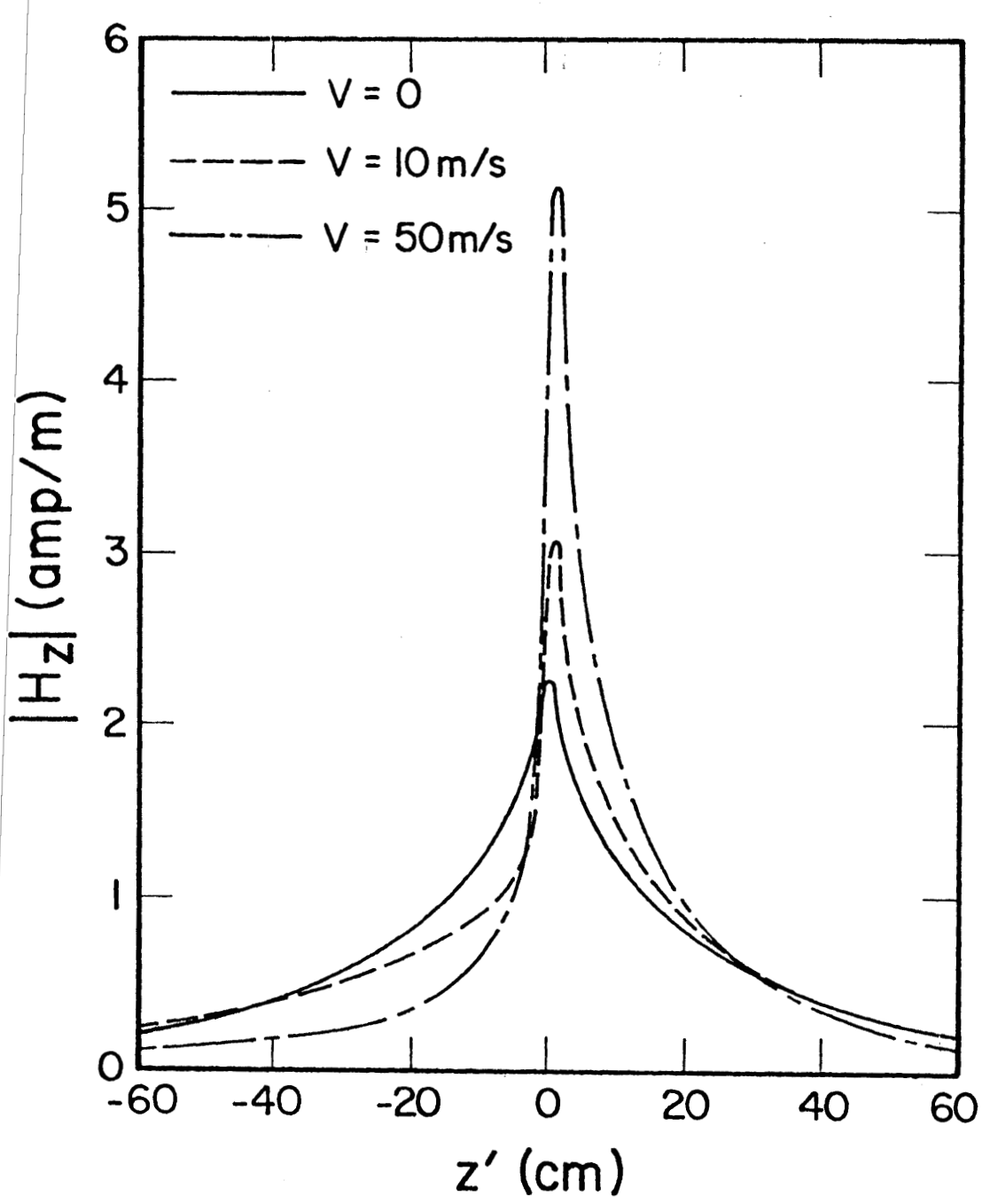

Fig. 3. Axial magnetic field at axis, $\rho = 0$, for same conditions as in Fig. 2.

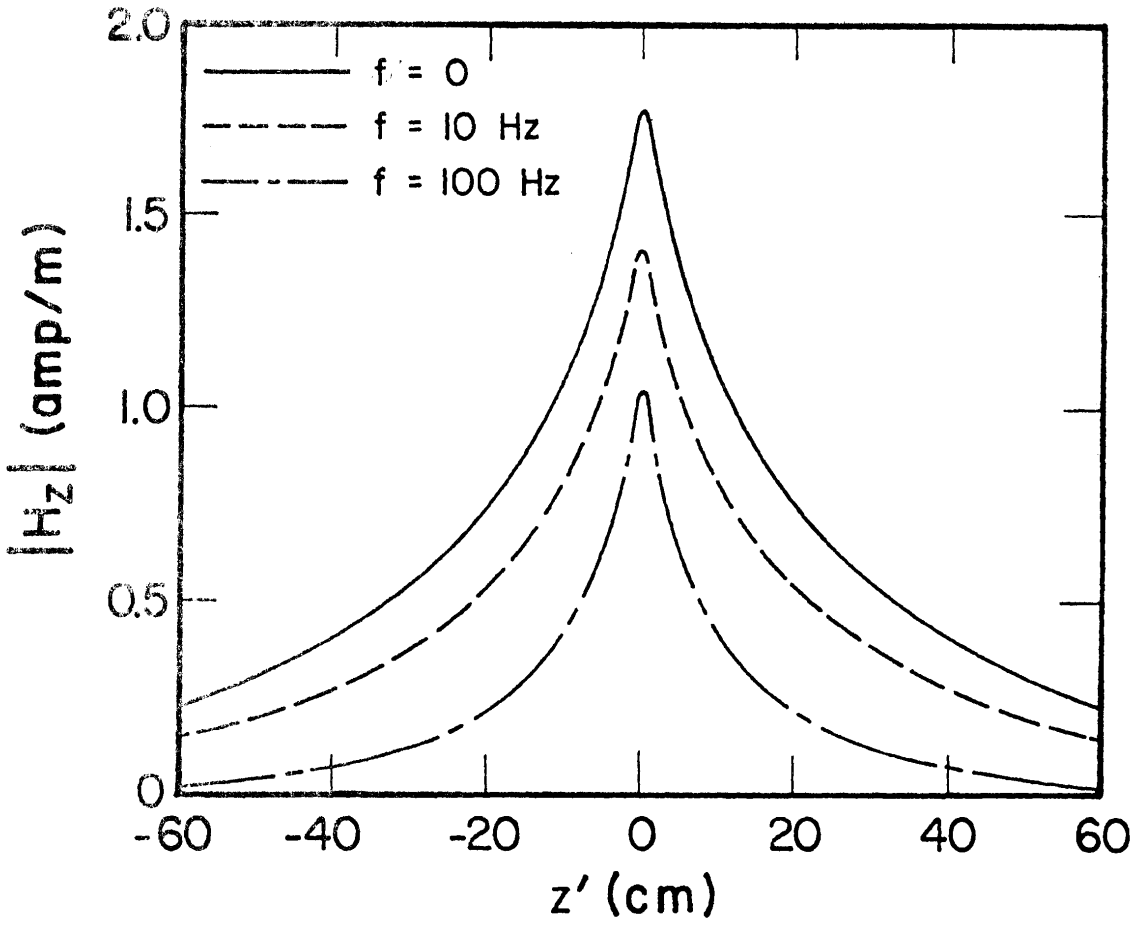

Fig. 4. Field at surface = a, for velocities v = 0, 10 and 50 m/s, for f = 10 Hz and other conditions as above.

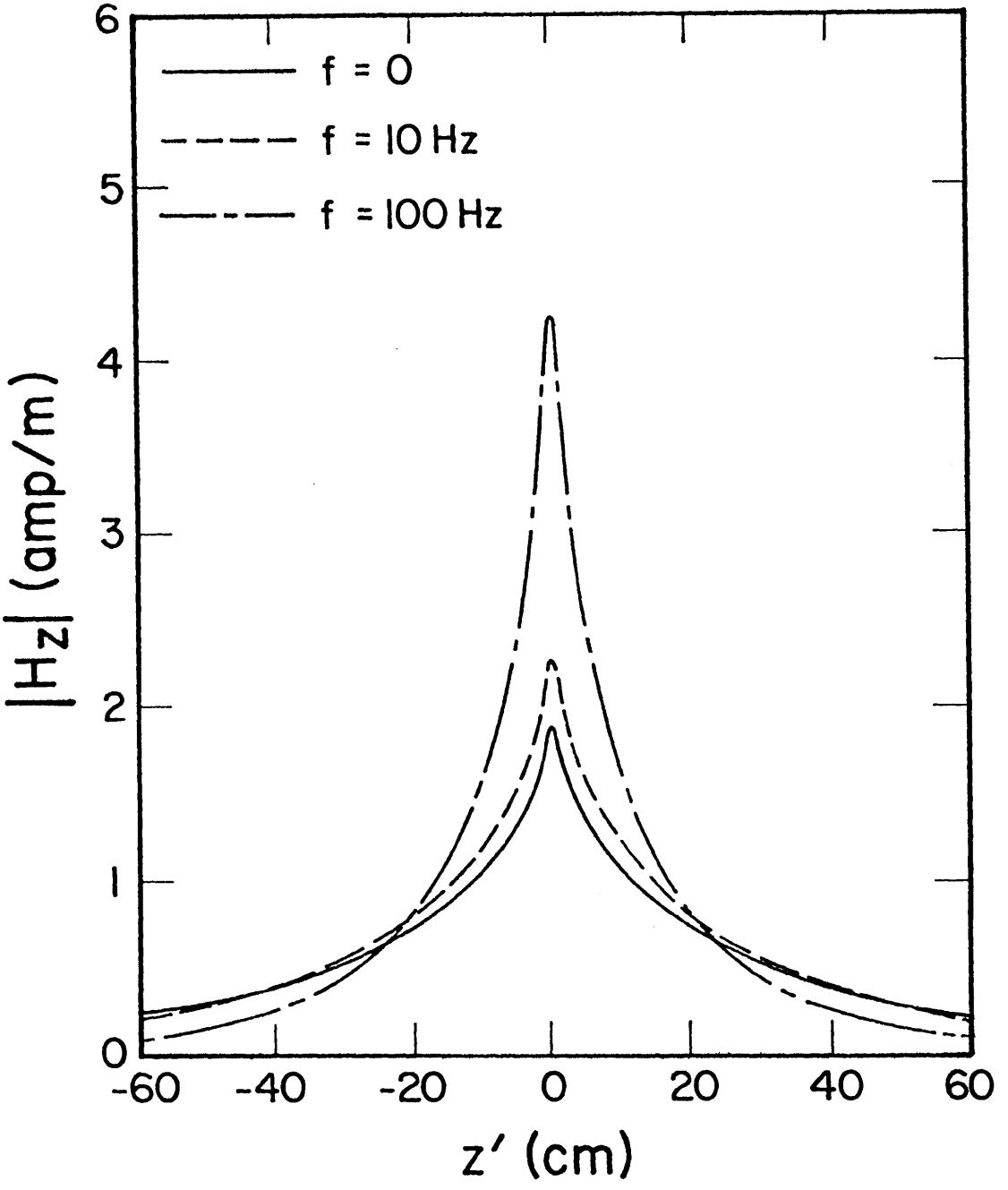

Fig. 5. Field at axis $\rho = 0$, for conditions as in Fig. 4.

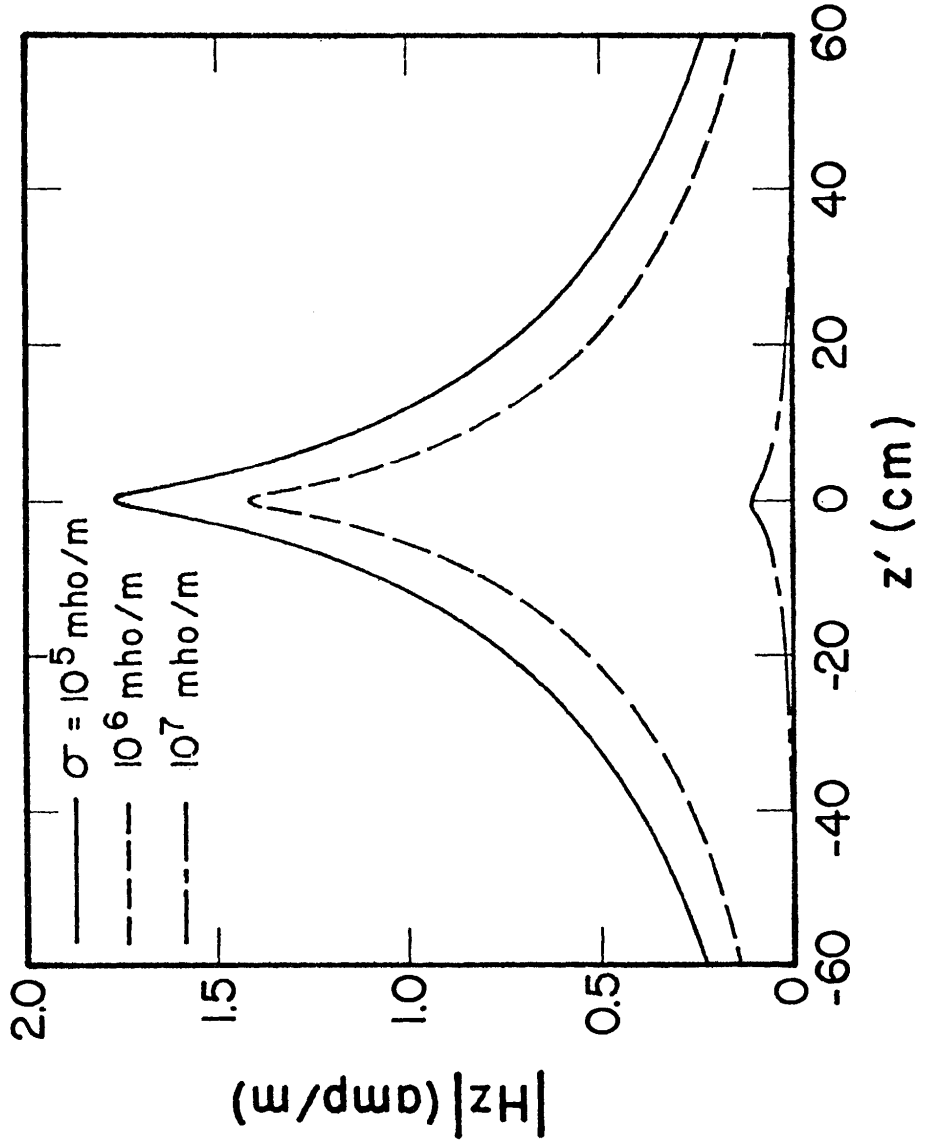

Fig. 6. Field at axis $\rho = 0$ for $f = 10$ Hz, $v = 0$, $\sigma = 10^6$ mho/m and $\mu/\mu_o = 1$, 20 and 200.

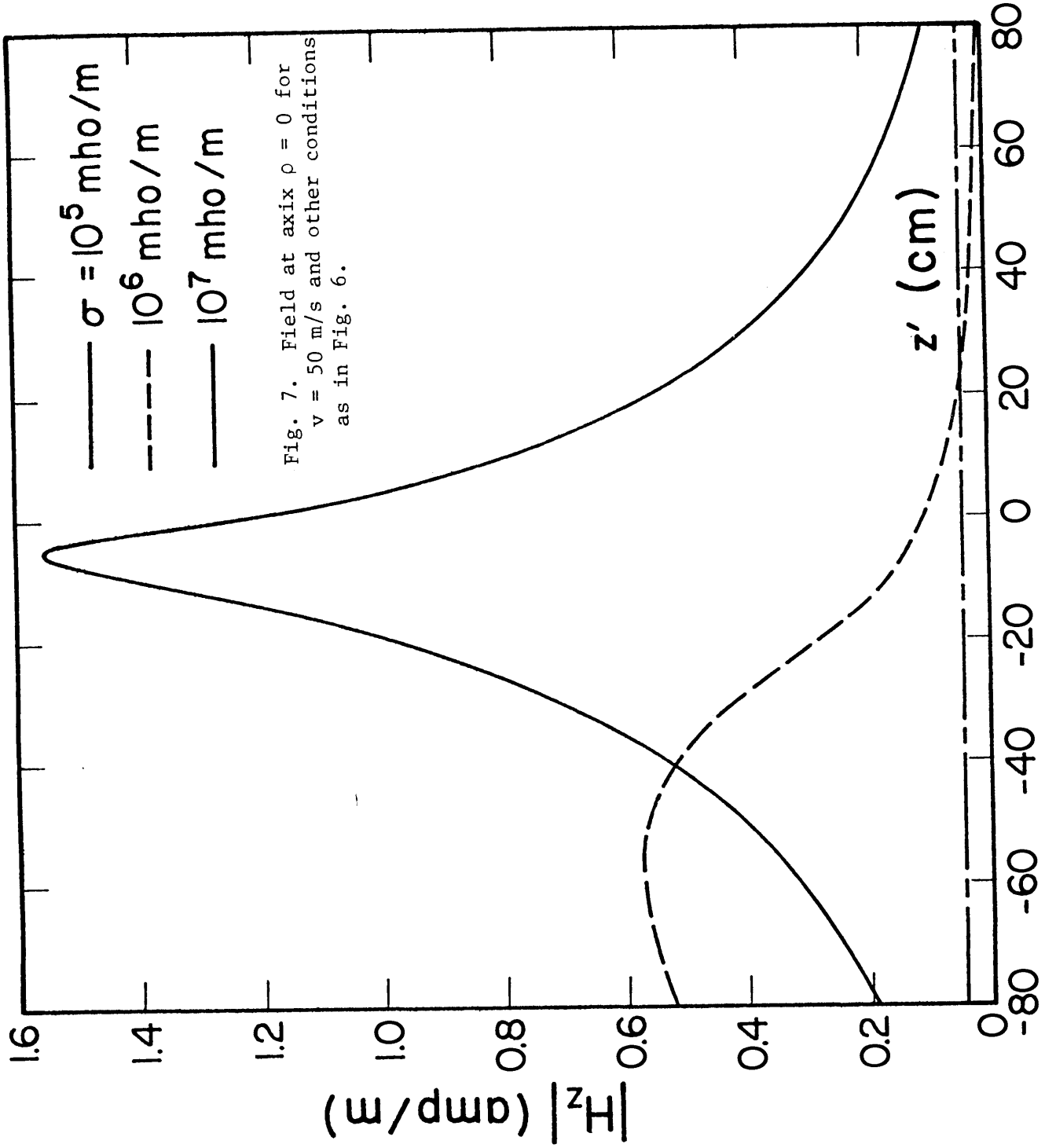

Fig. 7. Field at axix ρ = 0 for v = 50 m/s and other conditions as in Fig. 6.

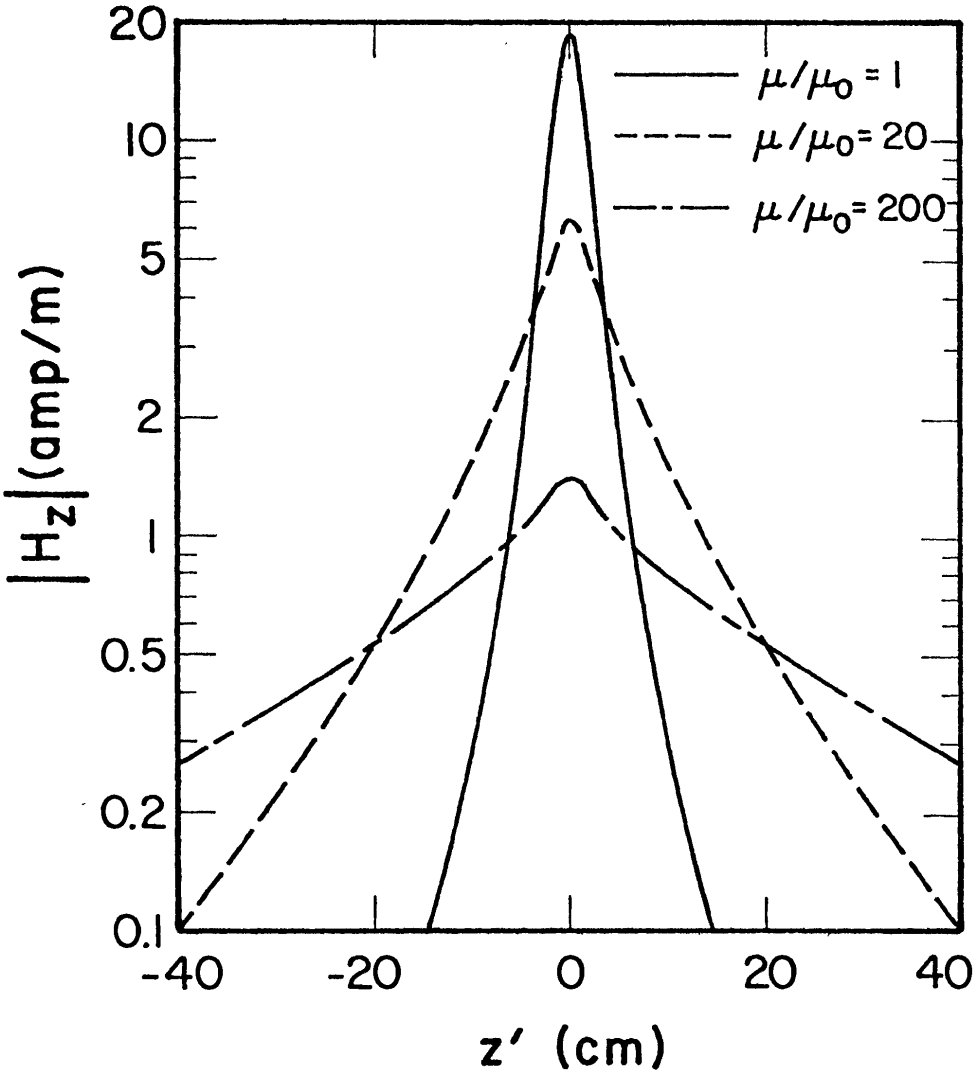

Fig. 8. Field at axis $\rho = 0$ for $v = 0$, $f = 10$ Hz, $\mu/\mu_o = 200$ and $\sigma = 10^5$, 10^6 and 10^7 mho/m.

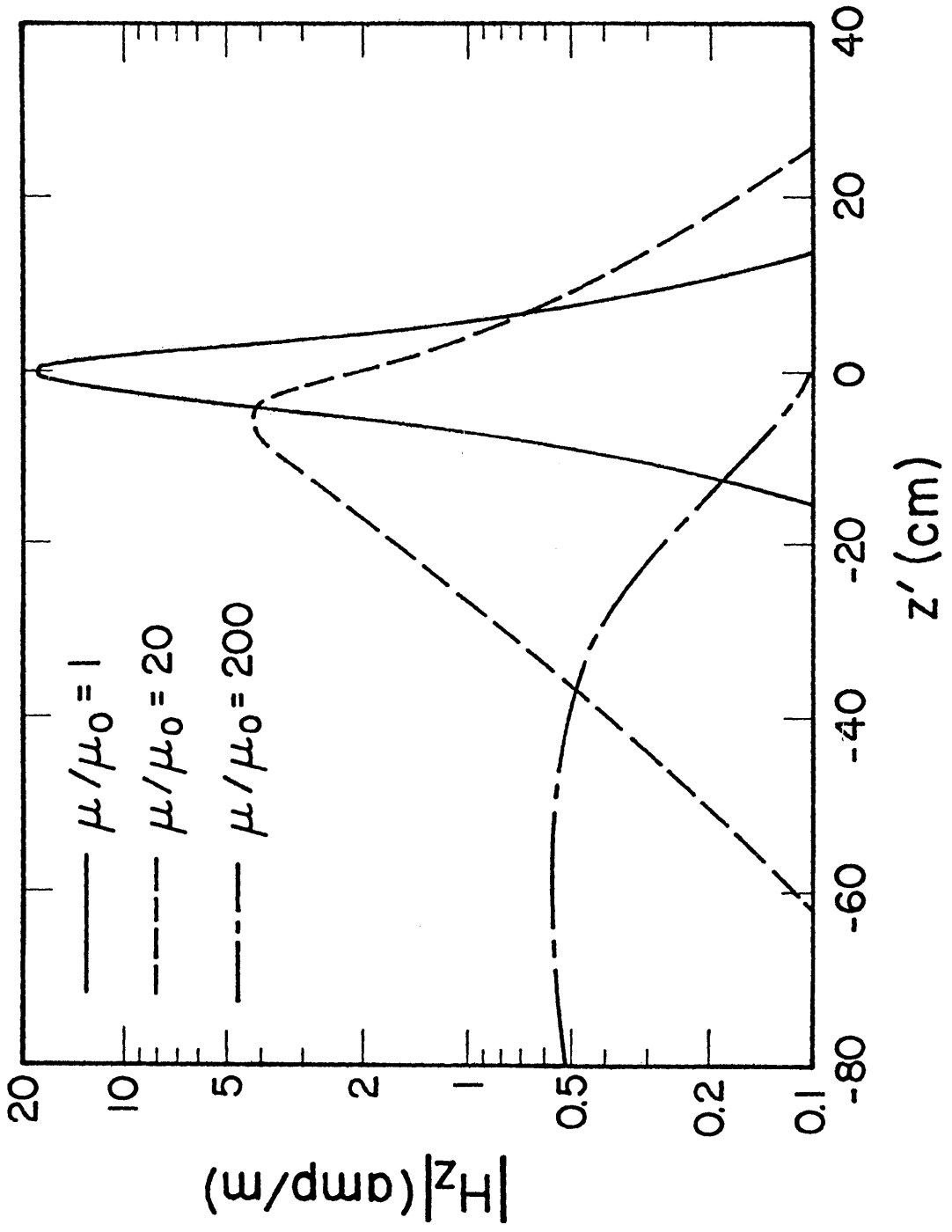

Fig. 9. Field at axis $\rho = 0$ for $v = 50$ m/s and other conditions as in Fig. 6.

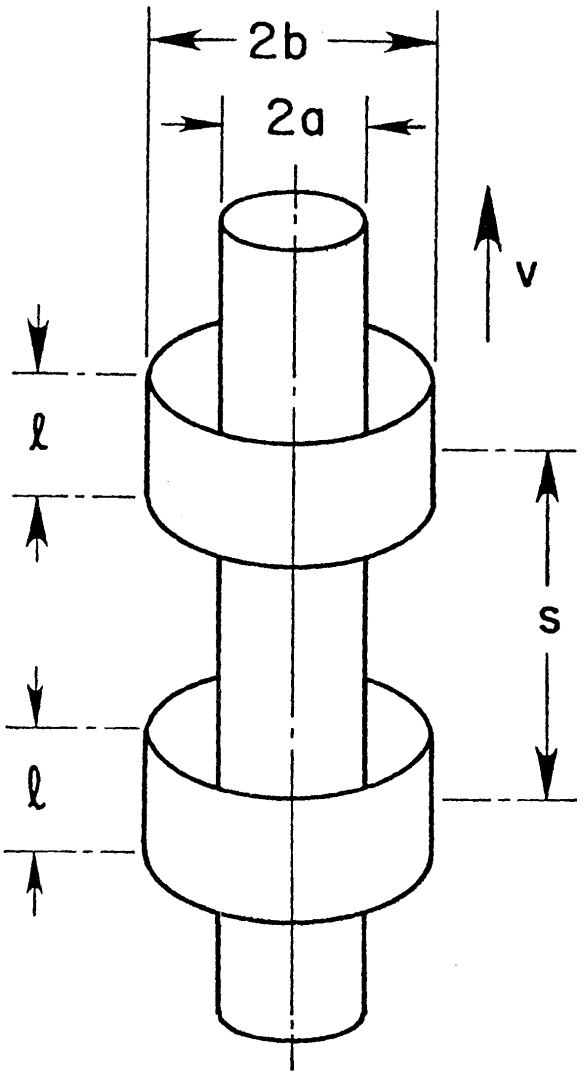

Fig. 10. Coaxial solenoid arrangement that moves with velocity v (upwards in figure) relative to cylindrical conductor or rope.

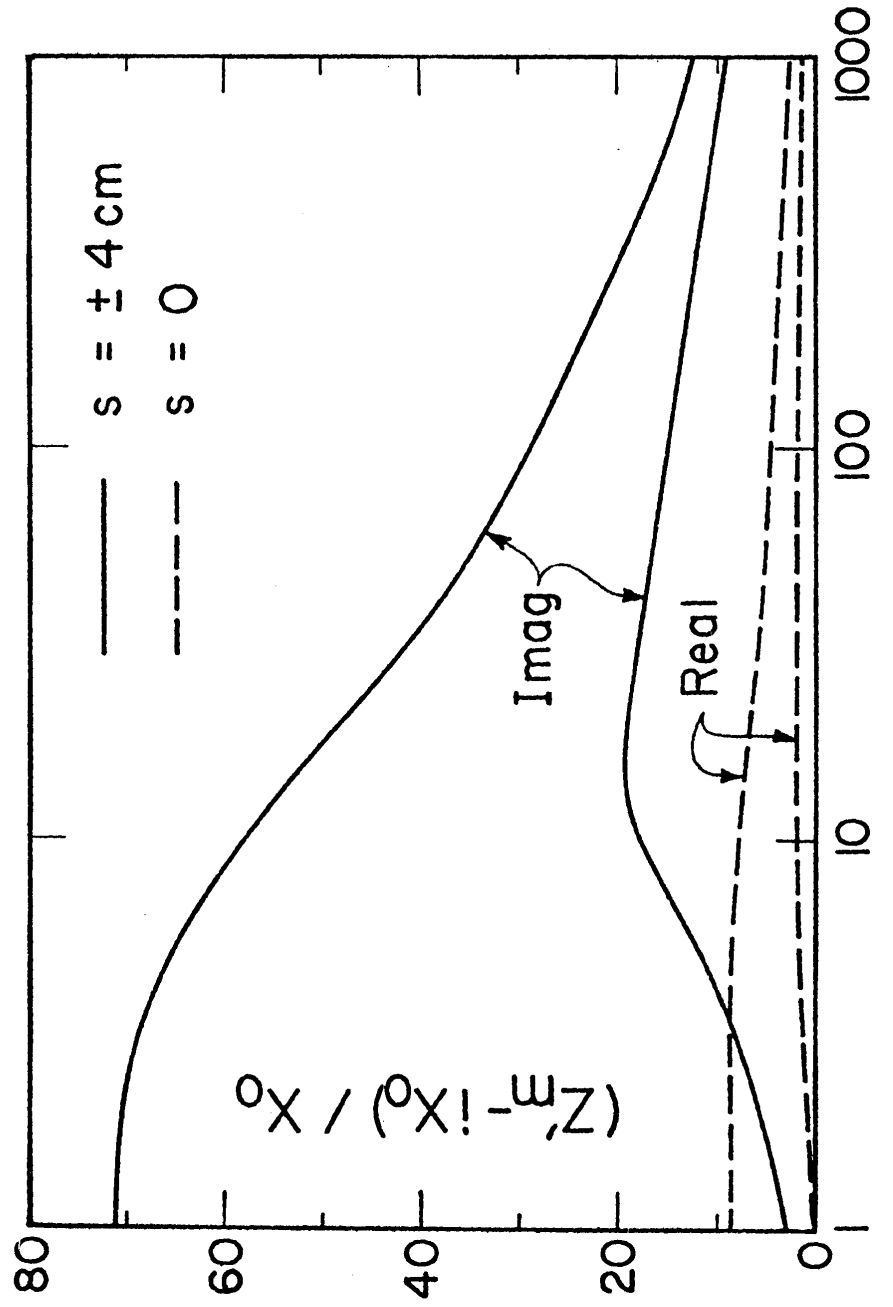

Fig. 11. Normalized response for sensor shown in Fig. 10 due to cylindrical conductor as a function of frequency for $v = 0$, $\sigma = 10^6$ mho/m, $\mu/\mu_o = 200$, $s = \pm 4$ cm and $s = 0$.

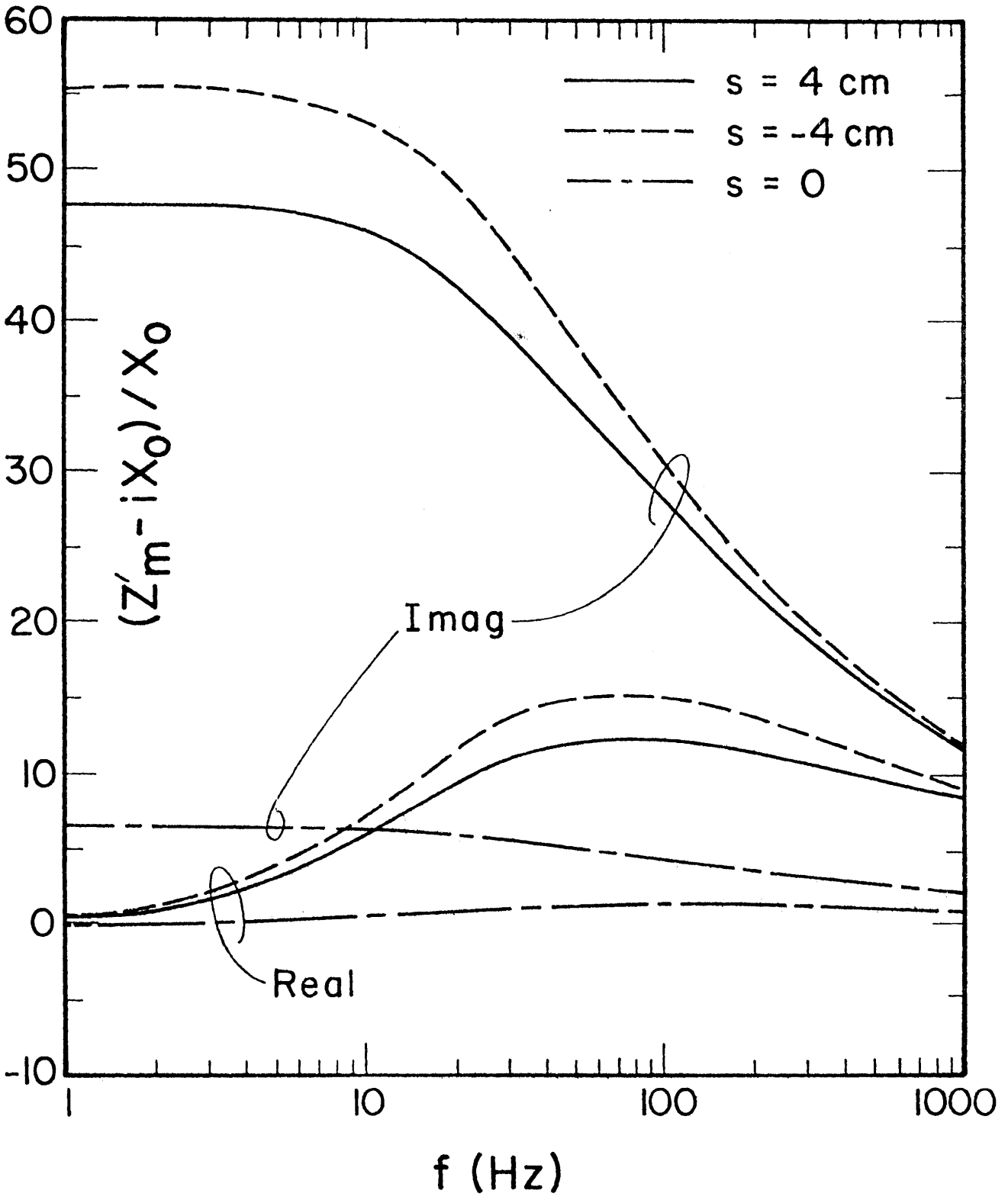

Fig. 12. Normalized response for v = 50 m/s and other conditions as in Fig. 11.

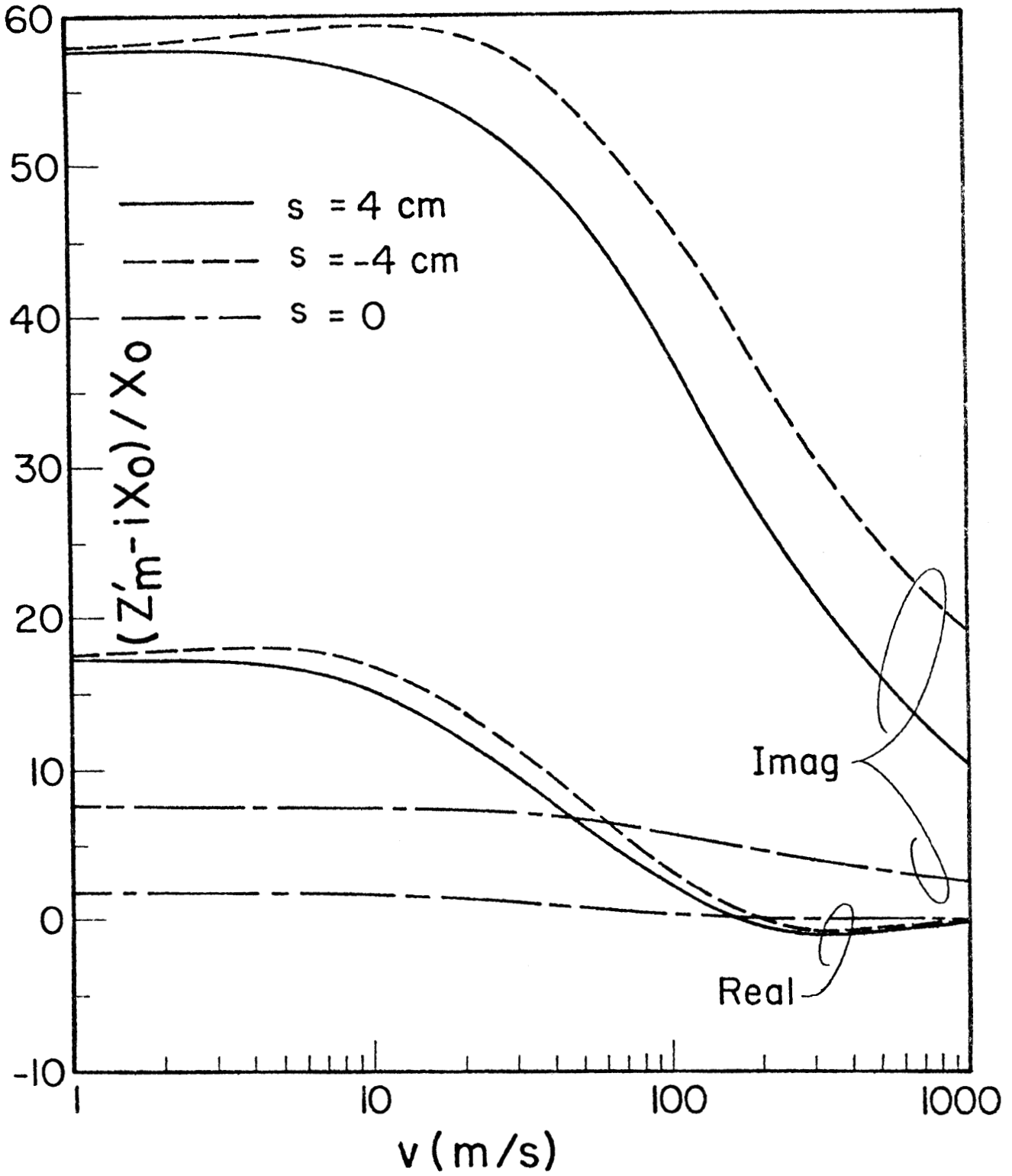

Fig. 13. Normalized response for coaxial sensor a function of v for f = 10 Hz, $\sigma = 10^6$ mho/m and $\mu/\mu_o = 200$, s = 0, -4 and +4 cm.